

High performance capillary electrophoresis using Van de Graaff generator

Dissertation
zur Erlangung des Grades
des Doktors der Ingenieurwissenschaften
der Naturwissenschaftlich-Technische Fakultät
der Universität des Saarlandes

Von

Seung Jae, Lee

Saarbrücken

2017

Tag des Kolloquiums:

13. July 2017

Vorsitzender:

Prof. Dr. Georg Frey

Dekan:

Univ.-Prof. Dr. Guido Kickelbick

Gutachter:

Prof. Dr. Andreas Manz
Prof. Dr. Matthias Nienhaus

Akademischer Mitarbeiter:

Dr. Haibin Gao

Contents

1. Introduction

1.1 Motivation	1
1.2 Capillary Electrophoresis	2
1.2.1 Electrical double layer	3
1.2.2 Electroosmotic flow	8
1.2.3 Electrophoresis	9
1.2.4 Experimental setup of Capillary electrophoresis (CE)	10
1.2.5 Separation efficiency & resolutions in CE	11
1.2.6 Joule heating in capillary electrophoresis	13
1.2.7 Electrical breakdown	14
1.3 Van de Graaff Generator (VDG)	16
1.3.1 Classic Van de Graaff Generator	16
1.3.2 Pelletron accelerator	17
1.4 Laser induced fluorescence (LIF) system	19
1.5 References	20

2. Van de Graaff generator for Capillary electrophoresis 27

2.1 Introduction	27
2.2 Theoretical background	28
2.3 Materials and Methods	29
2.3.1 Reagents	29
2.3.2 Experimental setup	31
2.3.3 Experimental procedure for capillary electrophoresis	32
2.4 Results and discussion	33
2.4.1 Effect of BGE concentration	33
2.4.2 Effect of capillary diameter	34
2.4.3 Comparison of the VGD to a conventional DC power supply	36
2.4.4 Determination of the voltage applied with the VDG	38
2.4.5 Outlook	43
2.5 Conclusions	44

2.6 Reference	45
3. Application of CE with VDG for carbohydrate separation	48
3.1 Sample from HIPs (Helmholtz center for infection research)	48
3.2 Labelling protocols and results for FITC labelling	49
3.3 Labelling protocols and results for APTs labelling	50
3.4 Conclusion	54
4. Outlook	59
5. Appendix	
5.1 Chip fabrication and Sample injection method for CE	60
5.1.1 Glass chip fabrication	60
➤ Design structure and glass wafer preparation	60
➤ Patterning structure and etching metal layers	62
➤ Powder blasting and glass bonding	63
5.1.2 Sample injection method for CE	64
➤ Electrokinetic sample injection method	64
➤ Hydrodynamic sample injection method	66
5.1.3 On chip capillary electrophoresis	67
➤ Electrokinetic sample injection method	67
➤ Detection method for on-chip CE	69
5.1.4 References	70
5.2 Split flow on-chip capillary electrophoresis (SCE)	71
5.2.1 Introduction	71
5.2.2 Materials and Methods	72
➤ Reagents	72
➤ Chip preparation	72
➤ Electrical equipment	74
➤ Electric field simulation	75

➤ On-chip CE experiment	75
5.2.3 Theoretical background	75
➤ Equation for theoretical number of plate	75
➤ Calculation for joule heating in CE chip	76
5.2.4 Results and Discussions	77
➤ Sample dividing in split flow channel	77
➤ Simulation of electric filed for normal CE chip and SCE	77
➤ Comparison experiment of separation efficiency	78
5.2.5 Conclusion.	80
5.2.6 Reference	81

5.3 Supplement materials

5.3.1 Fabrication process for split flow CE glass chip	83
5.3.2 Calculation for hydrodynamic sample injection system	102
5.3.3 High voltage measurement of VDG	104
➤ Theoretical understanding for voltage divide	104
➤ Using resistive capacitive voltage divider for VDG	105
➤ Electric field meter	107
5.3.4 Electrical breakdown and heating problem from the AC motor of VDG	108
➤ Electrical breakdown	108
➤ Heating problem from the AC motor of VDG	110
5.3.5 Presentation materials for conferences	114
➤ MicroTas 2014 (Poster presentation)	114
➤ 40 th ISCC Riva del Garda (Oral presentation)	115
➤ 20 th Nanobiotech Montereux (Flash presentation & Poster presentation)	116
5.3.6 Contributed publications	
➤ Short-term effect of humid airflow on antimicrobial air filter using <i>Sophora flavescens</i> nanoparticles, <i>Science of the Total Environment</i> (2012), 273-279	
➤ Effect of Antimicrobial Air filters on the Viability and Culturability of Airborne Bacteria, <i>Clean-Soil, Air, Water</i> (2016), 44 (9999), 1-10	

List of Figures

Figure 1.1: (Left) The schematic diagram of the Helmholtz double layer. (Right) Initial potential (ψ_0) at the inner Helmholtz plane (IHP) drop linearly to zero potential by the distance of outer Helmholtz plane (OHP) which comprises the absorbed anions.

Figure 1.2. (Left) The schematic diagram of the Gouy-Chapman model. (Right) The potential is dropped exponentially and the model follows the Boltzmann statistical distribution.

Figure 1.3: (Left) The schematic diagram of the stern model (Right) The potential changes exponentially and, follows the Boltzmann statistical distribution.

Figure 1.4: The schematic diagram of the zeta potential (ζ potential) for the dispersed particle

Figure 1.5: The schematic diagram of the zeta potential (electrokinetic potential) for the glass capillary

Figure 1.6: Schematic diagram of differences between electroosmotic flow (green) and parabolic flow (purple), green line represent electroosmotic flow by electrokinetic force and purple line indicate parabolic flow which can be generated by pressure driven flow.

Figure 1.7: Schematic diagram of electrophoretic mobility. Total electrophoretic mobility of electrolyte can be determined the sum of the original mobility for electrolyte and electroosmotic flow.

Figure 1.8: Schematic diagram of conventional CE setup. Normally, Laser induce fluorescence (LIF) system is used for detector.

Figure 1.9: Schematic diagram for comparison of separation efficiency and resolution. Normally, separation efficiency can be achieved by higher applied voltage and the resolution can be

achieved by slower total electrophoretic mobility or longer separation channel (longer analysis time).

Figure 1.10: (upper) Schematic diagram of joule heating phenomena in capillary electrophoresis. When the temperature at inside of capillary tube than the boiling point of BGE by current, small bubble is generated and block the capillary (or, become an obstacle by smaller bubble) tube. (bottom) heat gradient inside of capillary tube, the temperature at the core of capillary is the highest because of the heat dissipation at capillary wall.

Figure 1.11: : (Upper) Schematic diagram of Corona discharge which can be occurred by high electric field by Van de Graaff generator. (Bottom) Schematic diagram of electrical breakdown for fused silica capillary tubes by high electric field.

Figure 1.12: Early stage of Van de graaff generator in 1933 by Robert J. Van de Graaff at MIT.

Figure 1.13: (Left) Schematic diagram of Van de Graaff generator. Major components of VDG are two pulleys, two combs and rubber belt which can be driven by AC motor. Metal sphere can be a capacitance for electrons and it makes very high electric potentials. (Right) commercial VDG which can generate up to 350kV with 10 μ A constant current.

Figure 1.14: Schematic diagram of Pelletron accelerator which has similar mechanism with classic Van de Graaff generator. Pelletron consists two pulleys (drive pulley and terminal pulley), 2 high power supply which need to generate high current to metal pellets-nylon links and Terminal shell.

Figure 1.15: Schematic diagram of laser induced fluorescence (LIF) system. Which has 470nm excitation laser source, excitation filter, emission filter for 520nm wavelength, dichroic mirror and photomultiplier module.

Figure 2.1 Experimental setup for Van de Graaff (VDG) generator-based capillary electrophoresis. (A) Schematic diagram of the platform, illustrating the connection of a capillary tube to sample/buffer reservoirs connected to a conventional 30 kV power supply at the capillary

inlet and the VDG at the capillary outlet. Sample injection was achieved electro-kinetically using the DC power supply (5 kV for 3 s). And also, for direct measurement of field strength for the VDG, electric field meter was placed 140mm away from the dome (B) Laser induced fluorescence (LIF) detection system, consisting of a 473 nm laser directed into a filter cube. The excitation light passed into an optical fiber that was connected to a detection stage near to the outlet of the capillary. A photomultiplier tube (PMT) was attached to the filter cube for detection of fluorescence light collected from a sample. (C) Detection stage in which the capillary was held near to the outlet, allowing detection via a microscope objective connected to the optical fiber of the LIF system. The capillary outlet was inserted into a stainless steel buffer reservoir that was electrically connected to the VDG via a platinum wire. And also, electric field meter was placed 140mm distance from the sphere for measuring direct voltage from VDG.

Figure 2.2 The effect of background electrolyte (Borax solution) concentration on the migration times of three amino acids using the VDG CE platform with a 50 μm ID capillary.

Electropherograms showing amino acid migration times in (a) 2 mM Borax buffer, and (b) 10 mM Borax buffer.

Figure 2.3 The effect of capillary diameter on the migration times of three amino acids using the VDG CE platform (2 mM Borax background electrolyte). (a) Separation obtained using a 5 μm ID capillary, and (b) using a 50 μm ID capillary.

Figure 2.4 Comparison of the migration times of amino acids using different power supplies. (a) Separation using a Van de Graaff (VDG) generator power supply, with 2 mM Borax buffer and a 5 μm ID capillary. (b) Separation using a conventional 30 kV CE power supply (Normal PS), with 10 mM Borax buffer and a 50 μm ID capillary.

Figure 2.5 Comparison of Theoretical plate per second for 3 amino acids separations using the conventional 30 kV power supply and the VDG generator with varying background electrolyte concentrations (2 and 10 mM Borax) and capillary diameters (5 and 50 μm).

Figure 2.6 Upper) Electric field strength by measuring with electric field meter for different diameter of capillary tubes and concentrations of BGE and, Bottom) Comparison of average voltages, an average voltage approximately 3.4 times higher than the reference was achieved using the VDG

Figure 3.1 Chemical structure of Sialylglycopeptide (SGP)

Figure 3.2 Separation result for SGP with FITC labelling. Two SGP peaks and two free FITC peaks were separated.

Figure 3.3 Separation result for SGP with APTs labelling. For labelling SGP with APTs, sample was cleaved off with reducing reagent and then APTs was labelled. By the separation process with VDG, one “big peak flock” was separated. A) raw data for the separation, B) 1st Zoom in for red dot box, there has several hundred peaks were separated, C) 2nd Zoom in for red dot box, still there has very well separated peaks were observed, D) 4th Zoom in for red dot box, one peak was selected and the sigma value and FWHM value was extracted and the separation efficiency was calculated.

Figure 3.4 Repeating experiment to check the reproducibility. (upper) Peaks were appeared at 370sec. respectively. (middle) Peaks were zoomed in. Peaks were not non-reproducible. (bottom) peaks were not appeared regularly and the CE system looked that it had a problem for the reproducibility.

Figure 3.5 Separation experiment only with APTs fluoropore. (upper) 5times repeating experiement only with APTs and couldn`'t find the peak which has same reproducibility but, the calculation of separation efficiency was very good as like previous result (bottom).

Figure 5.1. (Upper) Design the structure for glass chip fabrication process with AutoCAD software. (Bottom) control plot for 5inch Mask design.

Figure 5.2. Making layer deposition onto the glass wafer to prevent photoresist layer.

Figure 5.3. Spin coating photo resist onto the masking layer at 4000rpm for 30sec.

Figure 5.4. Glass wafer is exposure with UV light by Mask Aligner.

Figure 5.5. Exposure glass wafer is developed by developer

Figure 5.6. Metal layer etching and glass etching by specific etchant.

Figure 5.7. Schematic diagram of Electrokinetic injection method. Power supply connected into sample reservoir (red line) and ground electrode (black line) is connected into outlet side of buffer reservoir. Sample is injected by electrokinetic force by power supply (red dot rectangular box) which is occurred by the flow of EOF that is predominant inside of capillary tube.

Figure 5.8. (Upper) Flow chart and flow calculation for hydrodynamic injection method. Hydrodynamic injection system consists with high pressure pump, injection, flow splitter and solenoid valve. (Bottom) Schematic diagram of hydrodynamic sample injection system.

Figure 5.9. Electrokinetic sample injection method for on-chip CE (upper). Sample can be flow only upper to bottom and BGE can be flow to cross section area by electro kinetic force therefore, sample is squeezed (red dot box). Sample is separated by total electrical mobility (bottom). Total electrical mobility is determined the summation of electroosmitic flow and mobility of electrolyte.

Figure 5.10 Microscopic detection system for on-chip CE. Emission light can be detected with photomultiplier tube (PMT) and oscilloscope is used for collecting signal from PMT.

Figure 5.11 Experimental picture for split flow CE chip which has 30 μ m width and 5 μ m depth. It was fabricated MESA+ at Twente University.

Figure 5.12 (Upper) Schematic diagram for sample loading process for SCE and normal CE chip, sample was squeezed in cross section by electro kinetic force (A) and sample injection process through SCE (B), sample was injected by electro kinetic force and the sample was divided at the split flow channel in the middle of separation channel. Each red dot circle and line indicate pictures from the experiment. Sample loading process for normal cross shape CE chip (C) and sample separation process in normal CE chip (D). (Bottom) Experimental picture for separation process at the split flow channel in the middle of SCE chip. Sample electrolytes are split at the star shape geometry.

Figure 5.13 Experimental setup for split flow CE. 8 channel sequencer was used to apply voltage to each reservoirs and fluorescence microscope with PMT was used for detection. Data was collected with Oscilloscope.

Figure 5.14. SCE (A) and circuit diagram for SCE (B) and Normal CE chip (C) and circuit diagram for normal CE chip (D)

Figure 5.15. amino acids separation with SCE (Left) and normal cross shape CE chip (Right) at 18.5mm from the cross section. Each number represent 1: free FITC, 2: GLU, 3: GLN, 4: Ala, 5: Arg, 6: Lys

Figure 5.16. Comparison of theoretical number of plate for SCE and normal CE chip. SCE has approximately 300% better separation efficiency than normal CE chip.

Figure 5.17 Schematic diagram of hydrodynamic sample injection system. (upper) Position of injector for sample loading process. (bottom) Position of injector for sample separation process.

Figure 5.18 Hydrodynamic injection system with “Flow splitter” for pressure pulse injection.

Figure 5.19 2-position flow injector for hydrodynamic sample injection system.

Figure 5.20 Solenoid valve for pressure pulse control

Figure 5.21 Flow splitter and T-connector for precise sample injection method into very narrow ID capillary tube (5 μ m)

Figure 5.22 Schematic circuit diagram for resistive voltage divider.

Figure 5.23 Resistive capacitive voltage divider for measurement of high voltage from VDG (upper), Measurement design with CVD 600 for high voltage measurement from VDG (Bottom).

Figure 5.24 Schematic diagram of constant capacitor. Ideal capacitor consists with two plates which has certain distance in between. Charges inside of plates can make an internal electric field.

Figure 5.25 Schematic diagram of electric field meter. It consists with two pairs of measurement sensors, grounding shutter which connect with rotating motor and AC amplifier (upper). Commercialized electric field meter for measurement of high voltage from VDG (bottom).

Figure 5.26 Corona discharge from VDG during separation experiment for CE.

Figure 5.27 Broken fused silica capillary by high electric field from VDG. When the electric field is too high, capillary is damaged (red arrow) and broken (red dot circle).

Figure 5.28 PEEK shielding to prevent breaking capillary tube by high voltage from VDG. By the shielding, total dielectric strength of capillary could be increased to 23.2~26.5kV/1180 μ m.

Figure 5.29 Heat control units from AC motor and speed control knob by Peltier elements.

Acknowledgements

I would like to thank to the god and I will give all of my glory to Jesus. First of all, I would like to thank to Professor Andreas Manz. It was really great honor to work with him. Moreover, I would like to thank to my team members (Dr. Matthias O. Altmeyer, Dr. Mark D. Tarn, Dr. Eric R. Castro, Dr. Jukyung Park, Dr. Christian Ahrberg, Ana Vanessa, Zeynep, Mi Jang), Professor Leon Abelman and Professor Rosanne R. Guijt. Also, many thanks to members of Magnetics. Finally, thanks to the members of Korean church in Kaiserslautern, Germany. Also, Special thanks to my parent, parents in law, my sister, my brother in law, sister in law and my nephew Sihyung Joo. From their cheering for me I can overcome obstacles during my PhD time.

I am really thanks to my lovely wife Eunmi Park and my son Junwoo Lee. With their love and encouragement, I can keep patient and keep going during my PhD time.

Eidesstattliche Versicherung

Hiermit versichere ich an Eides statt, dass ich die vorliegende Arbeit selbstständig und ohne Benutzung anderer als der angegebenen Hilfsmittel angefertigt habe. Die aus anderen Quellen oder indirekt übernommenen Daten und Konzepte sind unter Angabe der Quelle gekennzeichnet. Die Arbeit wurde bisher weder im In- noch im Ausland in gleicher oder ähnlicher Form in einem Verfahren zur Erlangung eines akademischen Grades vorgelegt.

Ort, Datum

Unterschrift

Abstract

Capillary electrophoresis (CE) is one of the most powerful separation technique in the field of analytical chemistry and biology. Applying high voltage to CE system is the most important factor to increase separation efficiencies and resolutions. In this thesis, I describe about the theoretical explanation of CE to understand the electrical and chemical properties for achieving high performance CE system, on-chip capillary electrophoresis with star shape geometry which can be used for precise sample injection method by connecting with high voltage CE. The usage of Van de Graaff generator (VDG) for CE which was used successfully higher applied voltage without joule heating problem also, natural component was separated and ultra-high separation efficiency was obtained with our high performance CE system. Moreover, in this thesis, many trials and errors were shown and described which was happened during set up the instrumentation for CE with VDG and experiment. For the further work by the result on this thesis, combination between high voltage CE system and on-chip injection method will be performed and additional system optimizing process for ultra-high performance CE system will be planed and achieved in near future.

Zusammenfassung

Kapillar-Elektrophorese (capillary electrophoresis; CE) ist eine der effektivsten Trenntechniken im Feld der analytischen Chemie und Biologie. Die Anwendung von Hochspannung für CE ist der wichtigste Faktor zur Steigerung der Auflösung und Trenn-Effizienz. In dieser Arbeit werden die theoretischen Hintergründe erläutert um die elektrischen und chemischen Eigenschaften zu verstehen und um eine Hochleistungs-CE, namentlich eine „on-chip“ Kapillar-Elektrophorese in Sternenform, welche in Verbindung mit Hochspannungs-CE zur einer präziseren Probenaufgabe führt. Ein Van de Graff Generators (VDG) wurde erfolgreich für unsere Hochleistungs-CE verwendet um Naturstoffe mit extrem hoher Effizienz voneinander zu trennen ohne dass hohe Temperaturen auftraten, entsprechend des Stromwärmegesetzes. Des Weiteren werden in dieser Arbeit nach der *Versuch-und-Irrtum* Methode der Aufbau der Instrumentalisierung, sowie der Experimentalvorgang mit der Kombination der CE und des VDG gezeigt. Weiterführende Arbeiten, basierend auf den hier gezeigten Ergebnissen, erlauben die Kombination von Hochspannungs-CE mit den „on-chip“ Probenaufgabe sowie eine Systemoptimierung welche in naher Zukunft zu einer „Ultra-Hochleistungs“-CE führen wird.

Chapter 1

Introduction

1.1 Motivation

Capillary electrophoresis (CE) is one of the most powerful separation techniques in the field of analytical chemistry [1]. Because CE can achieve very high separation efficiency and resolution [2, 3], it has been widely used for the separation of complex chemical components and biological substances, and in classical DNA sequencing since the early 1980s [4-12]. However, nowadays DNA can be amplified and analyzed very easily by PCR [13] also, small DNA fragments can be sequenced by high resolution and efficiency sequencing methods [14]. Furthermore, Western blot [15], Matrix-assisted laser desorption/ionization time of flight (MALDI-TOF) [16], and Liquid chromatography – Mass spectrometer (LC-MS) [17] are normally used to detect proteins. But, until now separation of similar or same molecular weight and size chemical compounds such as carbohydrates has a big challenge among separation scientists. Therefore, people try to establish high performance capillary electrophoresis systems. In order to obtain superior separations and/or to separate extremely complex samples, the immediate apparent solution would be to increase the applied voltage (V) [18], which would, in theory, increase the separation efficiency (N) proportionally and the separation resolution (R) by the square root of the voltage [19]. However, increasing the applied voltage brings further challenges in terms of excessive Joule heating [20-25] and electrical breakdown [26, 27]. Joule heating is generated as a result of passing current through a conductive medium and occurs inside a capillary in CE as a current passes through the background electrolyte (BGE). The heat generated inside the capillary can only be dissipated at the surface; inadequate heat dissipation will lead to a temperature gradient along the capillary radius resulting in decreased separation efficiency. In the worst case, Joule heating can interrupt the separation when bubbles caused by boiling of the BGE disrupt the electric field. Another potential pitfall of using very high voltage is electrical breakdown, which can be caused by the difference in electric potential between the inside and outside of the fused silica capillary.

By above reasons, increasing separation efficiency in CE is the most important achievement which needs to be improved or developed. If the separation efficiency can be increased dramatically by overcoming present problems and developing new methods, new paradigm of separation science

will be faced. Because, with the present technology for separation science has limitations to separate certain molecules for example, carbohydrate and isotope molecules because of low separation efficiencies and resolutions. Usually for carbohydrate separation needs to use NMR [28], HPLC [29] because it has very similar or same molecular weight and size, however those analysis method need an expensive instrumentation and complicate analysis processes. And for the separation of isotope needs more complicate, expensive and huge instrumentations and analysis tools such as huge magnetic field generator, huge cyclotron resonance accelerator, special features of guide rings and so on[30-32]. Hence, if the separation efficiency of CE can be dramatically increased by using ultra high voltage, there will be gotten the chance to extremely good analysis and separate for “extremely hard separation materials” easily, less usage of expensive instrumentation, less consumption of sample and so on. Therefore, during my PhD time, I have thought about how I can increase the separation efficiency easily by using the extremely high applied voltage for capillary electrophoresis without commercial DC power supply or in the same experimental condition (same length of separation channel, same power supply for applying voltage, same concentration buffer and so on.). Therefore, in this thesis, theoretical explanation of capillary electrophoresis, instrumentation for high voltage CE, on-chip capillary electrophoresis for precise sample injection and many trials & errors will be shown and described.

1.2 Capillary electrophoresis (CE)

CE is the separation of electrolyte in uniform electric field. Since early 1800`s electro-kinetic phenomena was observed in water by Ferdinand Frederic Reuss, Capillary electrophoresis (CE) was dramatically developed until now by a lot of researchers because of its high separation efficiencies and resolutions [33]. Also, the simplicity and convenience of the experimental setup for CE could be possible to commercialize early 1990`s and widely used for analytical chemistry, molecular biology and etc. Normally CE is performed with microscale capillary tube for the separation process, this means CE can be performed with sub-nano liter sample [34-36] for separation of electrolyte in complex chemical components and biological substances. This is one of the biggest benefit of CE and this can make a possibility to use CE in proteomics [37, 38], single cell analysis [39] and metabolomics [40-42] which need to be separated with very tiny amount of sample volume. Due to this reason, CE is one of the most promising separation technique in these days. Electrokinetic techniques can be classified such as gel electrophoresis (CGE) [43, 44], capillary isoelectric

focusing (CIEF) [45-47], capillary isotachopheresis [48-50] and micellar electrokinetic chromatography (MECK) [51-54]. In this classification, normally capillary electrophoresis can be pretended to capillary zone electrophoresis (CZE).

Analytical chemistry -A study of determination for the constituents of a chemical compound or a mixture of chemical compounds- has various applications for example, biology, environmental science, materials science and etc. In these areas, one of the most difficult problem is the analysis of complex sample. Therefore a very good separation technique is needed to separate the specific compound from the complex mixtures with high separation efficiencies and resolutions. CE is a separation method based on the electrical mobility of electrolytes in complex sample mixture by applying an electric field. A detail explanation will be given in the chapter 1.2.1. CE is a very good separation method for many practical application in analytical chemistry and molecular biology. According to the equation 1, the efficiency of CE is proportionally increased by applied voltage by high voltage power supply [55].

$$N = \frac{\mu V}{2D} \quad (1.1)$$

Where, μ is electrical mobility of electrolyte, D is diffusion coefficient of electrolyte and V is applied voltage through the capillary tube. When the applied voltage is increased also the electroosmotic flow can be increased which relate with migration time of electrolyte because of the relation between the electrolyte and electrical double layer inside of capillary tube. Therefore, in this chapter, theory of capillary electrophoresis will be discussed.

1.2.1 Electrical double layer

1.2.1.1 Helmholtz double layer

The concept of Helmholtz double layer was introduced at 1850s by Herman von Helmholtz. Helmholtz double layer constitutes two layers having opposite charges, one being negatively charged and the other positively charged [56]. The ions inside of capillary tube are formed electric double layer as like as capacitor. According to the theory of this model, when an electronic conductor (metal) dissolves continuously into liquid conductor (electrolyte), it become increasingly negative charge. Because, ions in solution are adsorbed at the surface of the capillary tube which has negative charge on surface. The excess of negative charge on the solid surface attract the positive charge

ion of the solution (Figure 1.1). The negatively charged layer is called as the inner Helmholtz layer and the positive layer is called as an outer Helmholtz layer. In this model, a potential (ψ) drop from the surface to the Outer Helmholtz layer (OHL). The potential drop is given in equation 1.2.

$$\psi = \psi_0 \left(1 - \frac{1}{X_{OHP}} X\right) \quad (1.2)$$

Where, ψ (psi) is the potential at the certain distance (X) from the surface of capillary tube and, X_{OHP} indicate the distance from the outer Helmholtz plane.

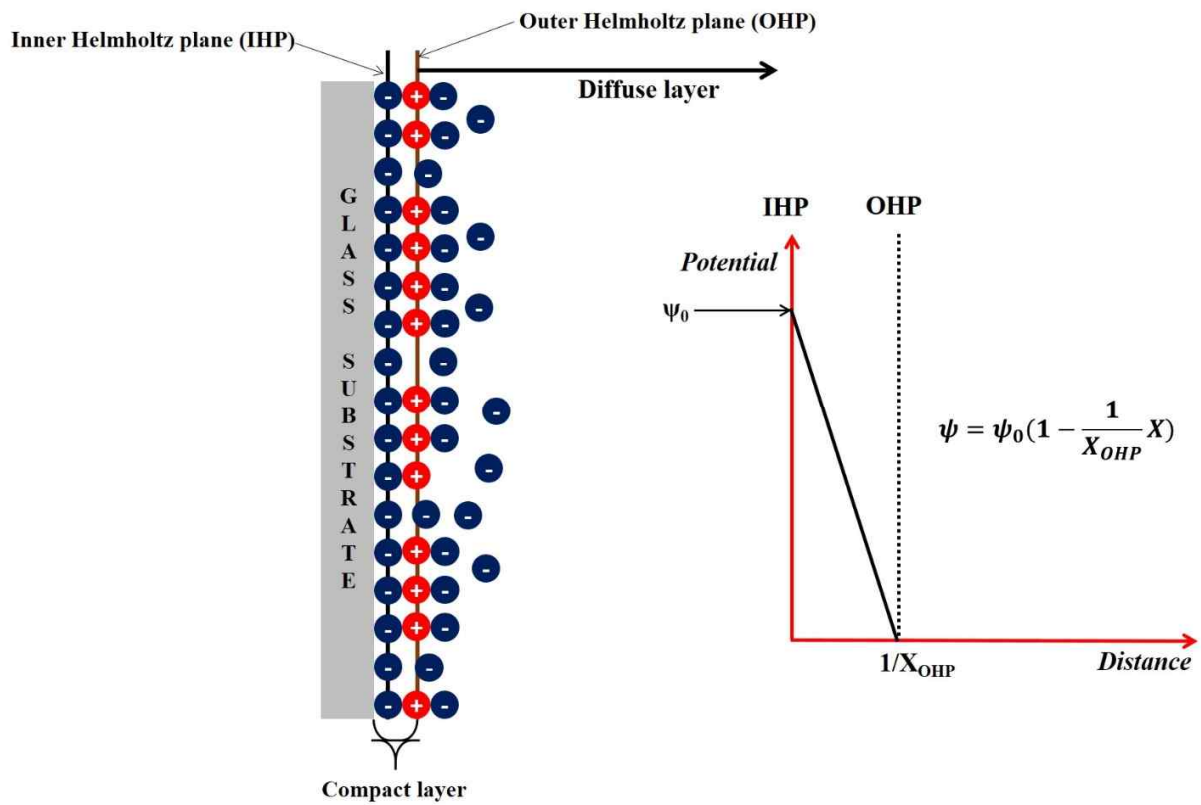


Figure 1.1: (Left) The schematic diagram of the Helmholtz double layer. (Right) Initial potential (ψ_0) at the inner Helmholtz plane (IHP) drop linearly to zero potential by the distance of outer Helmholtz plane (OHP) which comprises the absorbed anions.

1.2.1.2 Gouy-Chapman double layer

The Helmholtz model could be explained generally about the electrical double layer inside of capillary tube. However it does not consider some important factors such as diffusion of electrolyte,

thermal motion, adsorption of ions onto the surface of capillary tube, solvent/ surface interactions and etc.. Therefore, more realistic description of the electrostatic double layer was suggested by Gouy and Chapman in 1910 (Equation 1.2). For this model, the surface assumed flat, infinite and uniformly charged. According to this theory, the counter ions are considered as point charges and the Boltzmann statistical distributions are also considered near the surface of capillary tube [57]. The kinetic energy of the counter ions is the thickness of double layer which knows as the Debye length ($1/k$). The charge distribution of ions can be determined with the function of distance from the solid surface which follows Maxwell-Boltzmann statistics. The potential is dropped exponentially by the distance that is given in equation 1.3.

$$\psi = \psi_0 e^{-kX} \quad (1.3)$$

Where, ψ is the potential at the certain distance (X) from the surface of capillary tube and, k is the thickness of the Debye length.

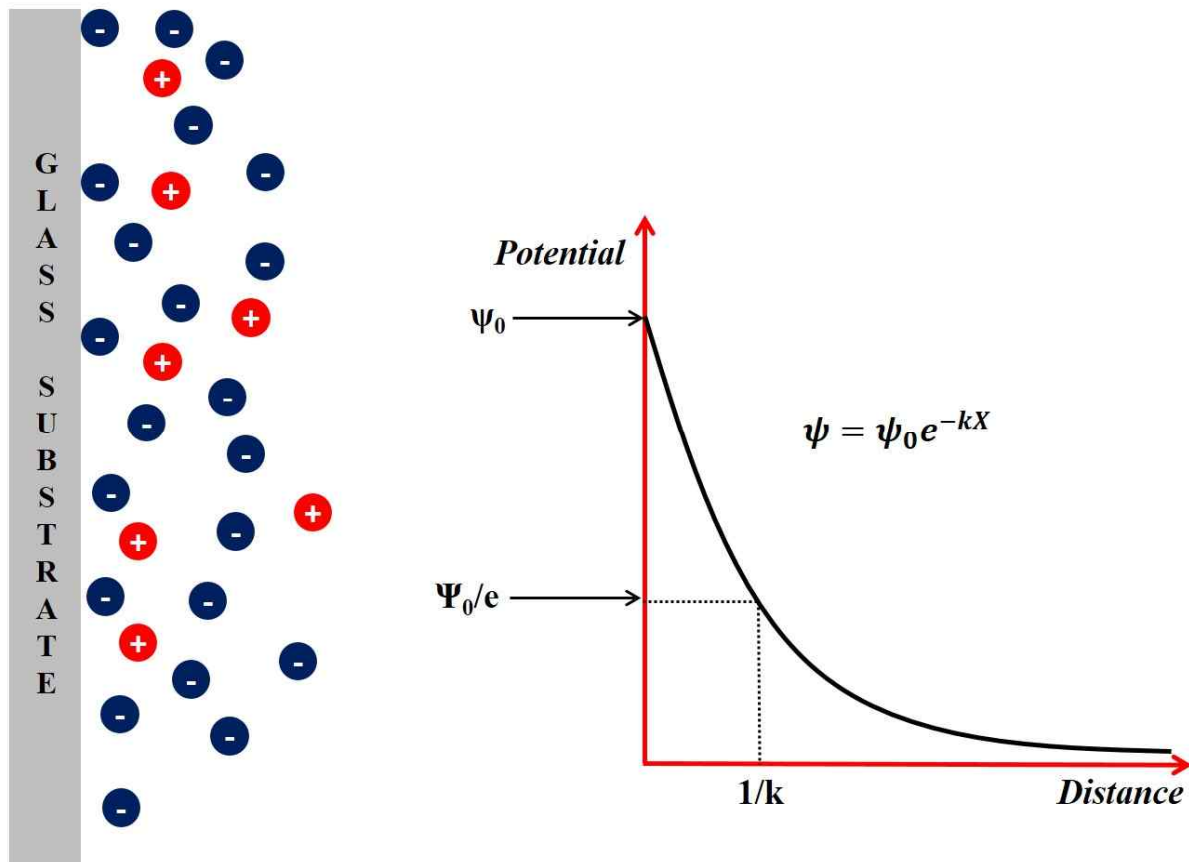


Figure 1.2. (Left) The schematic diagram of the Gouy-Chapman model. (Right) The potential is dropped exponentially and the model follows the Boltzmann statistical distribution.

1.2.1.3. Stern double layer

The Gouy-Chapman model provided a better approach of reality than the Helmholtz model, but it still has limitation of quantitative application [58]. It assumed that ions behave as point charges which cannot be behaved in reality, and it assumes that there has no physical limitation for the ion at their approach to the surface, which is cannot be exist. In 1924, Stern double layer was introduced by Otto Stern which is the combining Helmholtz layer with Gouy-Chapman layer. According to the stern motel, ions solvated to the wall as like as Helmholtz double layer, and the internal layer can be formed like Gouy-Chapman diffuse layer. Also, in this model shear plane is existed at the boundary of the diffuse layer [54]. And, we called zeta potential (ζ) or electrokinetic potential which is the potential at the shear plane (Equation 1.4).

$$\psi = \psi_0 \left(1 - \frac{1}{X_{OHP}} X\right), \psi = \psi_{st} e^{-k(X-X_{OHP})} \quad (1.4)$$

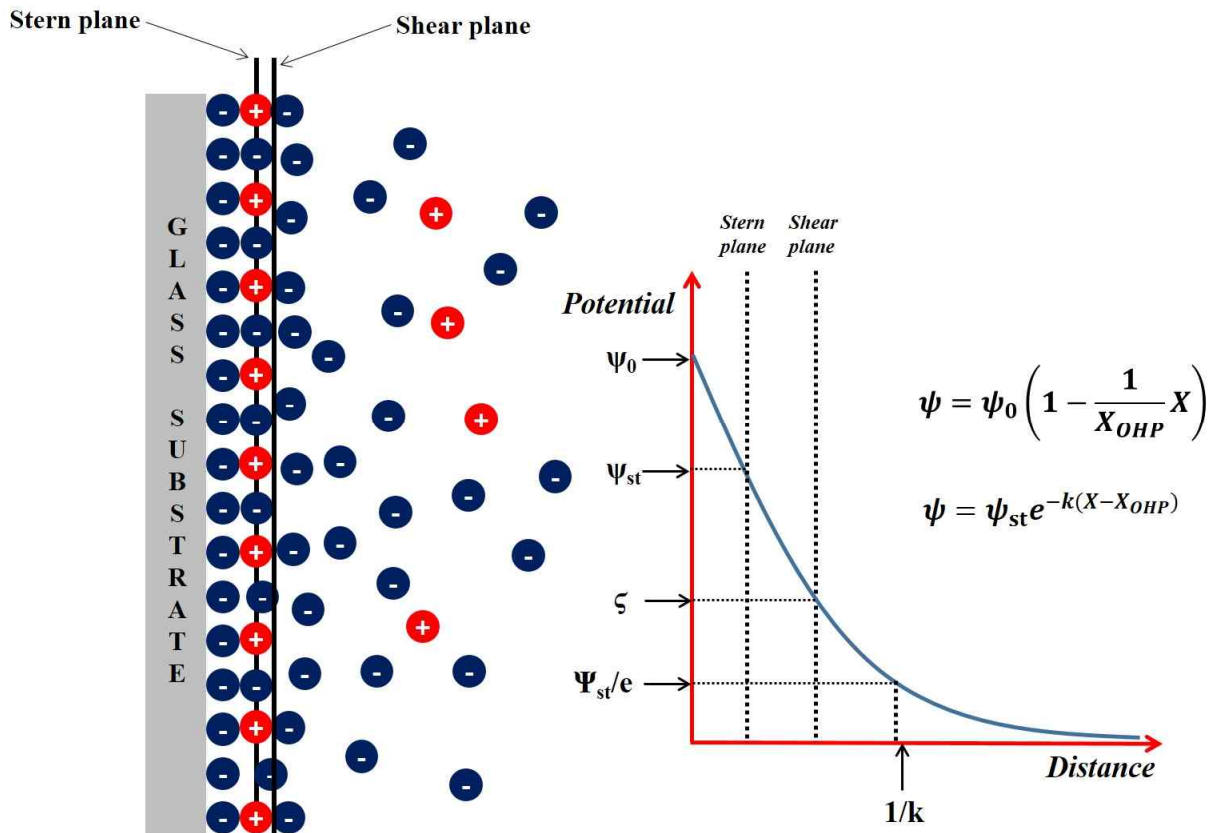


Figure 1.3: (Left) The schematic diagram of the stern model (Right) The potential changes exponentially and, follows the Boltzmann statistical distribution

1.2.1.4 Zeta potential (ζ potential)

The zeta potential (same as electrokinetic potential) is one of the important electric potential to explain electrical double layer and electrokinetic potential onto the wall of capillary. Zeta potential can be determined with the distance of location for slipping plane which has a relation in a point of the bulk fluid away from the surface of particle. The amount of zeta potential can be determined by the Debye length which represent the measurement of a charge carrier's net electrostatic effect in specific solutions [59]. But, in this thesis, Debye length will not be explained.

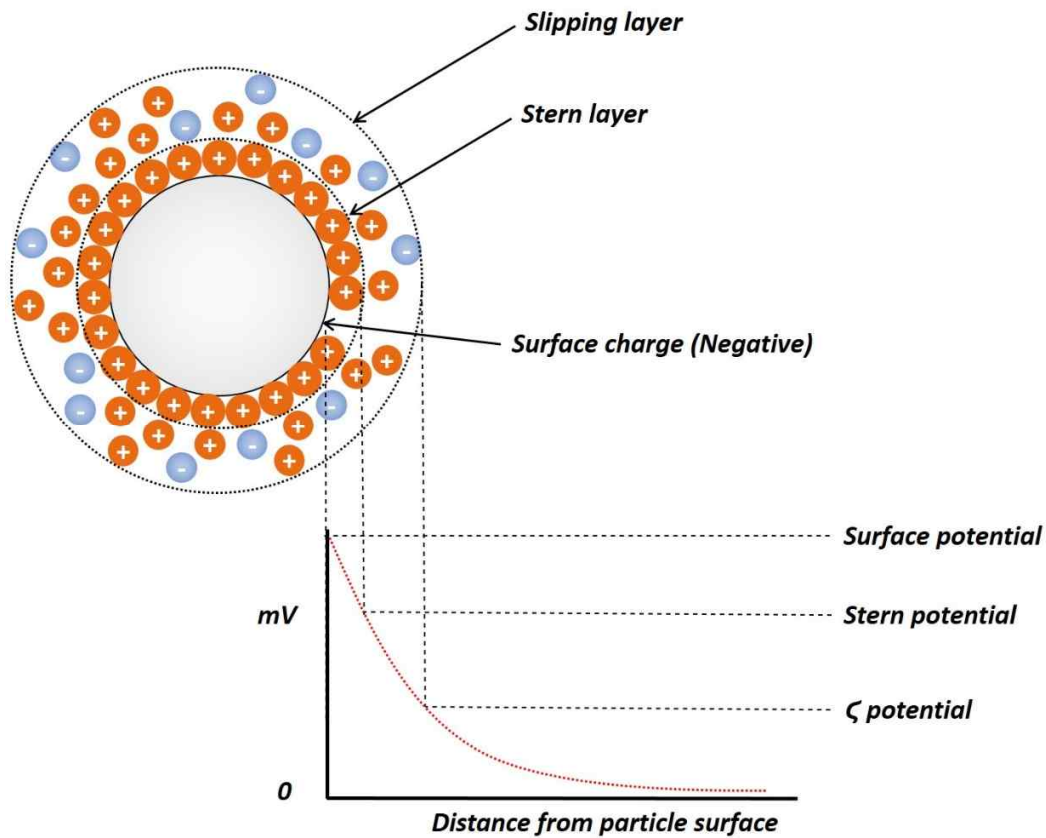


Figure 1.4: The schematic diagram of the zeta potential (ζ potential) for the dispersed particle

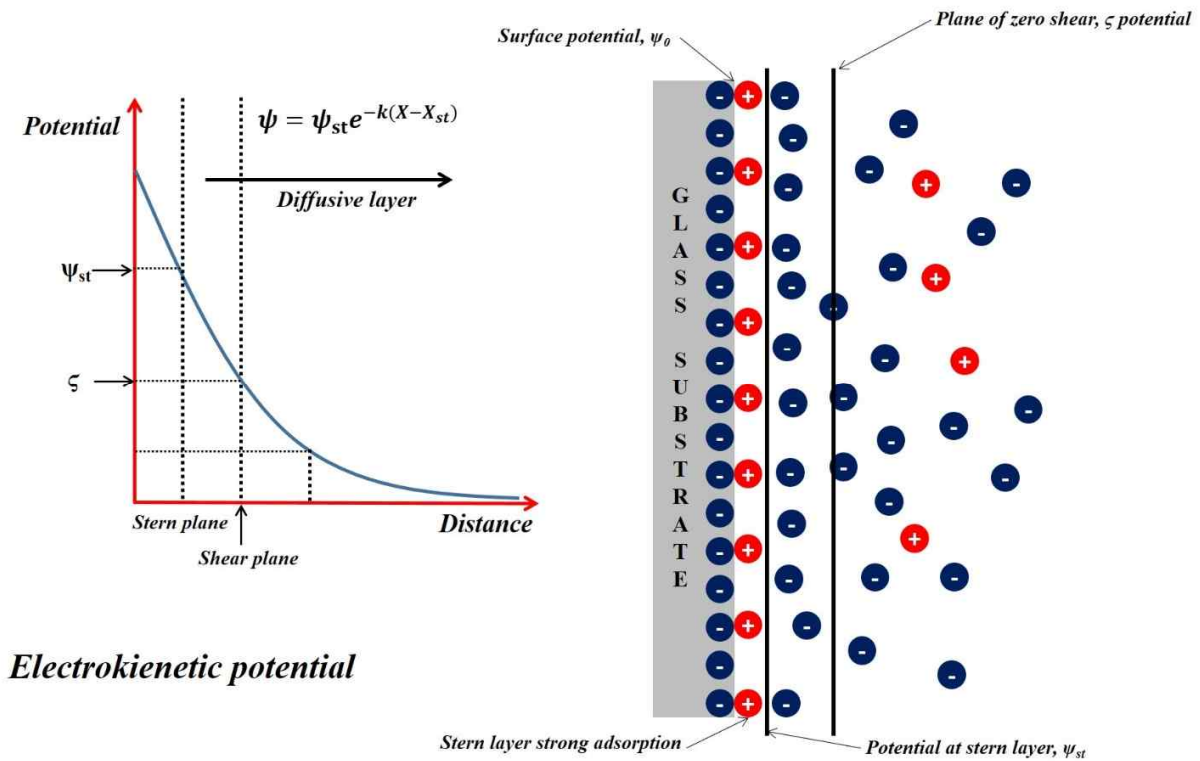


Figure 1.5: The schematic diagram of the zeta potential (electrokinetic potential) for the glass capillary

1.2.2 Electroosmotic flow (EOF)

The definition of electroosmotic flow is the motion of liquid which is driven by electric potential across a porous material such as capillary tube, microfluidic chip and so on [60, 61]. In CE, EOF is one of the most important factor to determine the total electrophoretic mobility of electrolyte and it makes predominant flow inside of capillary by forming electrical double layer onto the wall of capillary tube. When the back ground electrolyte (BGE) is injected into the capillary, positive or negative ions are linked onto the wall which is depends on the surface charge of the wall. Normally capillaries are made with fused silica which means numerous silanol (SiOH) groups cause the charge of the first layer to become negative (Inner Helmholtz plane, IHP) [62, 63]. The second layer is made up with electrolyte of BGE which are electrically attractive to the surface of capillary (Outer Helmholtz plane, OHP). This layer is not fixed so, this layer can be moved by electrical potential through the capillary, which called the diffuse layer (See fig. 1.2 Gouy-Chapman layer) or mobile layer. When an electrical potential is applied through the capillary, the diffuse layer is

pulled to one side. As the diffuse layer moves to the one side of the capillary, it drags the bulk solution along with it and, generate a flow (electroosmotic flow) of the solution forward to the cathode. As shown in figure 1.6, a plug flow can be generated by the result of applying an electrical potential, where the flow profile (green) is approximately planar, except of the variation near the electric double layer.

Electroosmotic flow

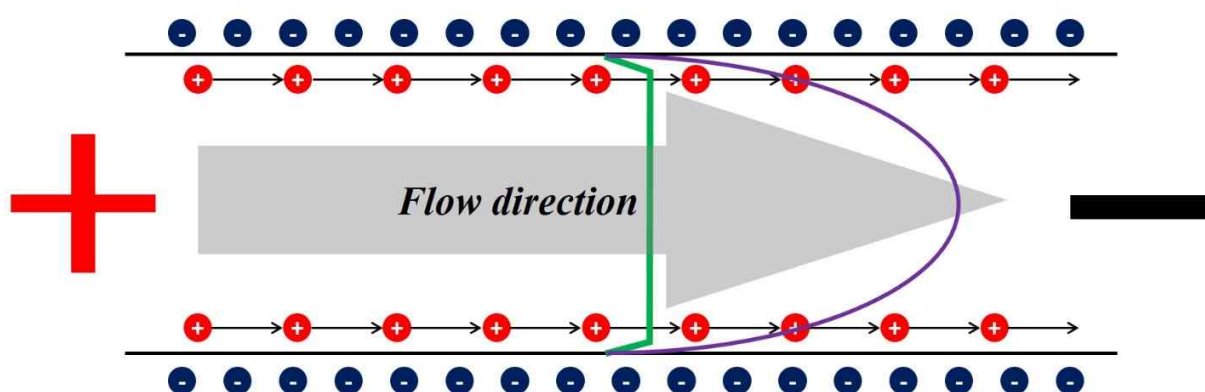


Figure 1.6: Schematic diagram of differences between electroosmotic flow (green) and parabolic flow (purple), green line represent electroosmotic flow by electrokinetic force and purple line indicate parabolic flow which can be generated by pressure driven flow.

1.2.3 Electrophoresis

Electrophoresis is one of the most powerful separation techniques in the field of analytical chemistry and biology because of its higher separation efficiency and resolution than other separation methods such as HPLC (High performance liquid chromatography) [64-66] or MALDI-TOF (Matrix Assisted Laser Desorption Ionization – Time of Flight) [67] and also relatively easy to operate and inexpensive technique. Electrophoresis is the motion of electrolyte at the uniform electric field. Especially, capillary electrophoresis is the movement of electrolyte inside of capillary tube at uniform electric field through the capillary. Total electrophoretic mobility is determined with the sum of electrophoretic mobility of electrolyte and electroosmotic flow by back ground electrolyte by applied voltage (Equation 1.5).

$$\mu_{tot} = \mu_{electrolyte} + \mu_{EOF} \quad (1.5)$$

And also, electrophoretic mobility can be expressed with the equation 1.6 which was introduced by Smoluchowski at 1903.

$$\mu_{\text{electrolyte}} = \frac{v}{E} = \frac{\epsilon_r \epsilon_0 \zeta}{\eta} \quad (1.6)$$

Where, ϵ_r is the dielectric constant of medium, ϵ_0 is the permittivity of free space, η is dynamic viscosity of the medium and ζ is the zeta potential.

Electrophoretic mobility

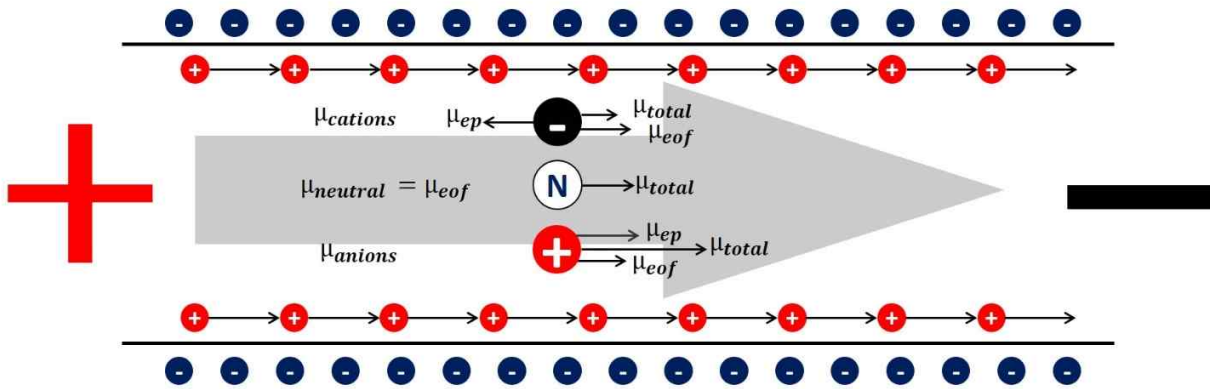


Figure 1.7: Schematic diagram of electrophoretic mobility. Total electrophoretic mobility of electrolyte can be determined the sum of the original mobility for electrolyte and electroosmotic flow.

1.2.4 Experimental setup of Capillary electrophoresis (CE)

Capillary electrophoresis is a part of electrokinetic separation methods which is performed with micron or sub-micron size of capillary tubes. Usually, CE represents capillary zone electrophoresis (CZE) however, CE also includes capillary gel electrophoresis (CGE), capillary isoelectric focusing (CIEF), capillary isotachopheresis and micellar electrokinetic chromatography (MEKC). In CE, electrolytes in specific sample can be separated by uniform electric field because of the total electrophoretic mobility which can be determined by ionic mobility of electrolyte and partitioning into an alternate phase via non-covalent interactions. The instrumentation of CE [68] is simple, usually the components of conventional CE setup (Figure 1.8) is sample and BGE reservoirs, capillary tube, electrodes, a high voltage power supply, detection system, data collection system and so on. The reservoir of BGE need to be filled with buffer solutions and also capillary tube. To apply the sample into the capillary tube, usually two different method can be used electrokinetic force injection method and pressure driven injection method. For the detection system, generally optical detection system is used such as laser induced fluorescence (LIF) system, photodiode and so on

[69-71]. Also, in these days, electrical detection system is frequently used for one of detection method [72, 73].

In capillary electrophoresis, back ground electrolyte (BGE) is the most important because, it can make a predominant flow inside of capillary tube so called, electroosmotic flow (EOF). By the sum of EOF and electrophoretic mobility of each electrolyte, the total electrophoretic mobility can be determined for electrolytes. Separated electrolytes passed detector that makes an electropherogram. According to the information of the electropherogram, separation efficiency can be calculated by the value of sigma (σ) or full width half max (FWHM).

Conventional CE system

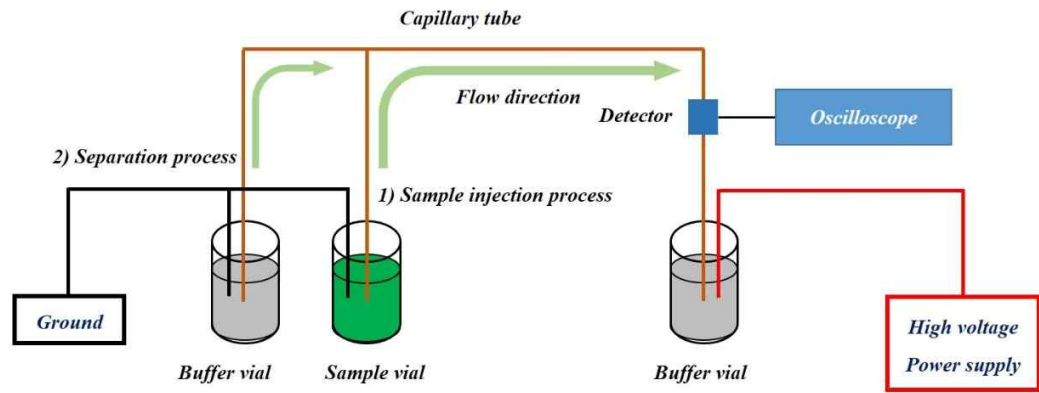


Figure 1.8: Schematic diagram of conventional CE setup. Normally, Laser induce fluorescence (LIF) system is used for detector.

1.2.5 Separation efficiency & resolutions in CE

In CE, separation efficiency and resolution represents how good separation was done. Separation efficiency is defined with the combination of applied voltage, electrical mobility, diffusion coefficient and migration time [54]. One of the most important factor to increase the separation efficiency in CE is applied voltage, according to the equation 1.1 separation efficiency is proportionally increased by applied voltage. Equation of separation efficiency can explain separation resolution in CE (Equation 1.7, 1.8).

$$N = \frac{V\mu}{2Dt_m} = \frac{L^2}{\sigma^2} = 5.54 \left(\frac{t_m}{FWHM} \right)^2 \quad (1.7)$$

$$R_s = \frac{1}{4} \left(\frac{\Delta\mu_p \sqrt{N}}{\mu_p + \mu_0} \right) = \frac{X_2 - X_1}{\frac{1}{2}(W_1 + W_2)} \quad (1.8)$$

Where, V is the applied voltage, μ is electrical mobility in separation medium, D is diffusion coefficient of analyte, t_m is migration time of electrolyte, L is length of capillary tube, σ is total variance of band broadening, μ_p is the mobility of electrolyte and N is the separation efficiency.

According to the above equation, the maximum resolution can be achieved when the electrical mobility of electrolyte has similar flow rate with electroosmotic flow in opposite direction. In addition, higher resolution can be made when the total electrical mobility is slower or the separation channel is longer (longer analysis time need to be required, Figure 1.9). Moreover, achieving higher resolution can be achieved by higher separation efficiency which can be achieved by higher applied voltage. However, separation efficiency cannot be determined only the applied voltage but also, total variance of band broadening which is the sum of band broadening by diffusion coefficient of medium, the length of injected sample plug, detection limitation and so on (Equation 1.9, 2.0) [74].

$$\sigma_{\text{total}} = \sigma_{\text{diff}}^2 + \sigma_{\text{inj}}^2 + \sigma_{\text{det}}^2 + \dots \quad (1.9)$$

$$\sigma_{\text{diff}}^2 = 2D_m t, \sigma_{\text{inj}}^2 = \frac{w^2}{12} \quad (1.10)$$

Where, D_m is diffusion coefficient of medium, t is migration time and, w is the length of injected sample plug.

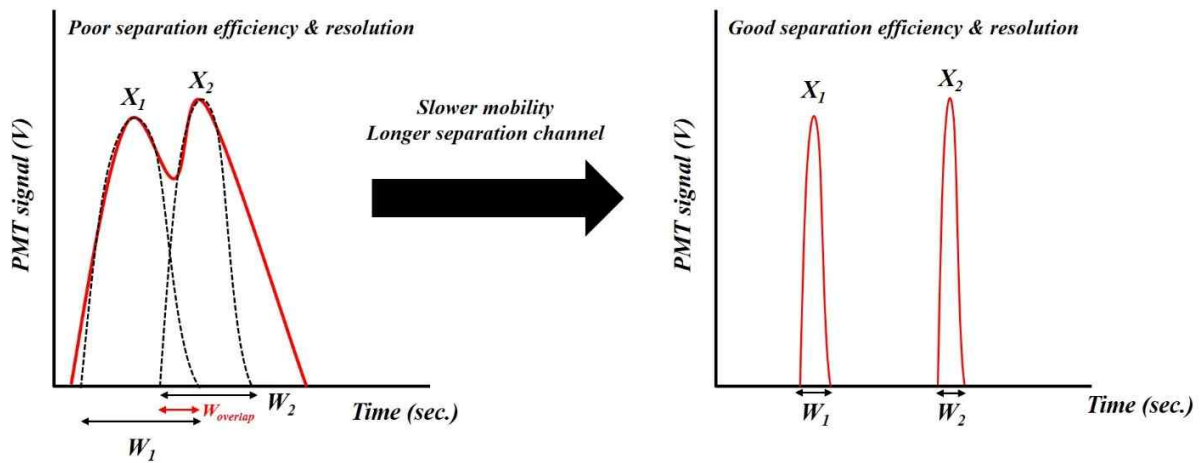


Figure 1.9: Schematic diagram for comparison of separation efficiency and resolution. Normally, separation efficiency can be achieved by higher applied voltage and the resolution can be achieved by slower total electrophoretic mobility or longer separation channel (longer analysis time).

1.2.6 Joule heating in capillary electrophoresis

Joule heating is occurred by electrical current which passes through a high resistor. When the high current flow through capillary, BGE can be heated up by the current and when the inner temperature higher than boiling point of BGE then bubble is generated inside of capillary tube (Figure 1.10). In capillary electrophoresis, radical joule heating causes changing viscosity of BGE which can make a result to change the electric mobility of electrolyte across the capillary tubes. And also, changing the temperature inside of capillary can be caused the changing ionization of buffer which so called self-ionization or auto dissociation that can make a changing of pK_a value of electrolyte [2, 19-24, 75, 76].

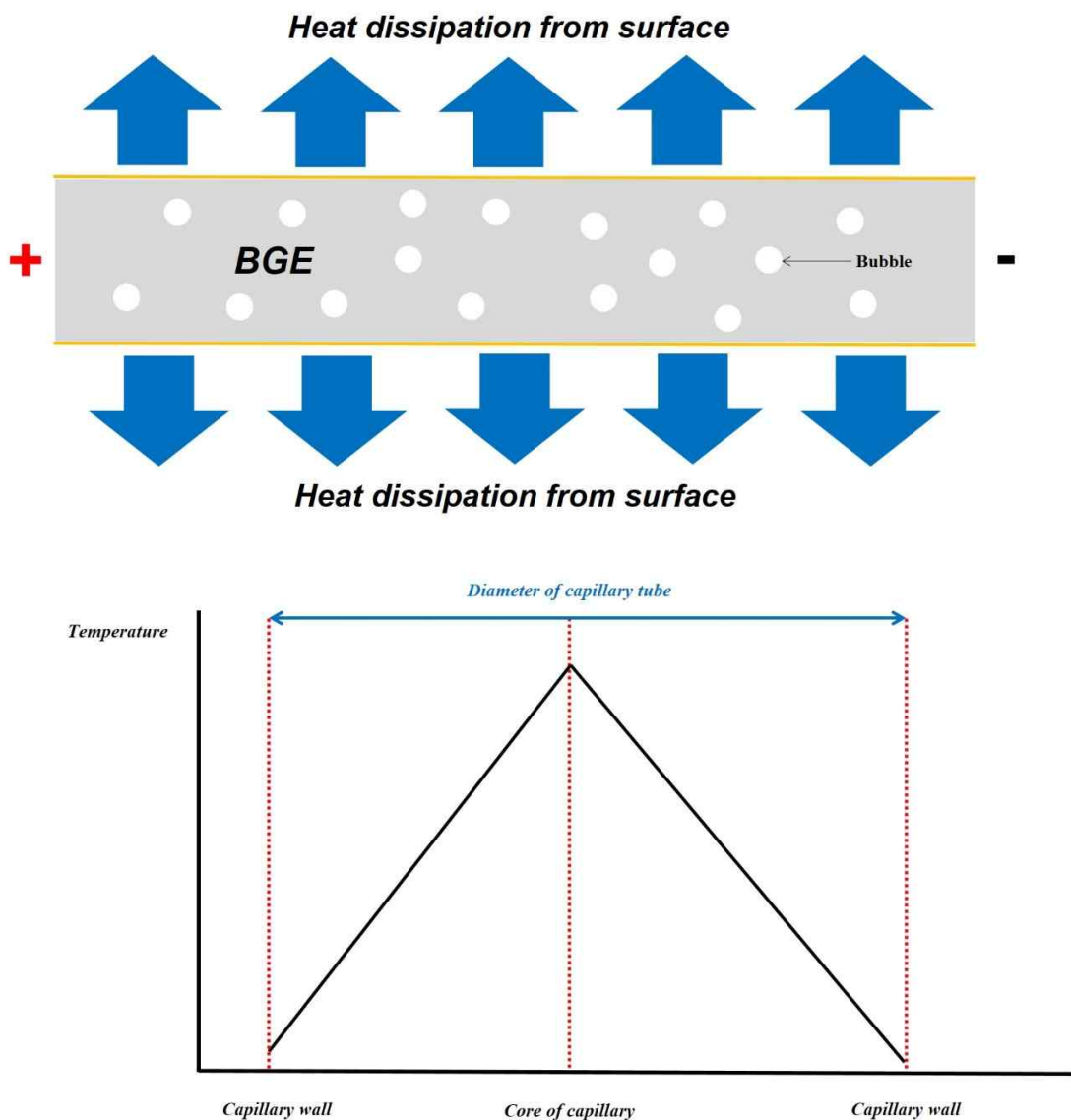


Figure 1.10:(upper) Schematic diagram of joule heating phenomena in capillary electrophoresis. When the temperature at inside of capillary tube than the boiling point of BGE by current, small bubble is generated and block the capillary (or, become an obstacle by smaller bubble) tube. (bottom) heat gradient inside of capillary tube, the temperature at the core of capillary is the highest because of the heat dissipation at capillary wall.

When the joule heating is occurred during separation process, BGE can be boiled by heating and made a bubble inside of the capillary tube. This can make no separation of electrolyte and lower separation efficiency and resolution of the result.

1.2.7 Electrical breakdown

Electrical breakdown (same as dielectric breakdown) is occurred by a reduction of an electrical insulator when the voltage applied across it. So, the corona discharge is occurred through air when the electrical potential is reached 3.0MV/m (30kV/cm). Also, dielectric strength of fused silica capillary tube is 25MV/m to 40MV/m so, in case of 50 μ m ID and 360 μ m OD capillary can be broken 4.1kV/165 μ m to 6.6kV/165 μ m. In CE, electrical breakdown need to be considered one of the most important parameter to be overcome for stable separation system with high voltage. So, people are try to put their system to vacuum chamber, oil tank or high pressure of gas chamber etc. [77, 78]. In this thesis, some problems by electrical break down will be describe and the solution will be suggested at chapter 6.

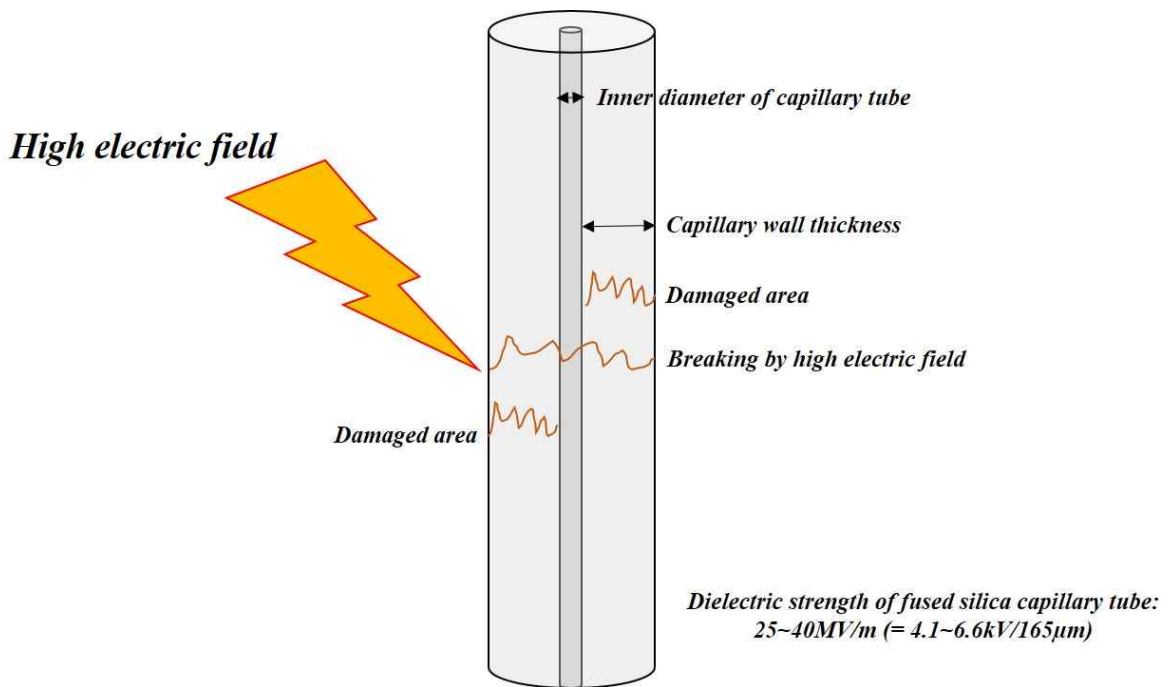
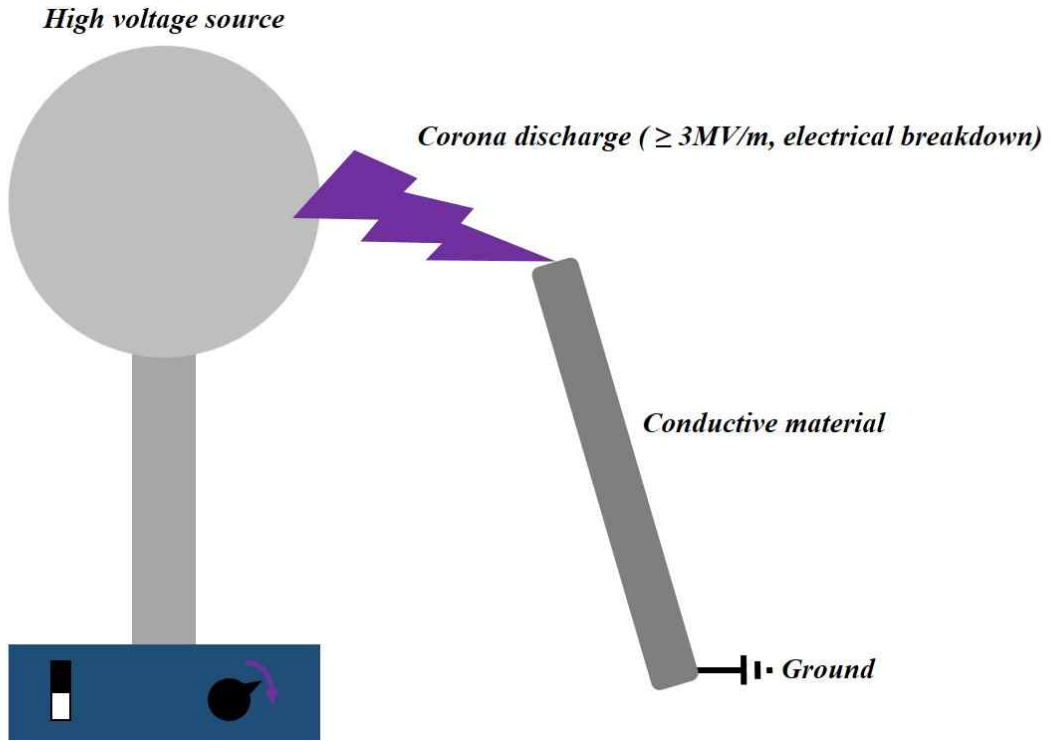
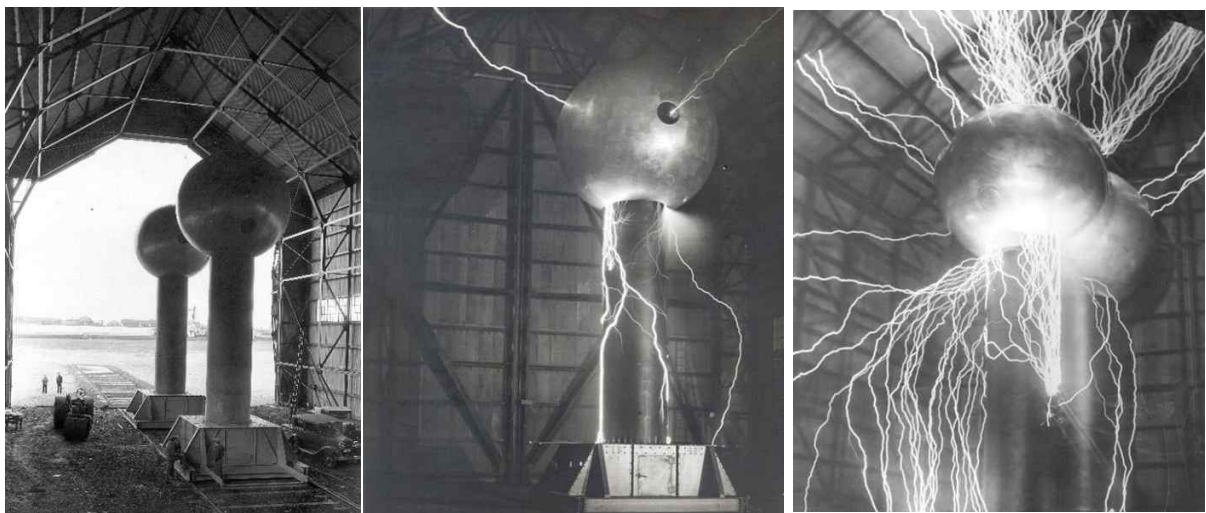


Figure 1.11: (Upper) Schematic diagram of Corona discharge which can be occurred by high electric field by Van de Graaff generator. (Bottom) Schematic diagram of electrical breakdown for fused silica capillary tubes by high electric field.

1.3 Van de Graaff Generator (VDG)

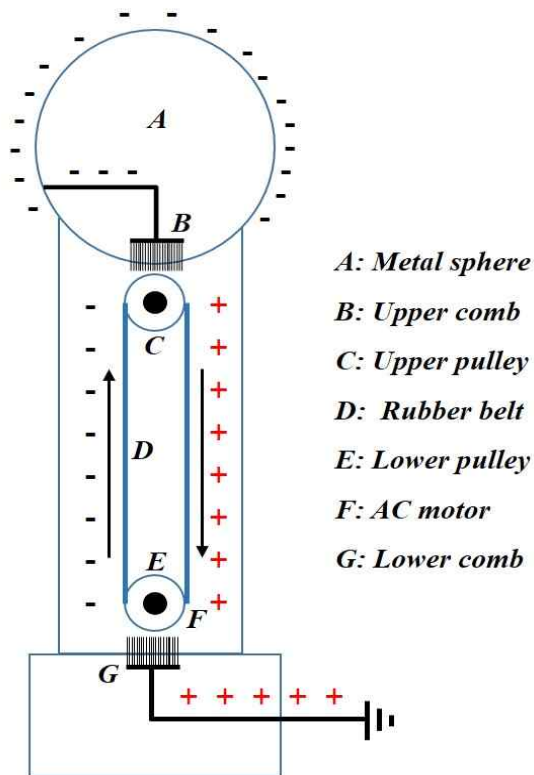
1.3.1 Classic Van de Graaff Generator

Van de graaff generator (VDG) was introduced by Robert J. Van de Graaff who is American physicist in 1929 [79,80] (figure 1.11). VDG is a constant current generator which is generated by the static electricity between two materials of pulleys (Figure 1.12). VDG generate very high electric potentials with very low constant current ($10\mu\text{A} \sim 60\mu\text{A}$) therefore, it has been used for physics class in middle school and high school because of its safeness. By the development of material science in these days, VDG can be achieved to reach 5 megavolts, doesn't need a huge construction like early stage of the equipment and also can be purchased very easily (500~600USD for 350~900kV) in market. After invented the VDG, it was developed to tandem Van de Graaff accelerator which has two different charged dome in parallel and this could generate up to 14MV at 1970s that was used in a tank of high pressure SF_6 which prevent sparking by trapping electrons for studying of light ion direct nuclear reactions [81,82]. After that, VDG was developed and used again to pelletron generator which is replaced rubber or fabric belt to chain of short conductive rods that were connected by insulating links.



Illustrations from "Progress Report on the M.I.T. High-Voltage Generator at Round Hill," by K. T. Compton, L. C. Van Atta, and R. J. Van de Graaff, December 12, 1933

Figure 1.12: Early stage of Van de graaff generator in 1933 by Robert J. Van de Graaff at MIT.



- A: Metal sphere*
- B: Upper comb*
- C: Upper pulley*
- D: Rubber belt*
- E: Lower pulley*
- F: AC motor*
- G: Lower comb*



Figure 1.13: (Left) Schematic diagram of Van de Graaff generator. Major components of VDG are two pulleys, two combs and rubber belt which can be driven by AC motor. Metal sphere can be a capacitance for electrons and it makes very high electric potentials. (Right) commercial VDG which can generate up to 350kV with 10 μ A constant current.

1.3.2 Pelletron accelerator

Pelletron (Figure 1.16) is the electrostatic particle accelerator which was developed in mid of 1960s and it has similar mechanism with classic Van de Graaff generator. However, pelletron needs more instrumentation to make higher and stable voltage or current generation such as high power supplies, inductors and suppressors. During the charging process, negatively charged inductor pushed electrons off from the pellet while the drive pulley is contacted with the ground. Only positive charges can be delivered to terminal shell by the chain and also this process is the same with negative charging mode. . With this charging process, pelletron accelerator can deliver

100~200 μA to high voltage terminal with very high voltage stability, no electrical breakdown (no corona charge in the air), high efficiency and also it has long lifetime chain (around 50,000 hours).

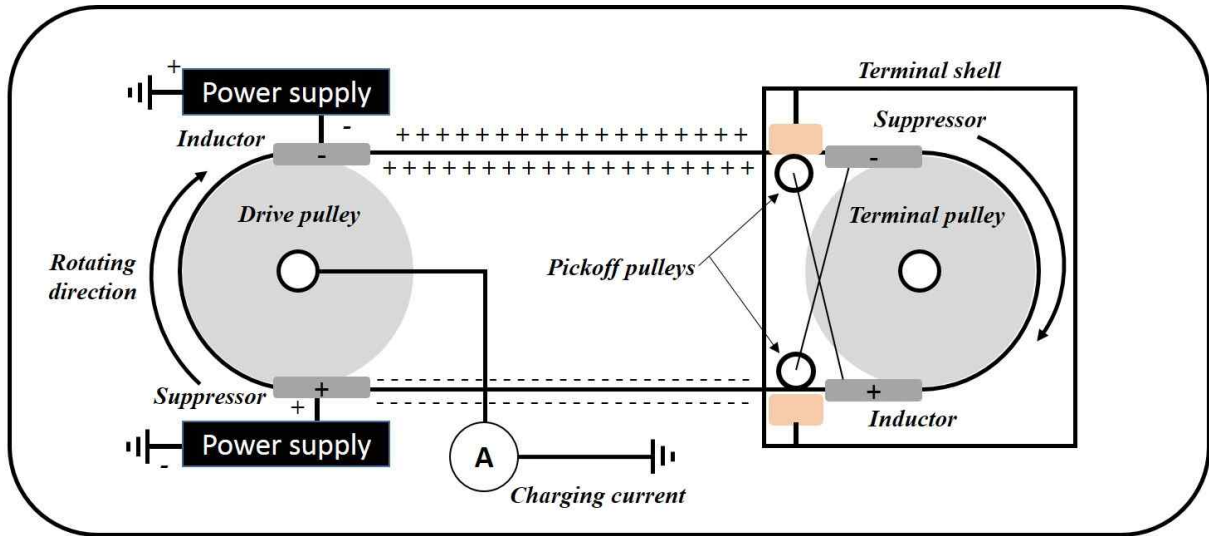


Figure 1.14: Schematic diagram of Pelletron accelerator which has similar mechanism with classic Van de Graaff generator. Pelletron consists two pulleys (drive pulley and terminal pulley), 2 high power supply which need to generate high current to metal pellets-nylon links and Terminal shell.

1.4 Laser induced fluorescence (LIF) system

LIF system was reported first time in 1968 by Zare and coworkers. LIF system is one of the most sensitive optical detection system which is used very frequently for the detection method of capillary electrophoresis. Figure 1.14 shows home build LIF system that consists with excitation laser light source (470nm), band path filter for excitation and emission light, dichroic mirror and photomultiplier tube. Main advantage of LIF system for CE is easy to modify for certain application and short response time. But, the needs of fluorescence labelling for sample is the limitation of LIF system. But, the most suitable detection method for high voltage capillary electrophoresis is LIF system because, other detection method for example, electric detection method cannot be used under high voltage CE because of high electric field from high applied voltage that can make a problem to detect separated sample precisely.

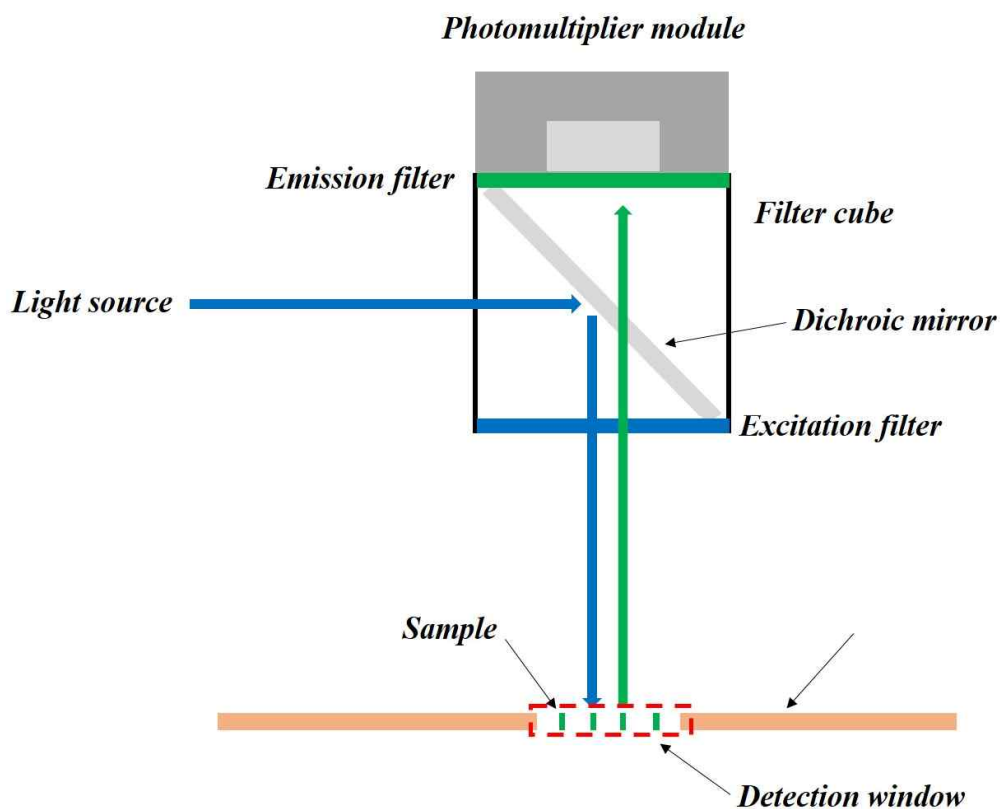


Figure 1.15: Schematic diagram of laser induced fluorescence (LIF) system. Which has 470nm excitation laser source, excitation filter, emission filter for 520nm wavelength, dichroic mirror and photomultiplier module.

1.5 References

1. Ewing, A.G., R.A. Wallingford, and T.M. Olefirowicz, *Capillary electrophoresis*. Analytical Chemistry, 1989. **61**(4): p. 292A-303A.
2. Palonen, S., et al., *Nonaqueous capillary electrophoresis with alcoholic background electrolytes: Separation efficiency under high electrical field strengths*. ELECTROPHORESIS, 2002. **23**(3): p. 393-399.
3. Palonen, S., et al., *Peak dispersion and contributions to plate height in nonaqueous capillary electrophoresis at high electric field strengths: Propanol as background electrolyte solvent*. ELECTROPHORESIS, 2003. **24**(10): p. 1565-1576.
4. Woolley, A.T. and R.A. Mathies, *Ultra-High-Speed DNA Sequencing Using Capillary Electrophoresis Chips*. Analytical Chemistry, 1995. **67**(20): p. 3676-3680.
5. Woolley, A.T., et al., *Functional Integration of PCR Amplification and Capillary Electrophoresis in a Microfabricated DNA Analysis Device*. Analytical Chemistry, 1996. **68**(23): p. 4081-4086.
6. Pedersen-Bjergaard, S. and K.E. Rasmussen, *Liquid–Liquid–Liquid Microextraction for Sample Preparation of Biological Fluids Prior to Capillary Electrophoresis*. Analytical Chemistry, 1999. **71**(14): p. 2650-2656.
7. Hutterer, K.M., et al., *High resolution of oligosaccharide mixtures by ultrahigh voltage micellar electrokinetic capillary chromatography*. Journal of Chromatography B: Biomedical Sciences and Applications, 2000. **745**(2): p. 365-372.
8. Hutterer, K.M. and J.W. Jorgenson, *Separation of hyaluronic acid by ultrahigh-voltage capillary gel electrophoresis*. ELECTROPHORESIS, 2005. **26**(10): p. 2027-2033.
9. James, M.H., *Protein Analysis by Capillary Electrophoresis*, in *Handbook of Capillary and Microchip Electrophoresis and Associated Microtechniques, Third Edition*. 2007, CRC Press. p. 75-107.
10. András, G. and S. Eszter, *Capillary Electrophoresis of Nucleic Acids*, in *Handbook of Capillary and Microchip Electrophoresis and Associated Microtechniques, Third Edition*. 2007, CRC Press. p. 227-250.
11. Julia, K., *Analysis of Carbohydrates by Capillary Electrophoresis*, in *Handbook of Capillary and Microchip Electrophoresis and Associated Microtechniques, Third Edition*. 2007, CRC Press. p. 251-294.

12. Timothy, D.V. and J.I. Haleem, *The Coupling of Capillary Electrophoresis and Mass Spectrometry in Proteomics*, in *Handbook of Capillary and Microchip Electrophoresis and Associated Microtechniques, Third Edition*. 2007, CRC Press. p. 295-303.
13. Woolley, A.T., et al., Functional Integration of PCR Amplification and Capillary Electrophoresis in a Microfabricated DNA Analysis Device. *Analytical Chemistry*, 1996. 68(23): p. 4081-4086.
14. Jensen, P.K., et al., Probing Proteomes Using Capillary Isoelectric Focusing-Electrospray Ionization Fourier Transform Ion Cyclotron Resonance Mass Spectrometry. *Analytical Chemistry*, 1999. 71(11): p. 2076-2084.
15. Ghaemmaghami, S., et al., Global analysis of protein expression in yeast. *Nature*, 2003. 425(6959): p. 737-741.
16. Vorm, O., P. Roepstorff, and M. Mann, Improved Resolution and Very High Sensitivity in MALDI TOF of Matrix Surfaces Made by Fast Evaporation. *Analytical Chemistry*, 1994. 66(19): p. 3281-3287.
17. Meiring, H.D., et al., Nanoscale LC-MS(n): technical design and applications to peptide and protein analysis. *Journal of Separation Science*, 2002. 25(9): p. 557-568.
18. Jorgenson, J.W. and K.D. Lukacs, *Zone electrophoresis in open-tubular glass capillaries*. *Analytical Chemistry*, 1981. 53(8): p. 1298-1302.
19. Jorgenson, J.W. and K.D. Lukacs, *Capillary zone electrophoresis*. *Science*, 1983.
20. Palonen, S., et al., *Peak dispersion and contributions to plate height in nonaqueous capillary electrophoresis at high electric field strengths: Ethanol as background electrolyte solvent*. *ELECTROPHORESIS*, 2004. 25(2): p. 344-354.
21. Xuan, X. and D. Li, *Analytical study of Joule heating effects on electrokinetic transportation in capillary electrophoresis*. *Journal of Chromatography A*, 2005. 1064(2): p. 227-237.
22. Palonen, S., M. Jussila, and M.-L. Riekkola, *Effect of initial voltage ramp on separation efficiency in non-aqueous capillary electrophoresis with ethanol as background electrolyte solvent*. *Journal of Chromatography A*, 2005. 1068(1): p. 107-114.
23. Evenhuis, C.J., et al., *Internal electrolyte temperatures for polymer and fused-silica capillaries used in capillary electrophoresis*. *ELECTROPHORESIS*, 2005. 26(22): p. 4333-4344.

24. Xuan, X., G. Hu, and D. Li, *Joule heating effects on separation efficiency in capillary zone electrophoresis with an initial voltage ramp*. ELECTROPHORESIS, 2006. **27**(16): p. 3171-3180.
25. Evenhuis, C.J. and P.R. Haddad, *Joule heating effects and the experimental determination of temperature during CE*. ELECTROPHORESIS, 2009. **30**(5): p. 897-909.
26. Effenhauser, C.S., G.J.M. Bruin, and A. Paulus, *Integrated chip-based capillary electrophoresis*. ELECTROPHORESIS, 1997. **18**(12-13): p. 2203-2213.
27. Monnig, C.A. and J.W. Jorgenson, *On-column sample gating for high-speed capillary zone electrophoresis*. Analytical Chemistry, 1991. **63**(8): p. 802-807.
28. Balakshin, M., et al., *Quantification of lignin-carbohydrate linkages with high-resolution NMR spectroscopy*. Planta, 2011. **233**(6): p. 1097-1110.
29. Wannet, W.J.B., et al., *HPLC Detection of Soluble Carbohydrates Involved in Mannitol and Trehalose Metabolism in the Edible Mushroom Agaricus bisporus*. Journal of Agricultural and Food Chemistry, 2000. **48**(2): p. 287-291.
30. Mazur, T.R., B. Klappauf, and M.G. Raizen, *Demonstration of magnetically activated and guided isotope separation*. Nat Phys, 2014. **10**(8): p. 601-605.
31. Mark, G.R. and K. Bruce, *Magnetically activated and guided isotope separation*. New Journal of Physics, 2012. **14**(2): p. 023059.
32. Noh, H.R., et al., *Isotope separation in a magneto-optical trap*. Review of Scientific Instruments, 1996. **67**(4): p. 1431-1433.
33. Vesterberg, O., *History of electrophoretic methods*. Journal of Chromatography A, 1989. **480**: p. 3-19.
34. Taylor, J.A. and E.S. Yeung, *Axial-beam laser-excited fluorescence detection in capillary electrophoresis*. Analytical Chemistry, 1992. **64**(15): p. 1741-1744.
35. Waldron, K.C. and N.J. Dovichi, *Sub-femtomole determination of phenylthiohydantoin-amino acids: capillary electrophoresis and thermo-optical detection*. Analytical Chemistry, 1992. **64**(13): p. 1396-1399.
36. Fang, Q., et al., *Sequential injection sample introduction microfluidic-chip based capillary electrophoresis system*. Analytica Chimica Acta, 1999. **390**(1-3): p. 27-37.
37. Pelzing, M. and C. Neusüß, *Separation techniques hyphenated to electrospray-tandem mass spectrometry in proteomics: Capillary electrophoresis versus nanoliquid chromatography*. ELECTROPHORESIS, 2005. **26**(14): p. 2717-2728.

38. Simpson, D.C. and R.D. Smith, *Combining capillary electrophoresis with mass spectrometry for applications in proteomics*. ELECTROPHORESIS, 2005. **26**(7-8): p. 1291-1305.
39. Stuart, J.N. and J.V. Sweedler, *Single-cell analysis by capillary electrophoresis*. Analytical and Bioanalytical Chemistry, 2003. **375**(1): p. 28-29.
40. Monton, M.R.N. and T. Soga, *Metabolome analysis by capillary electrophoresis–mass spectrometry*. Journal of Chromatography A, 2007. **1168**(1–2): p. 237-246.
41. Soga, T., et al., *Metabolomic Profiling of Anionic Metabolites by Capillary Electrophoresis Mass Spectrometry*. Analytical Chemistry, 2009. **81**(15): p. 6165-6174.
42. Soga, T., et al., *Quantitative Metabolome Analysis Using Capillary Electrophoresis Mass Spectrometry*. Journal of Proteome Research, 2003. **2**(5): p. 488-494.
43. Southern, E.M., *Detection of specific sequences among DNA fragments separated by gel electrophoresis*. Journal of Molecular Biology, 1975. **98**(3): p. 503-517.
44. Orita, M., et al., *Detection of polymorphisms of human DNA by gel electrophoresis as single-strand conformation polymorphisms*. Proceedings of the National Academy of Sciences, 1989. **86**(8): p. 2766-2770.
45. Rodriguez-Diaz, R., T. Wehr, and M. Zhu, *Capillary isoelectric focusing*. ELECTROPHORESIS, 1997. **18**(12-13): p. 2134-2144.
46. Jensen, P.K., et al., *Probing Proteomes Using Capillary Isoelectric Focusing–Electrospray Ionization Fourier Transform Ion Cyclotron Resonance Mass Spectrometry*. Analytical Chemistry, 1999. **71**(11): p. 2076-2084.
47. Zhu, M., R. Rodriguez, and T. Wehr, *Optimizing separation parameters in capillary isoelectric focusing*. Journal of Chromatography A, 1991. **559**(1): p. 479-488.
48. Baumann, G. and A. Chrambach, *A highly crosslinked, transparent polyacrylamide gel with improved mechanical stability for use in isoelectric focusing and isotachopheresis*. Analytical Biochemistry, 1976. **70**(1): p. 32-38.
49. Shihabi, Z.K., *Transient pseudo-isotachopheresis for sample concentration in capillary electrophoresis*. ELECTROPHORESIS, 2002. **23**(11): p. 1612-1617.
50. Kaniansky, D. and J. Marák, *On-line coupling of capillary isotachopheresis with capillary zone electrophoresis*. Journal of Chromatography A, 1990. **498**: p. 191-204.
51. Koji, O. and T. Shigeru, *Micellar electrokinetic chromatography*. Molecular Biotechnology, 1998. **9**(3): p. 253-271.

52. Nishi, H., T. Fukuyama, and S. Terabe, *Chiral separation by cyclodextrin-modified micellar electrokinetic chromatography*. Journal of Chromatography A, 1991. **553**: p. 503-516.
53. Terabe, S., et al., *Cyclodextrin-modified micellar electrokinetic chromatography: Separation of hydrophobic and enantiomeric compounds*. Journal of Chromatography A, 1993. **636**(1): p. 47-55.
54. Terabe, S., et al., *Separation of highly hydrophobic compounds by cyclodextrin-modified micellar electrokinetic chromatography*. Journal of Chromatography A, 1990. **516**(1): p. 23-31.
55. Lukacs, K.D. and J.W. Jorgenson, *Capillary zone electrophoresis: Effect of physical parameters on separation efficiency and quantitation*. Journal of High Resolution Chromatography, 1985. **8**(8): p. 407-411.
56. Conway, B.E., J.O.M. Bockris, and I.A. Ammar, *The dielectric constant of the solution in the diffuse and Helmholtz double layers at a charged interface in aqueous solution*. Transactions of the Faraday Society, 1951. **47**(0): p. 756-766.
57. Bolt, G.H., *Analysis of the validity of the Gouy-Chapman theory of the electric double layer*. Journal of Colloid Science, 1955. **10**(2): p. 206-218.
58. Torrie, G.M. and J.P. Valneau, *Electrical double layers. 4. Limitations of the Gouy-Chapman theory*. The Journal of Physical Chemistry, 1982. **86**(16): p. 3251-3257.
59. Yates, D.E., S. Levine, and T.W. Healy, *Site-binding model of the electrical double layer at the oxide/water interface*. Journal of the Chemical Society, Faraday Transactions 1: Physical Chemistry in Condensed Phases, 1974. **70**(0): p. 1807-1818.
60. Kirby, B.J. and E.F. Hasselbrink, *Zeta potential of microfluidic substrates: 1. Theory, experimental techniques, and effects on separations*. ELECTROPHORESIS, 2004. **25**(2): p. 187-202.
61. Rathore, A.S. and C. Horváth, *Capillary electrochromatography: theories on electroosmotic flow in porous media*. Journal of Chromatography A, 1997. **781**(1): p. 185-195.
62. Levine, S. and G.H. Neale, *The prediction of electrokinetic phenomena within multiparticle systems. I. Electrophoresis and electroosmosis*. Journal of Colloid and Interface Science, 1974. **47**(2): p. 520-529.

63. Schwer, C. and E. Kenndler, *Electrophoresis in fused-silica capillaries: the influence of organic solvents on the electroosmotic velocity and the zeta potential*. Analytical Chemistry, 1991. **63**(17): p. 1801-1807.
64. Gilges, M., M.H. Kleemiss, and G. Schomburg, *Capillary Zone Electrophoresis Separations of Basic and Acidic Proteins Using Poly(vinyl alcohol) Coatings in Fused Silica Capillaries*. Analytical Chemistry, 1994. **66**(13): p. 2038-2046.
65. Bridle, P. and C. García-Viguera, *Analysis of anthocyanins in strawberries and elderberries. A comparison of capillary zone electrophoresis and HPLC*. Food Chemistry, 1997. **59**(2): p. 299-304.
66. Lange, J., K. Thomas, and C. Wittmann, *Comparison of a capillary electrophoresis method with high-performance liquid chromatography for the determination of biogenic amines in various food samples*. Journal of Chromatography B, 2002. **779**(2): p. 229-239.
67. González-Peñas, E., et al., *Comparison between capillary electrophoresis and HPLC-FL for ochratoxin A quantification in wine*. Food Chemistry, 2006. **97**(2): p. 349-354.
68. Kazmaier, T., et al., *Quantitative analysis of malto-oligosaccharides by MALDI-TOF mass spectrometry, capillary electrophoresis and anion exchange chromatography*. Fresenius' Journal of Analytical Chemistry, 1998. **361**(5): p. 473-478.
69. Felhofer, J.L., L. Blanes, and C.D. Garcia, *Recent developments in instrumentation for capillary electrophoresis and microchip-capillary electrophoresis*. ELECTROPHORESIS, 2010. **31**(15): p. 2469-2486.
70. He, L., M.J. Natan, and C.D. Keating, *Surface-Enhanced Raman Scattering: A Structure-Specific Detection Method for Capillary Electrophoresis*. Analytical Chemistry, 2000. **72**(21): p. 5348-5355.
71. Schwartz, H.E. and K.J. Ulfelder, *Capillary electrophoresis with laser-induced fluorescence detection of PCR fragments using thiazole orange*. Analytical Chemistry, 1992. **64**(15): p. 1737-1740.
72. Lacroix, M., et al., *Laser-induced fluorescence detection schemes for the analysis of proteins and peptides using capillary electrophoresis*. ELECTROPHORESIS, 2005. **26**(13): p. 2608-2621.
73. Zemann, A.J., et al., *Contactless Conductivity Detection for Capillary Electrophoresis*. Analytical Chemistry, 1998. **70**(3): p. 563-567.

74. Sloss, S. and A.G. Ewing, *Improved method for end-column amperometric detection for capillary electrophoresis*. Analytical Chemistry, 1993. **65**(5): p. 577-581.
75. Effenhauser, C.S., et al., *High-Speed Separation of Antisense Oligonucleotides on a Micromachined Capillary Electrophoresis Device*. Analytical Chemistry, 1994. **66**(18): p. 2949-2953.
76. Chen, G., et al., *Influence of moderate Joule heating on electroosmotic flow velocity, retention, and efficiency in capillary electrochromatography*. Journal of Chromatography A, 2004. **1044**(1-2): p. 287-294.
77. Swinney, K. and D.J. Bornhop, *Quantification and evaluation of Joule heating in on-chip capillary electrophoresis*. ELECTROPHORESIS, 2002. **23**(4): p. 613-620.
78. Hutterer, K.M. and J.W. Jorgenson, *Ultrahigh-Voltage Capillary Zone Electrophoresis*. Analytical Chemistry, 1999. **71**(7): p. 1293-1297.
79. Frazer, W.D., S.M. Fischer, and R.K. Crawford, *Apparatus for delivering ions from a grounded electrospray assembly to a vacuum chamber*. 2006, Google Patents.
80. van Atta, L.C., et al., *The Design, Operation, and Performance of the Round Hill Electrostatic Generator*. Physical Review, 1936. **49**(10): p. 761-776.
81. Van Atta, L.C., et al., *Electrostatic Generator for Nuclear Research at M.I.T.* Review of Scientific Instruments, 1941. **12**(11): p. 534-545.
82. Allen, K.W., *Recent research in nuclear reactions using the Aldermaston Tandem generator*. Nuclear Instruments and Methods, 1961. **11**: p. 93-111.

Chapter 2

Van de Graaff generator for Capillary electrophoresis

2.1 Introduction

Capillary electrophoresis (CE) is one of the most powerful separation techniques in the field of analytical chemistry. Because CE can achieve very high separation efficiency and resolution, it has been widely used for the separation of complex chemical components and biological substances, [1-4] and in classical DNA sequencing since the early 1980s [5, 6]. In order to obtain superior separations and/or to separate extremely complex samples, the immediate apparent solution would be to increase the applied voltage (V), which would, in theory, increase the separation efficiency (N) proportionally and the separation resolution (R) by the square root of the voltage. However, increasing the applied voltage brings further challenges in terms of excessive Joule heating [7, 8] and electrical breakdown [9]. Joule heating is generated as a result of passing current through a conductive medium and occurs inside a capillary in CE as a current passes through the background electrolyte (BGE). The heat generated inside the capillary can only be dissipated at the surface; inadequate heat dissipation will lead to a temperature gradient along the capillary radius resulting in decreased separation efficiency [10]. In the worst case, Joule heating can interrupt the separation when bubbles caused by boiling of the BGE disrupt the electric field [11, 12]. Another potential pitfall of using very high voltage is electrical breakdown [13], which can be caused by the difference in electric potential between the inside and outside of the fused silica capillary.

Even in the face of such challenges, a handful of research groups have developed CE platforms capable of harnessing the benefits of high voltages while addressing the aforementioned concerns. The Jorgenson group developed an ultra-high voltage CE system, based on a Cockcroft-Walton voltage multiplier design, that was demonstrated for use with voltages as high as 330 kV, though special precautions and apparatus were required to use it [13-15]. A part of separation capillary tube was wound around an acrylic rod that was centered inside a series of Cockcroft-Walton modules and further cast in a polymer resin as a dielectric insulator to prevent electrical breakdown. A dedicated sample injection port was also developed. The system was applied to the separation of peptides, proteins and DNA, with peptide separations at 330 kV or 580 V/cm yielding Theoretical plates up to 10^7 plates in a tenth of the separation time required for a 10^6 plate separation conducted

at 30 kV. However, this significant achievement in resolution clearly comes at a cost in experimental complexity. The group of Riekkola developed a high voltage CE system with which they were able to apply up to 60 kV [16]. However, various alcoholic media were employed, rather than an aqueous buffer, to reduce the conductivity inside the capillary and thus limit the extent of Joule heating. This nonaqueous CE platform was employed for the separation of benzoic acids, demonstrating fast separations. Joule heating nonetheless proved somewhat problematic and the setup required a bespoke apparatus for electrical insulation [17-20]. Thus, while certainly not trivial, these examples show that it is possible to take advantage of higher voltages for greatly improved CE separations.

Here, we demonstrate that it is possible to achieve high voltage capillary electrophoresis separations without the need for complex instrumentation or unconventional media by employing a simple, inexpensive Van de Graaff (VDG) generator, the same type as those found in school laboratories [21]. We investigated the use of the platform for the separation of a mixture of amino acids (AAs) and studied the effects of background electrolyte concentration and capillary diameter on the migration times of the AAs, and employed a conventional 30 kV CE power supply as a reference system for comparison.

2.2 Theoretical background

In CE, separation efficiency is determined by the number of theoretical plates (N), as demonstrated in Equation 1.1. Thus, according to Eqn. (1.1), the separation efficiency (N) increases proportionally to the voltage (V) applied across the length of the capillary tube. The number of theoretical plates can also be obtained experimentally based on the migration time (t_m) of an analyte and the full-width at half maximum (FWHM) height of its signal peak [22]. The resolution (R_s) of a CE separation can be described based on the separation efficiency and the mobilities of two separated analytes, as shown in Equation 2.2:

$$R = \frac{1}{4} \sqrt{N} \left(\frac{\Delta\mu}{\mu_{avg}} \right) \quad (2.2)$$

Where, $\Delta\mu$ is the difference in electrophoretic mobility between two components, μ_{avg} is the average electrophoretic mobility of two components and N is the number of theoretical plates. Therefore, increasing the applied voltage of a CE separation not only increases the separation efficiency, but

also the resolution albeit to a lesser extent, thereby clearly demonstrating the advantages to be gained by striving for higher voltages. However, as described above, factors such as Joule heating and electrical breakdown become problematic as the voltage is increased.

2.3 Materials and Methods

2.3.1 Reagents

Sodium hydroxide, sodium tetraborate, fluorescein isothiocyanate isomer I (FITC) and amino acids (L-glutamic acid (Glu), L-glutamine (Gln) and L-alanine (Ala)) were purchased from Sigma-Aldrich (Germany). A 100 mM tetraborate buffer (Borax) solution at pH 9.21 was used as stock for preparing the background electrolyte (BGE). A sample stock solution containing 5 mM of each of the 3 amino acids (AAs) was prepared in BGE. The AAs were labelled with 5 mM FITC and stored in the dark for 12 hours [23]. For the CE experiments, the BGE was serially diluted using purified water (Milli-Q® Direct 8, Merck, Germany) to 10 mM and 2 mM. The sample containing the fluorescently labelled AAs was diluted to 100 μ M with purified water.

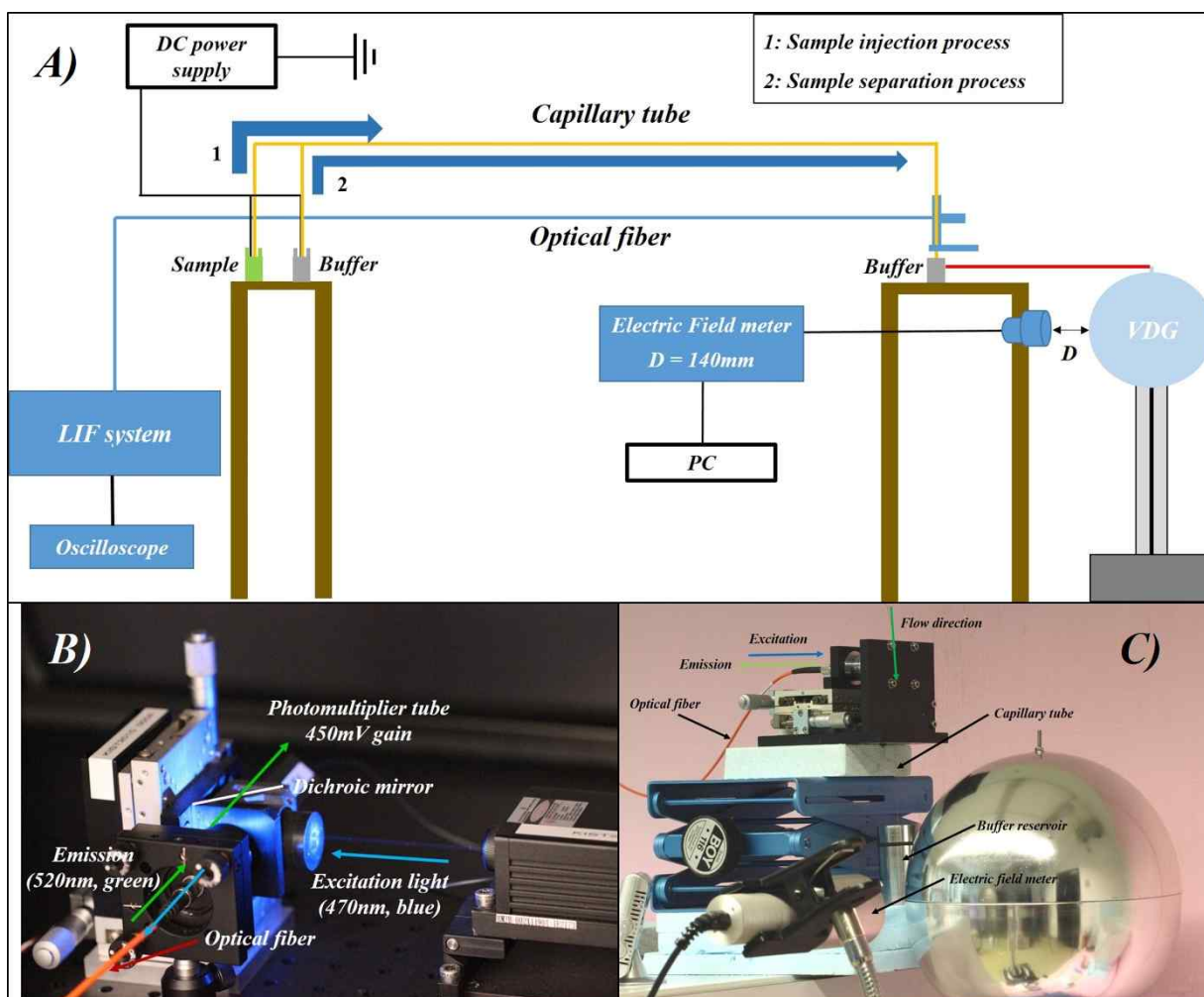


Figure 2.1 Experimental setup for Van de Graaff (VDG) generator-based capillary electrophoresis. (A) Schematic diagram of the platform, illustrating the connection of a capillary tube to sample/buffer reservoirs connected to a conventional 30 kV power supply at the capillary inlet and the VDG at the capillary outlet. Sample injection was achieved electro-kinetically using the DC power supply (5 kV for 3 s). And also, for direct measurement of field strength for the VDG, electric field meter was placed 140mm away from the dome (B) Laser induced fluorescence (LIF) detection system, consisting of a 473 nm laser directed into a filter cube. The excitation light passed into an optical fiber that was connected to a detection stage near to the outlet of the capillary. A photomultiplier tube (PMT) was attached to the filter cube for detection of fluorescence light collected from a sample. (C) Detection stage in which the capillary was held near to the outlet,

allowing detection via a microscope objective connected to the optical fiber of the LIF system. The capillary outlet was inserted into a stainless steel buffer reservoir that was electrically connected to the VDG via a platinum wire. And also, electric field meter was placed 140mm distance from the sphere for measuring direct voltage from VDG.

2.3.2 Experimental setup

Fused silica capillary with an ID of 5 and 50 μm (OD 375 μm) was obtained from Postnova (Germany) and used in 75 cm lengths (length to detector, LD = 60 cm). The inlet of the capillary was positioned at a sample introduction stage, and the outlet at a detection stage (Figure 2.1). A Van de Graaff (VDG) generator (N-100VB, Winsco, USA), which generated a negative charge at its dome, was placed near to the detection stage, and the two were electrically connected to ensure that they were at the same potential. The detection stage featured a capillary holder that fixed the capillary in place for laser-induced fluorescence (LIF) detection, as well as a custom-designed stainless steel BGE reservoir (with a volume of approximately 30mL) suspended beneath the detection stage by four screws, into which the outlet of the capillary was connected via a one-piece fitting (C360-100, LabSmith, USA) (Figure 2.1c). To electrically connect the reservoir to the VDG, a Pt wire was wound around one of the screws holding the reservoir in place and also wound to the dome of the VDG. At the sample introduction stage, sample and buffer reservoir were prepared from 2 mL micro centrifuge tubes for sample injection and separation processes. The reservoirs on both the sample introduction and detection stages were located at the same height in order to prevent hydrodynamic flow due to hydrostatic pressure. For sample injection during VDG experiments, and for performing control experiments, a conventional high voltage power supply was employed (CZE 2000, Spellman, USA), which was connected to the sample or buffer reservoirs of the sample introduction stage via a platinum electrode. An electric field meter (Statometer III, HAUG GmbH, Germany) was placed 140 mm from the sphere surface of VDG to serve as a proxy for the applied separation voltage. Field strength was measured with 5 to 50 μm ID capillary which has 100cm length with the same manner of experimental process for CE. During the measurement using the van de Graaff generator and the conventional power supply, the electric field strength was measured in real-time and the data was collected and stored using the supplied software interface (STOFEN, HAUG GmbH, Germany).

For LIF detection, a setup similar to the one which was established by Hernandez et al.[24] was used. A modified microscope filter cube (91015, Chroma Technology Corp., USA) was fitted with a dichroic mirror and bandpass filter sets (MF475-35 excitation filter, MD499 dichroic mirror, MF530-43 emission filter, Thorlabs, Germany). A section of polyimide coating was removed from the capillary approximately 15 cm from the outlet using a cigarette lighter to create a detection window, which was fixed in place in the detection stage. Laser light (nominal wavelength of 470 nm) was passed through the filter cube, coupled into an optical fiber (M31L10, ThorLabs, Germany) via a collimator (F220FC-A, ThorLabs) and focused onto the detection window of the capillary using a microscope objective (Epiplan Neofluar 100 \times , Zeiss, Germany) that was fixed to the detection stage. The emitted light was collected by the same objective and optical fiber setup, then passed through the dichroic mirror into a photomultiplier tube (PMT, H10722-01, Hamamatsu, Japan). The fluorescence signal from the PMT was recorded using an oscilloscope (MPO 6014, Tektronix, Germany).

2.3.3 Experimental procedure for capillary electrophoresis

The 75 cm long capillary was conditioned with 0.1 mM sodium hydroxide via a high pressure pump (L-7100, Hitachi, Japan) for 10 min and washed with deionized water for 10 min. The capillary was then flushed with BGE using the high pressure pump for 10 min and subsequently 30 kV was applied for 10 min to equilibrate under electric field conditions. On the sample introduction stage, the inlet of the capillary could be manually moved from the BGE reservoir to the sample reservoir, and likewise the Pt electrode connected to the 30 kV power supply could also be manually moved between the reservoirs. Sample injection was performed by positioning the capillary inlet and Pt electrode in the sample reservoir, and 5 kV was applied to the sample reservoir for 3 s. For the subsequent CE separation, the capillary inlet and Pt electrode were then placed in the BGE reservoir. CE separations were performed using the VDG and compared with separations conducted using a conventional 30 kV power supply (Spellman CZE 2000) in the same set-up. Grounding of the experiments with the VDG was achieved by connecting capillary inlet with the conventional power supply at 0 V, while the van de Graaff generator was connected with the capillary outlet to apply the high voltage (current limit 10 μ A). For the control experiments, the conventional CZE2000 power supply was used to apply +30 kV to the capillary inlet, with the outlet reservoir grounded to maintain normal separations towards the cathode (the van de Graaff generator acts as a negative power supply at the opposite end of the capillary).

2.4 Results and discussion

2.4.1 Effect of BGE concentration

When using a conventional DC power supply for CE, decreasing the electrical resistance for the separation does not impact the applied voltage because a DC power supply is a constant voltage generator. However, a VGD is a current source and, according to Ohm's Law, for a constant current the applied potential is increased when the capillary⁴ resistance increases. In CE, the resistance of the capillary can be adjusted by changing the ionic strength of the BGE, or the capillary diameter. Initial experiments focused on decreasing the ionic strength of the BGE concentration to increase the electrical resistance and achieve the desired increase in applied potential by the VDG. Using a 50 μm ID capillary, BGEs consisting of 10 mM and 2 mM Borax solution were used to measure the effect of ionic strength on the separation of a mixture of amino acids (AAs) (Figure 2.2). The migration time of the AAs was reduced by a factor two when using 2 mM BGE with 0.33×10^6 theoretical plates instead of the 10 mM BGE with 0.19×10^6 theoretical plates which are 1.74 times higher theoretical plates in comparison. For example, Gln migrated at approximately 600 s with the 2 mM BGE (Figure 2.2a) and at approximately 1200 s with the 10 mM BGE (Figure 2.2b), with the other amino acids behaving in the same manner. When diluting the BGE below 2 mM, the efficiency of the separation deteriorated due to electromigrational dispersion and possibly pH changes due to insufficient buffer capacity. With the BGE ionic strength optimized, further gains in separation efficiency would require decreasing the capillary diameter, hence this parameter is discussed in the following section.

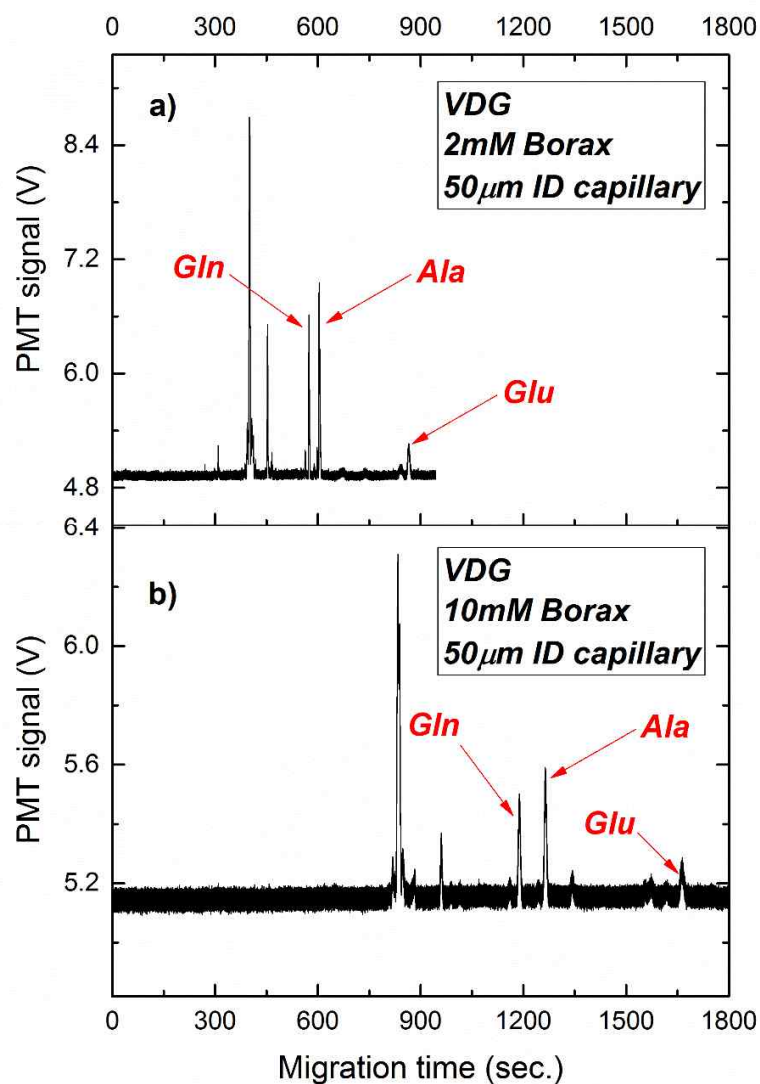


Figure 2.2 The effect of background electrolyte (Borax solution) concentration on the migration times of three amino acids using the VDG CE platform with a 50 μm ID capillary. Electropherograms showing amino acid migration times in (a) 2 mM Borax buffer, and (b) 10 mM Borax buffer.

2.4.2 Effect of capillary diameter

The electrical resistance (R) of the capillary tube can be expressed in terms of its length (l), cross-sectional area (A), and the electrical resistance of the material (ρ), as shown in Equation 2.3:

$$R = \rho \frac{l}{A} \quad (2.3)$$

According to Eqn. 2.3, the total resistance of the capillary can be increased by increasing the capillary length or by reducing the cross-sectional area by decreasing the inner diameter of the capillary. As increasing the length of the capillary would also decrease the electric field strength, decreasing the capillary ID was considered to be the best option. Furthermore, as the cross-sectional area is proportional to the square of the radius, a 10-fold decrease in capillary radius would yield a 100-fold increase in the capillary resistance. Therefore, the effect of ID on the separation of AA's was investigated using capillaries with 50 μm ID and 5 μm ID (Figure 2.3), with 5 μm being the smallest diameter readily available for commercial fused silica capillaries. For the 5 μm ID capillary (Figure 2.3a), the migration time of the AAs mixture was halved compared to a 50 μm ID capillary tube using the same 10 mM BGE (Figure 2.3b). For example, in case of Glu, the migration time was approximately 400 s with the 5 μm ID capillary (Figure 2.3a), while in the 50 μm ID capillary (Figure 2.3b) it was approximately 900 s (0.1×10^6 theoretical plates). Combining these results with the results from the BGE concentration study led to decreasing both the buffer ionic strength (from 10 to 2 mM) and the capillary ID (from 50 to 5 μm), and indeed a 4-fold decrease in migration time was achieved when using the VDG (see Figs. 2.2b and 2.3a (0.42×10^6 theoretical plates)).

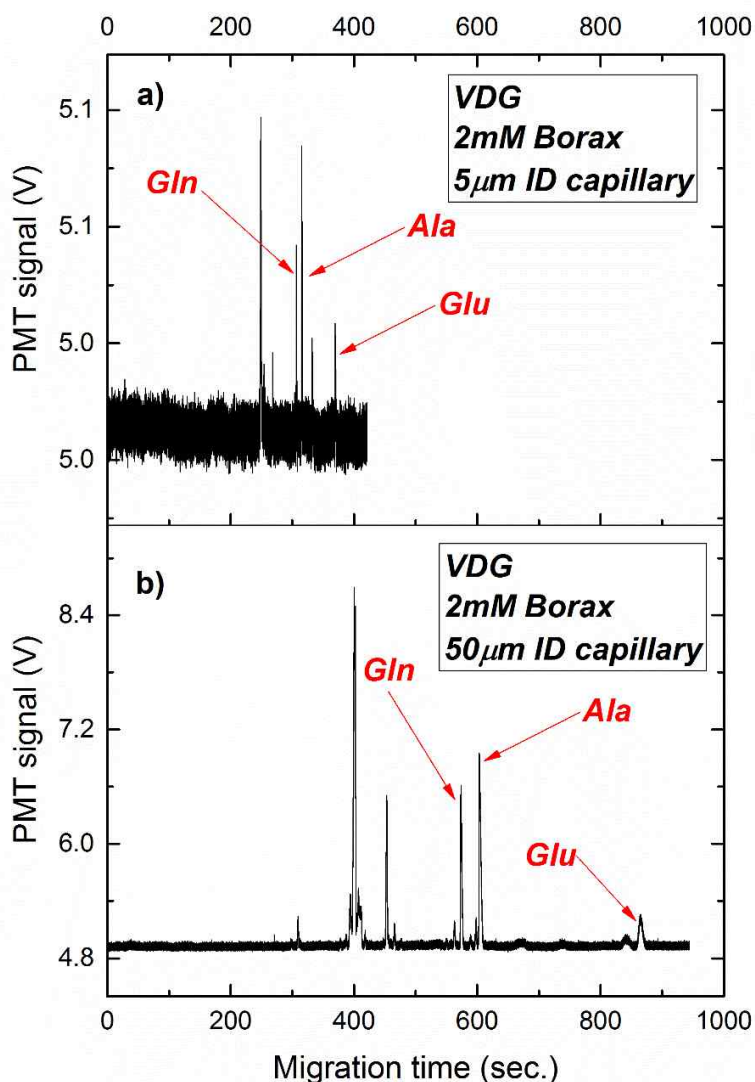


Figure 2.3 The effect of capillary diameter on the migration times of three amino acids using the VDG CE platform (2 mM Borax background electrolyte). (a) Separation obtained using a 5 μm ID capillary, and (b) using a 50 μm ID capillary.

2.4.3 Comparison of the VDG to a conventional DC power supply

In order to compare the performance of the VDG CE platform to a conventional system, the separation efficiencies of the AA mixture were calculated for CE experiments performed with both the VDG and a normal 30 kV power supply (CZE2000) under optimized experimental conditions (Figure 2.4). For the normal DC power supply (labelled as “Normal PS” in Figure 2.4), a voltage

generator, the separation efficiency is not related to the total electrical resistance of the capillary unless high currents lead to excessive Joule heating, and similar efficiencies were obtained for 2 mM and 10 mM electrolytes (Figure 2.4b). Conversely, for the VDG a lower BGE concentration (2 mM Borax, Figure 2.3), and the narrow ID capillary (5 μm , Figure 2.4a) led to increased separation efficiencies. Using the VDG with 2 mM BGE and 5 μm ID capillary, a separation efficiency (N) of 0.97×10^6 theoretical plates was obtained for Gln, which is approximately a 4-fold improvement over the efficiency obtained with the 30 kV DC power supply (0.23×10^6) with 10mM BGE, 50 μm ID capillary and same length of capillary tube (75 cm). For the other amino acids (Glu and Ala), the separation efficiencies were 2–3 times higher than obtained using the normal 30 kV power supply (Table 2.1). For repeat injections, the migration times obtained with the VDG had with RSDs better than 2.3 % (n = 5) for all amino acids (Table 2.2), which is similar to CE separations conducted with conventional power supplies (<1.5% RSDn=5).

An overview of separation efficiencies (N) obtained for the amino acids for the VDG and conventional power supply are given in in Figure 2.5, respectively. The data demonstrate that decreasing R when using the VDG allows for a significant enhancement of N, whereas the separation efficiency for the normal power supply remains relatively unaffected. It must be noted, however, that the theoretical plates for separations conducted with the VDG with a BGE concentration of 10 mM and a 50 μm ID capillary was around half that of the normal 30 kV DC power supply under the same conditions. This is the result of the lower voltage applied using the VDG under these low electrical resistance conditions (Equation (2.3)).

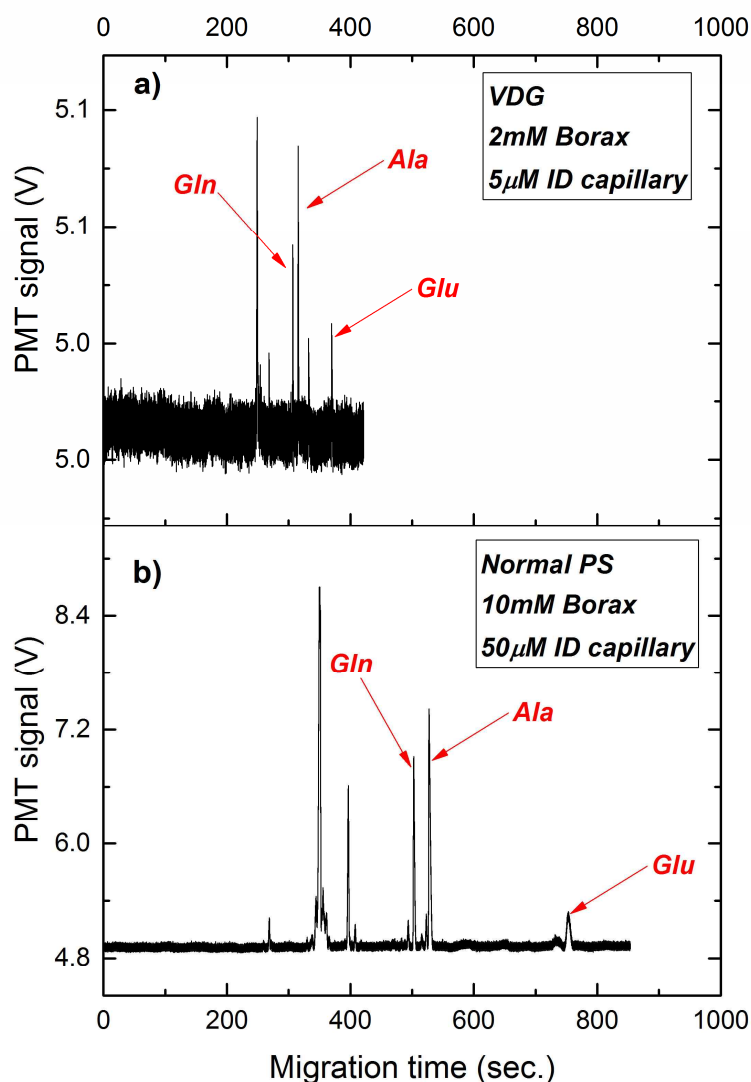


Figure 2.4 Comparison of the migration times of amino acids using different power supplies. (a) Separation using a Van de Graaff (VDG) generator power supply, with 2 mM Borax buffer and a 5 μm ID capillary. (b) Separation using a conventional 30 kV CE power supply (Normal PS), with 10 mM Borax buffer and a 50 μm ID capillary.

2.4.4 Determination of the voltage applied with the VDG

In electrophoresis, the apparent velocity v_{ap} of an ion is a function of its apparent mobility μ_{ap} and the applied field strength E , calculated by V/L_{tot} (L_{tot} is the capillary length) (Equation 2.4).

$$v_{ap} = \mu_{ap}E = \mu_{ap} \frac{V}{L_{tot}} \quad (2.4)$$

From the electroperogram, μ_{ap} can be calculated from the migration time t_m (Equation 2.5)

$$\mu_{app} = \frac{L_{tot} L_D}{V t_m} \quad (2.5)$$

Assuming μ_{ap} does not change when using the same BGE, the effective voltage applied by the Van de Graaff generator (VDG) can be derived from the migration times obtained by the conventional power supply ($t_{m, supplied}$) and the VDG (t_m, VDG), and the supplied voltage of the conventional power supply ($V_{supplied}$) when the detection and capillary lengths are the same, as illustrated in Equation 2.6

$$V_{VDG} = V_{supplied} \frac{t_{supplied}}{t_{VDG}} \quad (2.6)$$

Using this calculation, the voltage, and hence E was increased by a factor of 2 to approx. 75kV/m when using the VDG (Eqn. 2.6) (Figure 2.5) in case of Glu with the comparison between the normal supply (50 μ m ID, 10mM BGE) and VDG (5 μ m ID, 2mM BGE).

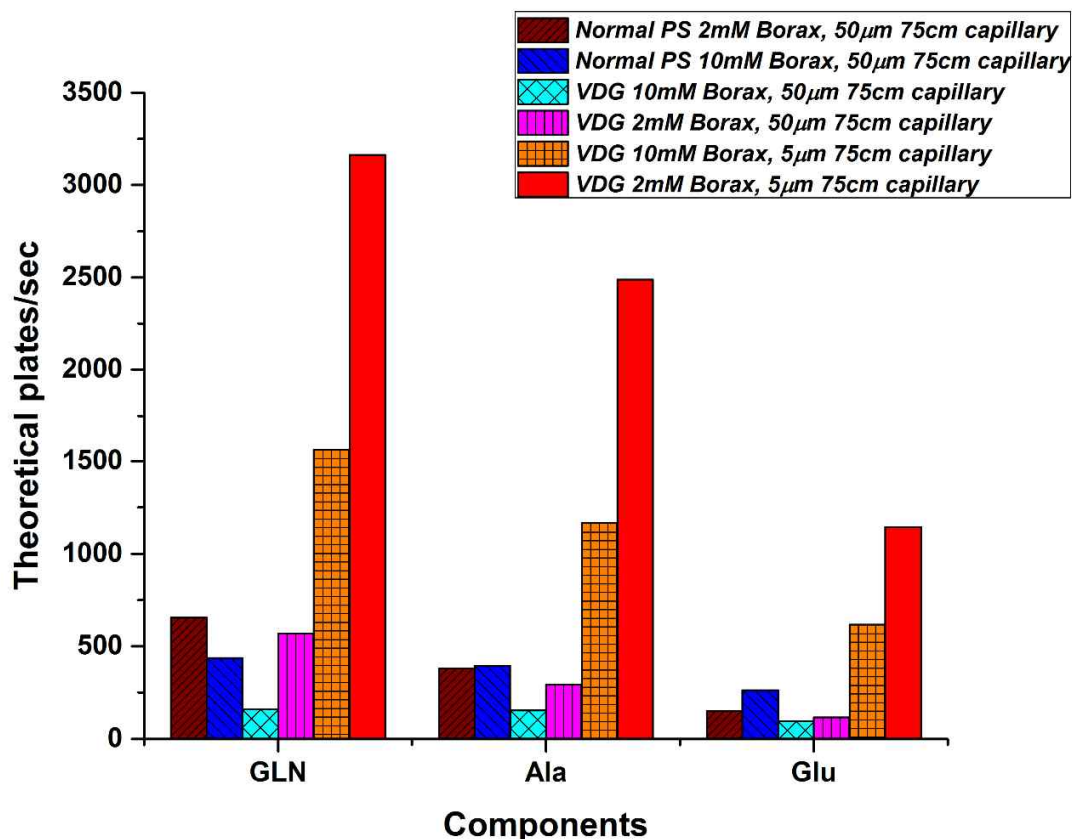


Figure 2.5 Comparison of Theoretical plate per second for 3 amino acids separations using the conventional 30 kV power supply and the VDG generator with varying background electrolyte concentrations (2 and 10 mM Borax) and capillary diameters (5 and 50 µm).

To provide a more direct measure of the applied electric field strength an electric field meter was used. First, the meter was characterized using the 30kV DC power supply was used and the measurement under controlled temperature (25°C) and humidity (50% RH). For different ID (50µm ID and 5µm ID) and BGE concentration (2mM and 10mM) for VDG and 30kV DC power supply the field strength was measured at – 25 kV, with no significant changes by capillary ID or BGE (Figure 2.6A). The 5 kV/m deviation from the applied field strength can be explained by the fact the electric field meter was positioned 140 mm away from the capillary. For the VDG, field strength increased dramatically by the reducing the capillary ID and the concentration of BGE. And also, by the result of field meter, average voltage for each cases were calculated and compared (Figure 2.6B). While E increased with decreasing the ID for 10mM BGE, no significant change in E was observed with reducing the ID from 50 to 5 µm for the 2mM BGE.

From these results, we conclude there may be parallel resistor in the system limiting the maximum voltage that be applied by the VDG through adjusting the capillary ID and BGE. In order to achieve higher voltages from the VDG, measures previously presented by the Jorgenson group including oil tank, vacuum chamber and etc. need to be considered, all impacting on the simplicity of the current set-up. As using the current set-up, electric breakdown of the capillary was sometimes observed after 2-3 repeat injections (Data is not shown). Working with a 360 μ m OD and 5 μ m ID capillary with a dielectric strength of 25~45 MV/m, or 4.5~7.2 kV/180 μ m field strengths of 75 kV/m appears to be the limit when aiming to work with a simple experimental set-up without the need to be wind the capillary with dielectric insulator.

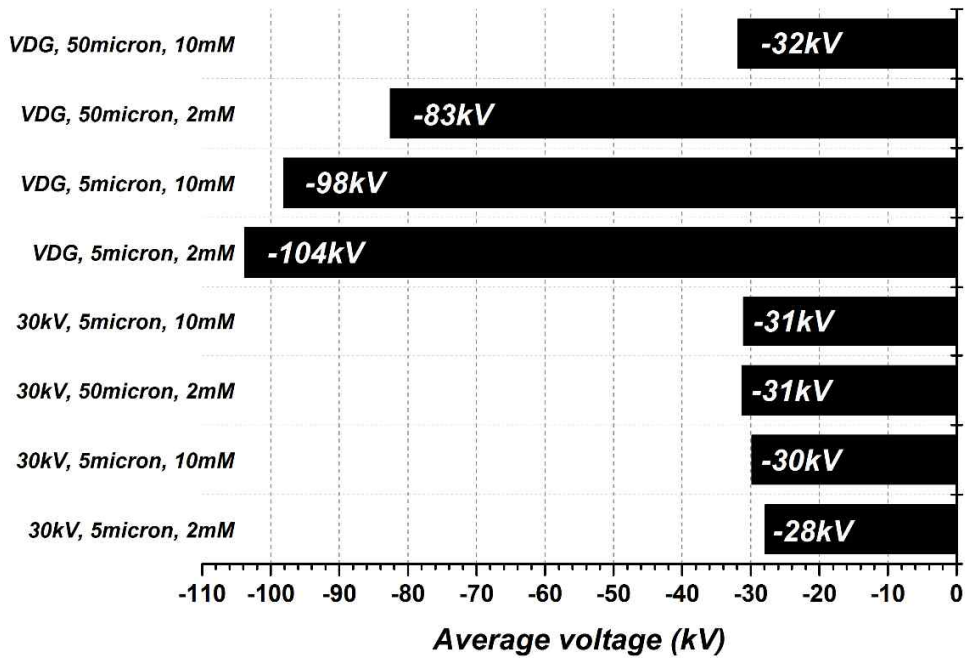
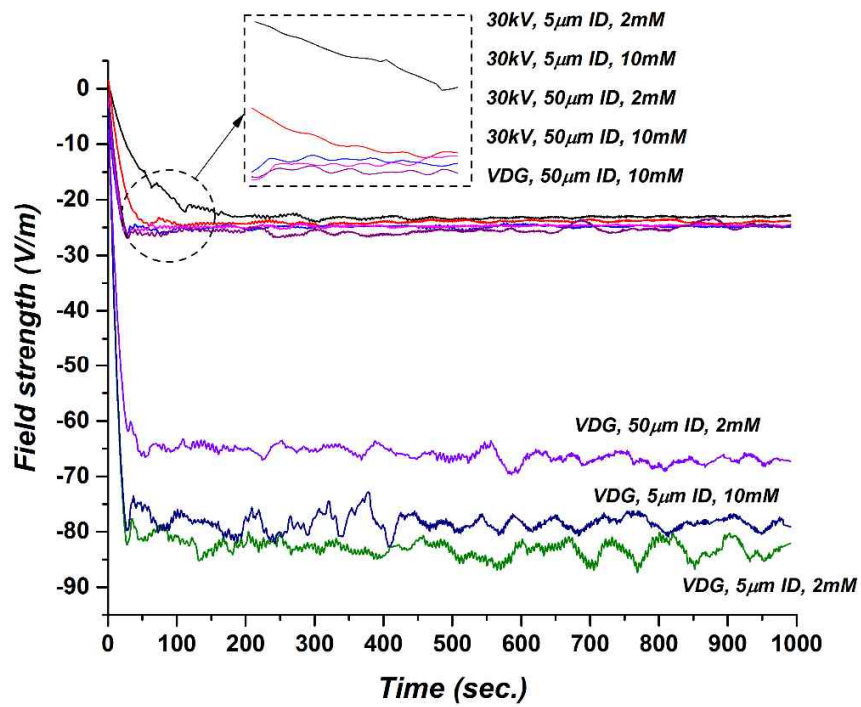


Figure 2.6 Upper) Electric field strength by measuring with electric field meter for different diameter of capillary tubes and concentrations of BGE and, Bottom) Comparison of average

voltages, an average voltage approximately 3.4 times higher than the reference was achieved using the VDG

2.4.5 Outlook

The results described above demonstrate, to our knowledge, the first successful application of a standard Van de Graaff (VDG) generator as a power supply for CE separations. A conventional high voltage power supply, which could generate up to 30 kV, was used as a reference platform for comparison with the VDG for CE separations. Decreasing the capillary ID and the BGE concentration resulted in decreased migration times for the AAs when using the VDG, and increased the separation efficiency (N) in comparison to the conventional 30 kV DC power supply. The low current (10 μ A) VDG generated a high applied voltage by increasing the total resistance of the capillary tube according to Ohm's law, hence the higher theoretical plates (\sim 4-fold) achieved than for the normal power supply (30 kV). The higher voltage results in a higher apparent velocity, and as band broadening in CE is dominated by longitudinal diffusion (expressed in terms of the diffusion coefficient, D, and the migration time, t_m , using Einstein's equation: $\sigma = \sqrt{2D t_m}$ through the standard deviation of the Gaussian peak σ), the separation efficiency can be increased by decreasing the separation time through increased apparent velocity.

Compared to previous examples of high voltage capillary electrophoresis with normal DC power supply, the Van de Graaff (VDG) generator-based platform developed here represents a far more simple and cost-effective (for example, the price range of commercial normal power supply is \$ 2,000 to \$ 25,000 (\pm 30kV to \pm 100kV)) approach.

While the VDG has been shown to offer advantages in separation efficiency compared to the conventional power supply used for reference, the theoretical plates were still below those reported by the group of Jorgenson who were able to apply much higher voltages with their ultra-high voltage platform [15]. Despite its impressive results, the application of the ultra-high voltage platform of Jorgenson et al. has been constrained by its significant complexity and expense. Our method, on the other hand, with its very simple and inexpensive setup, significantly lowers the entry barrier for research groups that wish to exploit the high efficiency gains associated with higher voltages, but are deterred by the high initial investment. In fact, even if a research group intended to perform CE separations at standard applied voltages, the VDG still represents a significant reduction in cost compared to conventional power supplies which is only \$ 665.

2.5 CONCLUSIONS

In this chapter, development of high voltage capillary electrophoresis platform based on a Van de Graaff (VDG) generator power supply is described. Previous high voltage CE techniques have required the use of complex setups or nonaqueous mobile phases in order to avoid problems with Joule heating. By limiting the current, a VDG can be used to deliver high voltages using a simple and low-cost setup. Using a narrow bore capillary and low concentrations of electrolyte solution, electrophoretic separations could be conducted at voltages up to 104 kV. The separation performance was characterized by separation of a mixture of amino acids in capillaries of differing diameters and with varying background electrolyte concentrations. The results showed that narrower capillaries and lower electrolyte concentrations yielded faster separations with higher separation efficiencies (approximately 4-fold improvement) and greater separation resolution (approximately 2-fold improvement) compared to a conventional DC power supply with the same capillary length (Fig 2.6.). These initial results demonstrate the great potential for achieving rapid, high quality separations using an economic platform. Future work will include the optimization of various separation parameters, including sample plug size and the prevention of the current leakage that currently limits the potential. Application areas for the high efficiency, highly resolution separations are expected in the analysis of complex chemical and biological samples, such as for chiral molecule and glycan analysis.

2.6 REFERENCES

1. K. Verleysen, P. Sandra, Separation of chiral compounds by capillary electrophoresis, *ELECTROPHORESIS*, 19 (1998) 2798-2833.
2. S.Y. Zhou, H. Zuo, J.F. Stobaugh, C.E. Lunte, S.M. Lunte, Continuous in Vivo Monitoring of Amino Acid Neurotransmitters by Microdialysis Sampling with Online Derivatization and Capillary Electrophoresis Separation, *Analytical Chemistry*, 67 (1995) 594-599.
3. K.M. Hutterer, H. Birrell, P. Camilleri, J.W. Jorgenson, High resolution of oligosaccharide mixtures by ultrahigh voltage micellar electrokinetic capillary chromatography, *Journal of Chromatography B: Biomedical Sciences and Applications*, 745 (2000) 365-372.
4. A. Rizzi, Fundamental aspects of chiral separations by capillary electrophoresis, *ELECTROPHORESIS*, 22 (2001) 3079-3106.
5. J.W. Jorgenson, K.D. Lukacs, Zone electrophoresis in open-tubular glass capillaries, *Analytical Chemistry*, 53 (1981) 1298-1302.
6. S. Terabe, K. Otsuka, K. Ichikawa, A. Tsuchiya, T. Ando, Electrokinetic separations with micellar solutions and open-tubular capillaries, *Analytical Chemistry*, 56 (1984) 111-113.
7. X. Xuan, D. Li, Analytical study of Joule heating effects on electrokinetic transportation in capillary electrophoresis, *Journal of Chromatography A*, 1064 (2005) 227-237.
8. C.J. Evenhuis, P.R. Haddad, Joule heating effects and the experimental determination of temperature during CE, *ELECTROPHORESIS*, 30 (2009) 897-909.
9. C.A. Monnig, J.W. Jorgenson, On-column sample gating for high-speed capillary zone electrophoresis, *Analytical Chemistry*, 63 (1991) 802-807.
10. C.J. Evenhuis, R.M. Guijt, M. Macka, P.J. Marriott, P.R. Haddad, Temperature Profiles and Heat Dissipation in Capillary Electrophoresis, *Analytical Chemistry*, 78 (2006) 2684-2693.
11. G. Chen, U. Tallarek, A. Seidel-Morgenstern, Y. Zhang, Influence of moderate Joule heating on electroosmotic flow velocity, retention, and efficiency in capillary electrochromatography, *Journal of Chromatography A*, 1044 (2004) 287-294.
12. X. Xuan, G. Hu, D. Li, Joule heating effects on separation efficiency in capillary zone electrophoresis with an initial voltage ramp, *ELECTROPHORESIS*, 27 (2006) 3171-3180.

13. K.M. Hutterer, J.W. Jorgenson, Ultrahigh-Voltage Capillary Zone Electrophoresis, *Analytical Chemistry*, 71 (1999) 1293-1297.
14. K.M. Hutterer, J.W. Jorgenson, Separation of hyaluronic acid by ultrahigh-voltage capillary gel electrophoresis, *ELECTROPHORESIS*, 26 (2005) 2027-2033.
15. W.H. Henley, J.W. Jorgenson, Ultra-high voltage capillary electrophoresis >300 kV: Recent advances in instrumentation and analyte detection, *Journal of Chromatography A*, 1261 (2012) 171-178.
16. S. Palonen, M. Jussila, S.P. Porras, T. Hyötyläinen, M.-L. Riekkola, Extremely high electric field strengths in non-aqueous capillary electrophoresis, *Journal of Chromatography A*, 916 (2001) 89-99.
17. S. Palonen, M. Jussila, S.P. Porras, T. Hyötyläinen, M.-L. Riekkola, Nonaqueous capillary electrophoresis with alcoholic background electrolytes: Separation efficiency under high electrical field strengths, *ELECTROPHORESIS*, 23 (2002) 393-399.
18. S. Palonen, M. Jussila, S.P. Porras, M.-L. Riekkola, Peak dispersion and contributions to plate height in nonaqueous capillary electrophoresis at high electric field strengths: Ethanol as background electrolyte solvent, *ELECTROPHORESIS*, 25 (2004) 344-354.
19. S. Palonen, M. Jussila, M.-L. Riekkola, Effect of initial voltage ramp on separation efficiency in non-aqueous capillary electrophoresis with ethanol as background electrolyte solvent, *Journal of Chromatography A*, 1068 (2005) 107-114.
20. S. Palonen, S.P. Porras, M. Jussila, M.-L. Riekkola, Peak dispersion and contributions to plate height in nonaqueous capillary electrophoresis at high electric field strengths: Propanol as background electrolyte solvent, *ELECTROPHORESIS*, 24 (2003) 1565-1576.
21. R.J. Van de Graaff, K.T. Compton, L.C. Van Atta, The Electrostatic Production of High Voltage for Nuclear Investigations, *Physical Review*, 43 (1933) 149-157.
22. S. Fanali, *Handbook of capillary electrophoresis*. James P. Landers (Ed.), CRC Press Inc., Boca Raton, FL, USA 1996, pp. 1-912, ISBN 0-8493-2498-X, \$ 135.00, *ELECTROPHORESIS*, 18 (1997) 2116-2117.

23. C.S. Effenhauser, A. Manz, H.M. Widmer, Glass chips for high-speed capillary electrophoresis separations with submicrometer plate heights, *Analytical Chemistry*, 65 (1993) 2637-2642.
24. L. Hernandez, J. Escalona, N. Joshi, N. Guzman, Laser-induced fluorescence and fluorescence microscopy for capillary electrophoresis zone detection, *Journal of Chromatography A*, 559 (1991) 183-196.

Chapter 3

Application of CE with VDG for carbohydrate separation

3.1 Sample from HIPs (Helmholtz center for infection research)

After the successful separation with VDG for amino acids, we could get the Sialylglycopeptide (SGP) which was extracted from the egg yolk. SGP can be differentiated or chemically synthesized to Man3GlcNac oxazoline (1) which can be differentiated to glycol-liposome, glycopeptides, glycoproteins and so on. Therefore, this compound is very important for the study of infectious diseases, cell structures and etc. (figure 3.1).

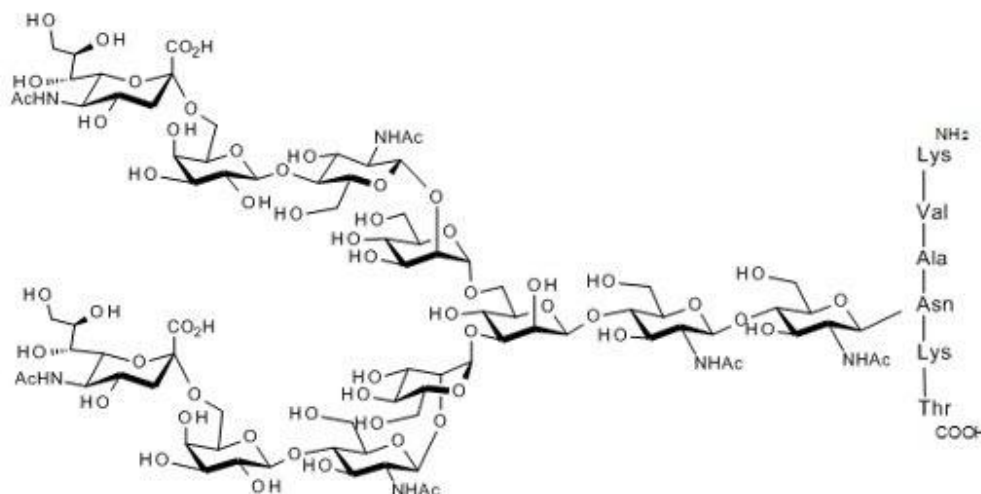


Figure 3.1 Chemical structure of Sialylglycopeptide (SGP)

So, we tried to separate this compounds with our VDG system and we labelled SGP with FITC because, SGP has amin-branch which can be bind with FITC.

3.2 Labelling protocols and results for FITC labelling

According to the preliminary separation with HPLC (high performance liquid chromatography) at HIPs, SGP has two main peaks which has 80% and 20% peak areas.

2mM tetraborate which has pH 9.20 was prepared as a BGE and 200 μ M concentration of HIPs sample was with same concentration of FITC at BGE then stored in dark condition at the room temperature overnight. 2m and 50 μ m ID fused silica capillary tube was prepared and conditioned with 100mM sodium hydroxide for 10 min. and DI water for 10 min. to make uniform and clean surface inside of capillary tube. And then, BGE was filled with HPLC pump with 0.1ml/min flow rate then 30kV applied voltage applied through the capillary for generating uniform electrical double layer inside of capillary tube. Sample was injected with electro kinetic sample injection method at 5kV for 5sec.. VDG was used as a voltage source for separation process. For the detection system, LIF system was used and the intensity of laser was measured over 19mW with optical power meter. According to figure 5.2, labelled SGP sample was separated and 4 peaks were appeared. By the identification experiment with FITC fluorophore, 4 peaks were identified and sigma (σ) and full width half max (FWHM) was extracted. According to the eqn. 3.2 separation efficiency was calculated. The separation efficiency of peak 1 is 1.7×10^6 and peak 2 has 8.1×10^5 separation efficiency.

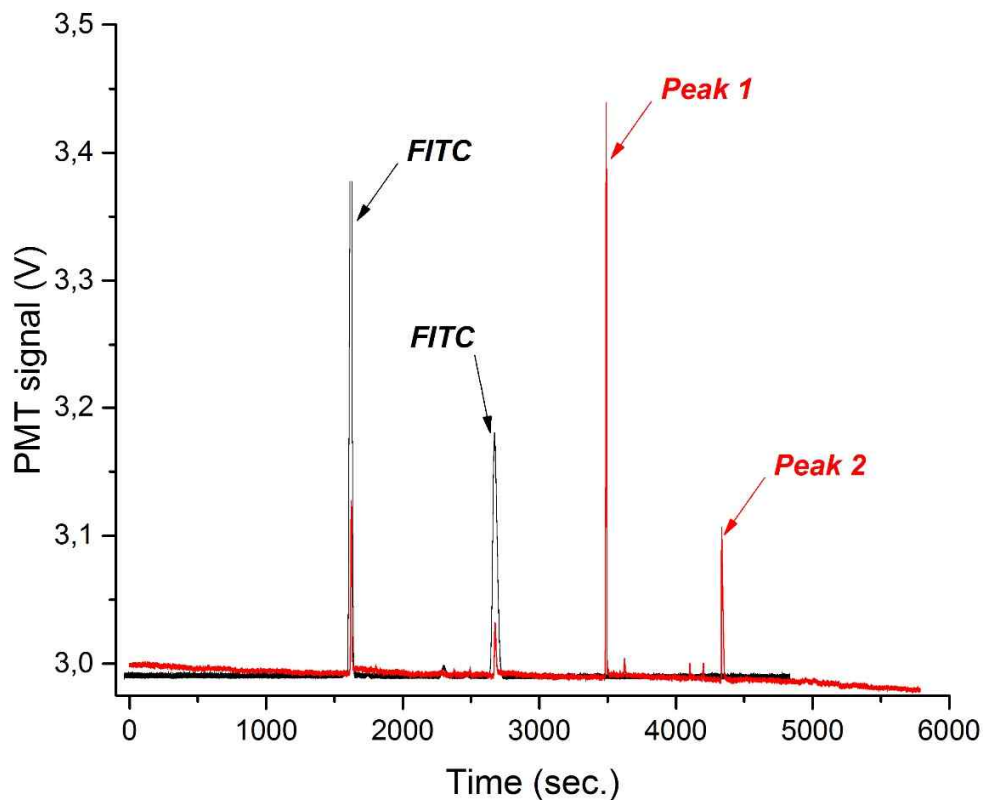


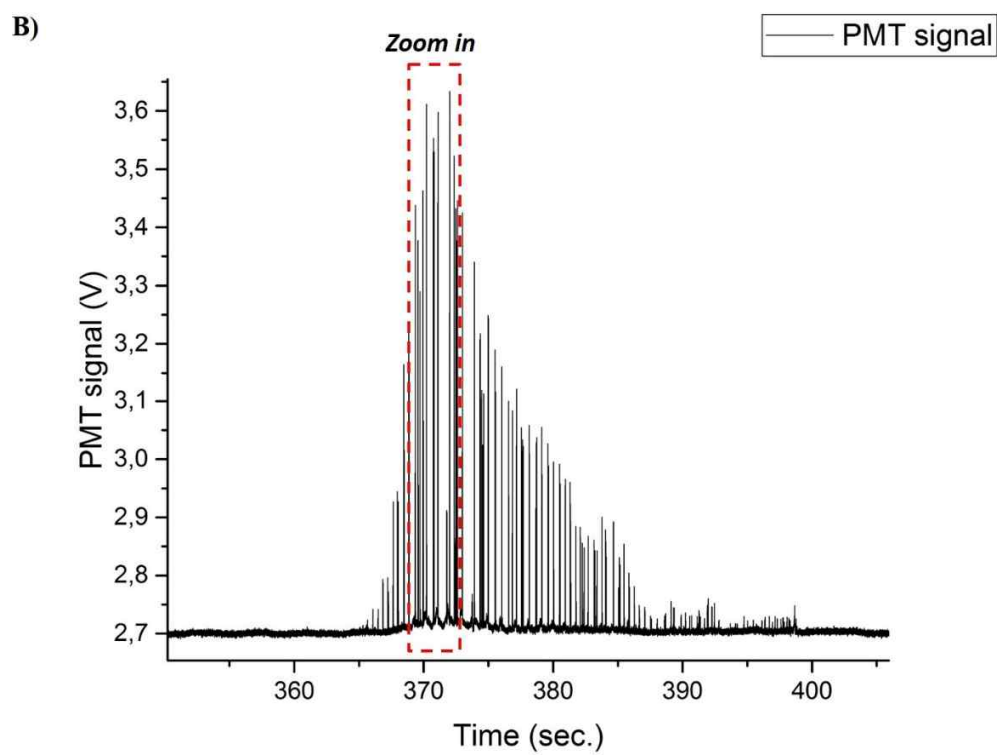
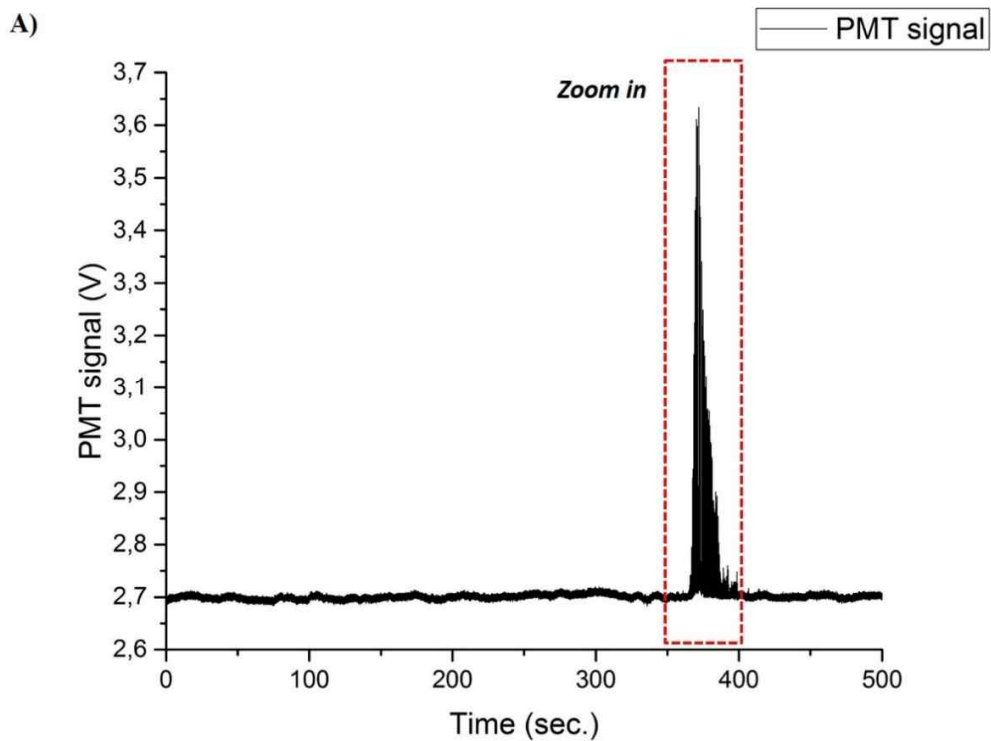
Figure 3.2 Separation result for SGP with FITC labelling. Two SGP peaks and two free FITC peaks were separated.

3.3 Labelling protocols and results for APTs labelling

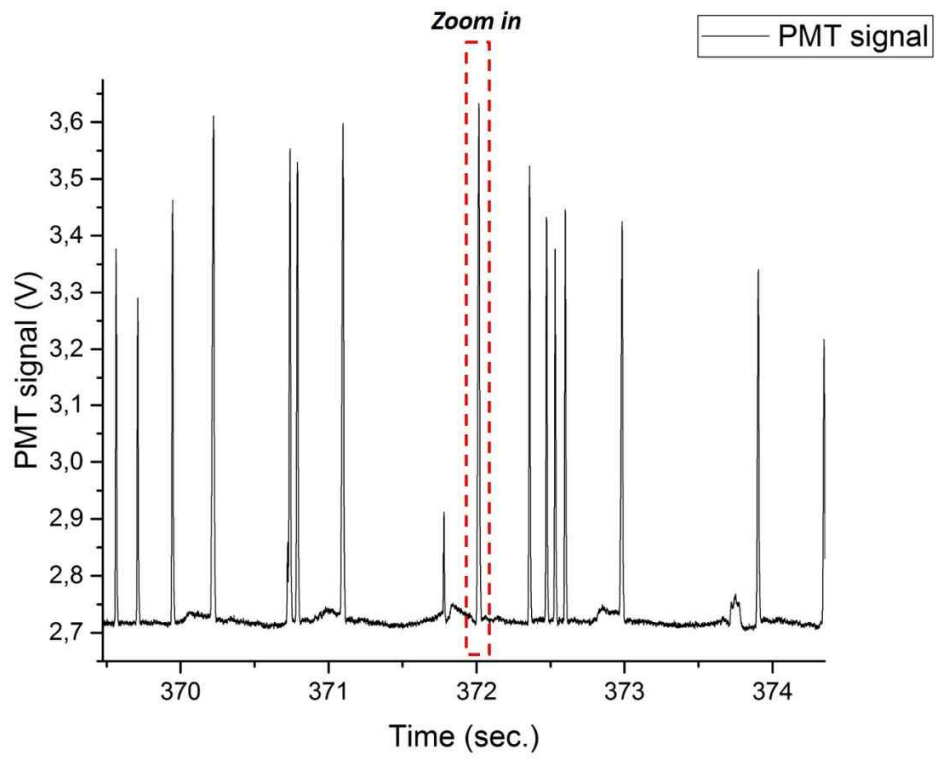
After separation experiment with FITC, we wanted to cleave off SGP with reducing reagent (Cyanoboro hydrate at 100mM THF (tetrahydrofuran)) and then label APTs which can be labelled with carbohydrate components. For the labelling, 20 μ l SGP sample was mixed with 20 μ l reducing agent and then sample mixture was mixed 40 μ l APTs mixtures (0.2M APTs + 40 μ l 1M citric acid). For the labelling reaction, sample mixture was stored in the dark at room temperature for overnight. After that, 1ml ice cold acetone was added to sample mixture and centrifuged at 12,000 rpm for 15min. to remove supernatant then, the sample was washed with acetone 2~3 times. For the

conditioning sample mixture 500 μ l DI was added to sample mixture and the sample was ready to use for separation experiment.

Separation process was done with 1m 5 μ m ID capillary, and 2mM tetraborate which has pH 9.20 was used as a BGE. VDG was used as a voltage source for CE and electrikinetic force injection (5kV, 10sec.) was used for sample injection process. Once separation was done with VDG CE system (expected voltage approx. 100kV), incredibly high resolution of separated peaks was appeared and extremely high separation efficiency was calculated. $2.7*10^9$ separation efficiency, this is the very much high separation efficiency than expected and when we compared with the separation efficiency of commercial CE system, it is 1000 times higher values (figure 3.3).



C)



D)

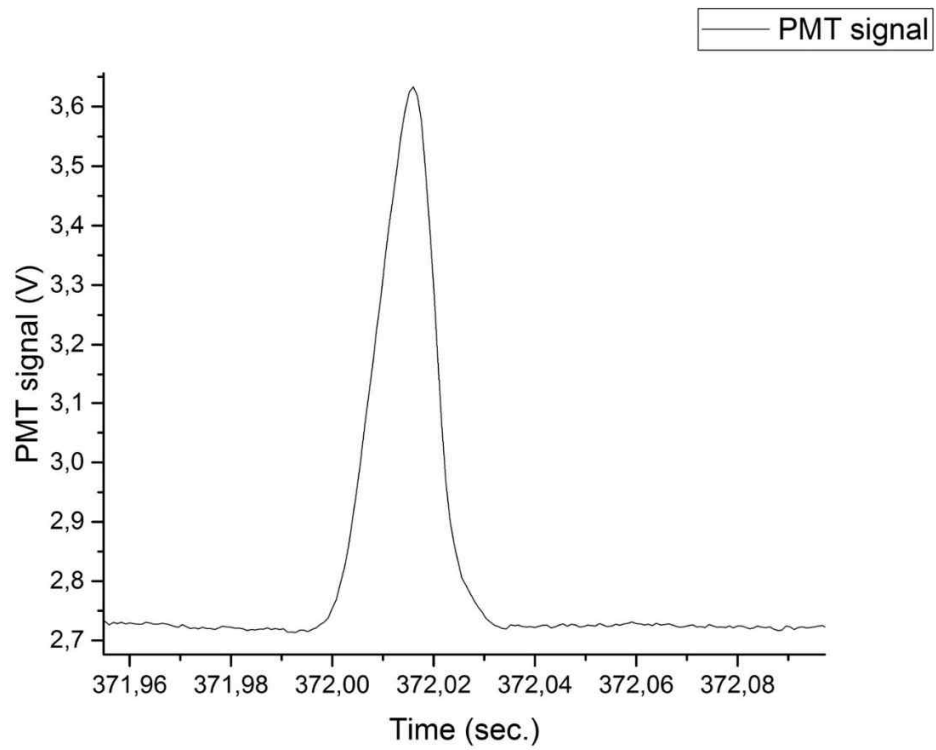
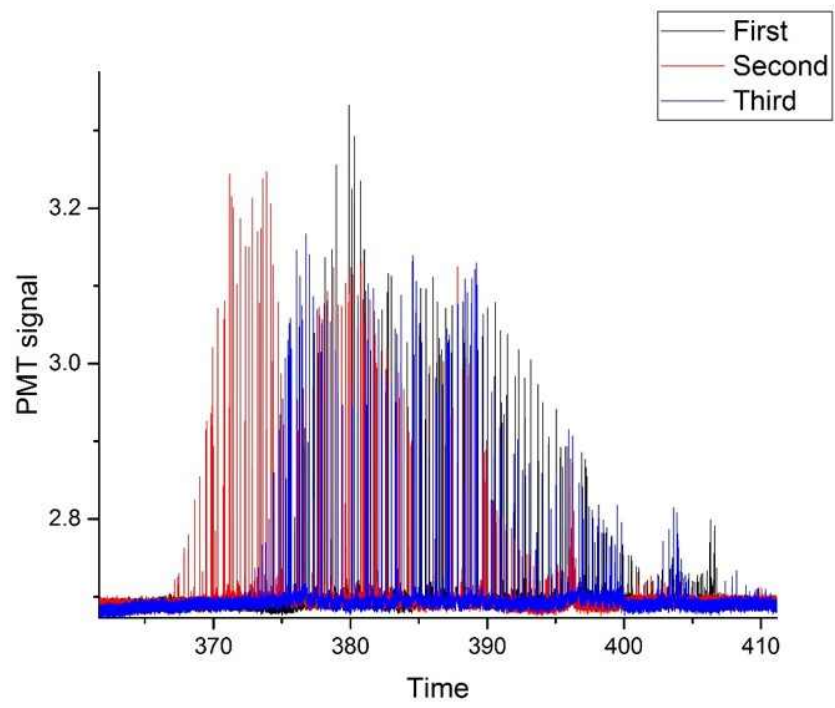
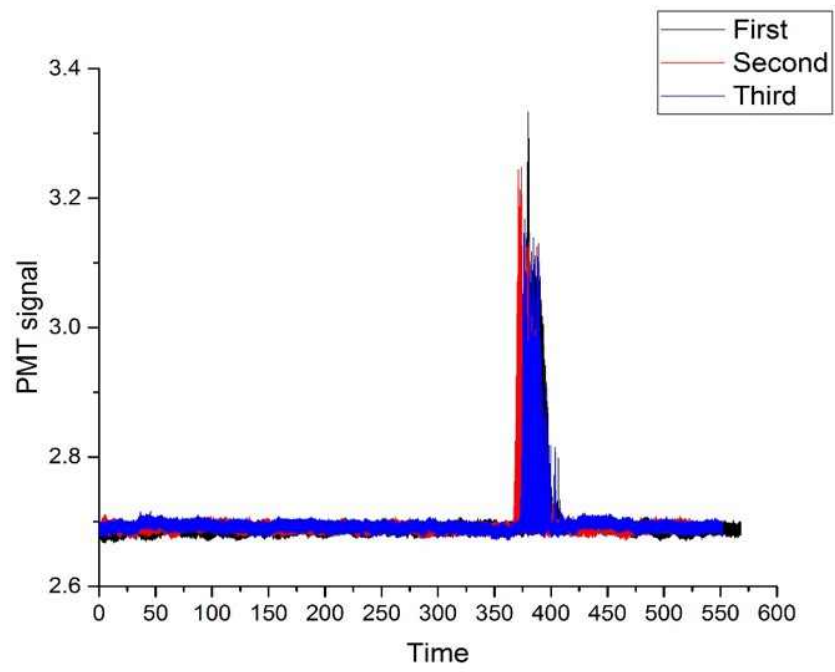


Figure 3.3 Separation result for SGP with APTs labelling. For labelling SGP with APTs, sample was cleaved off with reducing reagent and then APTs was labelled. By the separation process with VDG, one “big peak flock” was separated. A) raw data for the separation, B) 1st Zoom in for red dot box, there has several hundred peaks were separated, C) 2nd Zoom in for red dot box, still there has very well separated peaks were observed, D) 4th Zoom in for red dot box, one peak was selected and the sigma value and FWHM value was extracted and the separation efficiency was calculated.

3.4 Conclusion

After we got this results, we were very excited and we would like to analysis each single peaks. Hence, we repeated separation experiment to check the reproducibility and, we could see the peak flock at almost same time (when the VDG is full speed around 360sec., figure 3.4 upper) however, when peaks were zoomed in, irregular peak flock was observed (fig. 3.4 middle and bottom) which meant our system was not reproducible under certain experimental condition (1m length, 5 μ m ID and 100kV applied voltage). We assumed the peak flock was appeared at “the timing of braking capillary tube by high voltage.” Because, usually we could observed “braking capillary tube” after 2~3 runs of separation process. So, we prepared another sample which has only APTs and separated with same experimental condition to find out the problem for our system (fig 3.5). Precondition of this experiment is whether we could observe same flock of peak at fig 3.4 with this experiment or not. If yes, the peak flock at fig. 3.4 did not come from the sample but, if not, those peak came from the sample. As shown as in fig. 3.5, when only APTs was injected and separated, we could observe one big main peak and other small peaks which looks like when FITC was separated by CE. However, still “timing of peaks” is irregular so, we could assume there had an unknown factor to change the electric field such as, heating problem from AC motor for rotating rubber belt, electrical breakdown problem for capillary tube etc. (these will be described at chapter 6).

At the moment, this experiment still need an optimization process for reproducible and stable result. We cannot publish these data yet but, we can see the potential of this approach and after the experimental condition will be optimized then we will repeat the whole process again and submit the paper.



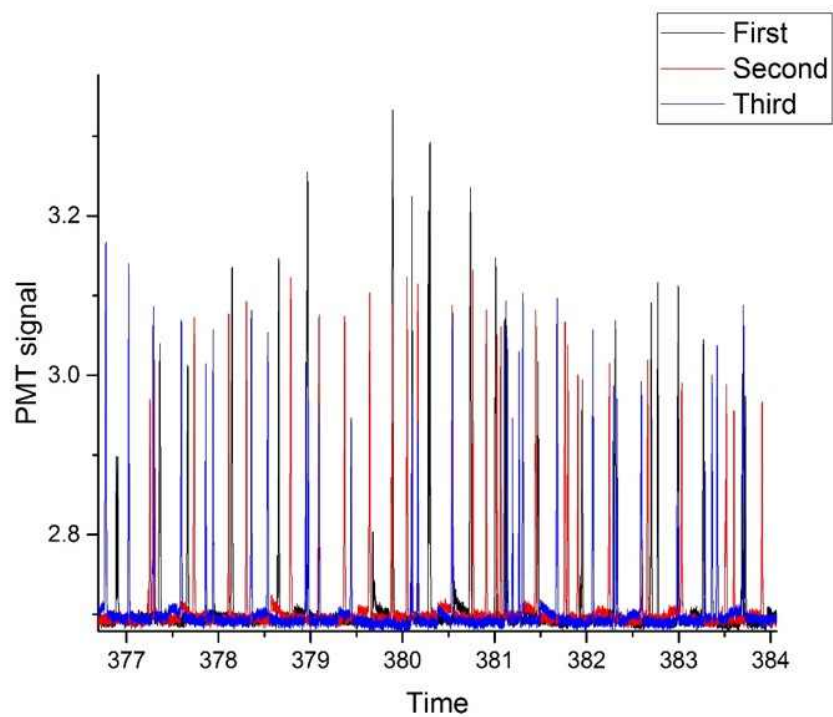


Figure 3.4 Repeating experiment to check the reproducibility. (upper) Peaks were appeared at 370sec. respectively. (middle) Peaks were zoomed in. Peaks were not non-reproducible. (bottom) peaks were not appeared regularly and the CE system looked that it had a problem for the reproducibility.

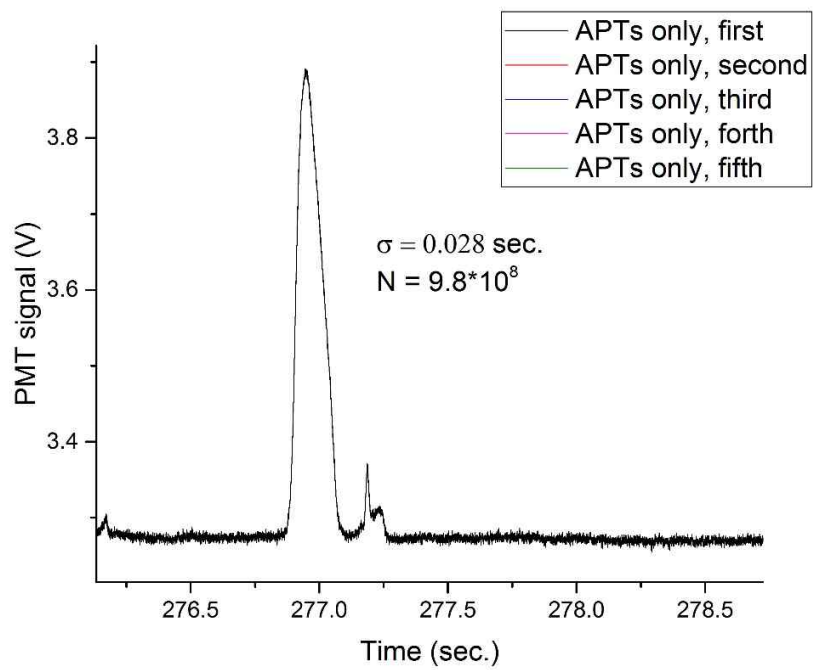
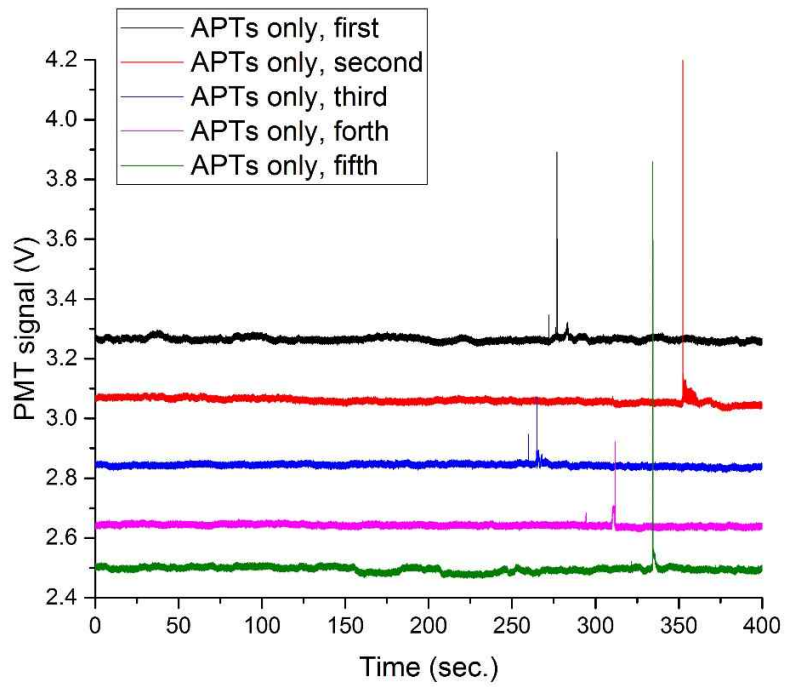


Figure 3.5 Separation experiment only with APTs fluoropore. (upper) 5times repeating experiement only with APTs and couldn't find the peak which has same reproducibility but, the calculation of separation efficiency was very good as like previous result (bottom).

Chapter 4

Outlook

As written from chapter 2 to chapter 5, the usage of VDG for CE and applications with amino acids and carbohydrates were successfully done. We used high applied voltage with VDG for CE which could be explained by ohm's law and, according to the theory, high applied voltage was generated by increasing total resistance of capillary tube which could be adjust by decreasing the ionic strength of BGE and decrease the inner diameter of capillary. Also, for precise sample injection, hydro-dynamic sample injection system with 2 phase injector and on chip-CE was considered and developed. Base on the development those things, integration between VDG CE system and precise sample injection (hydrodynamic sample injection method and using microfluidic chip) will be considered as a further work. Moreover, integration VDG CE system with mass spectroscopy (MS) will be also considered. After optimization process for preventing electrical breakdown of fused silica capillary, applying ultra-high voltage (over 1MV) by pelletron will be considered and performed.

Chapter 5

Appendix

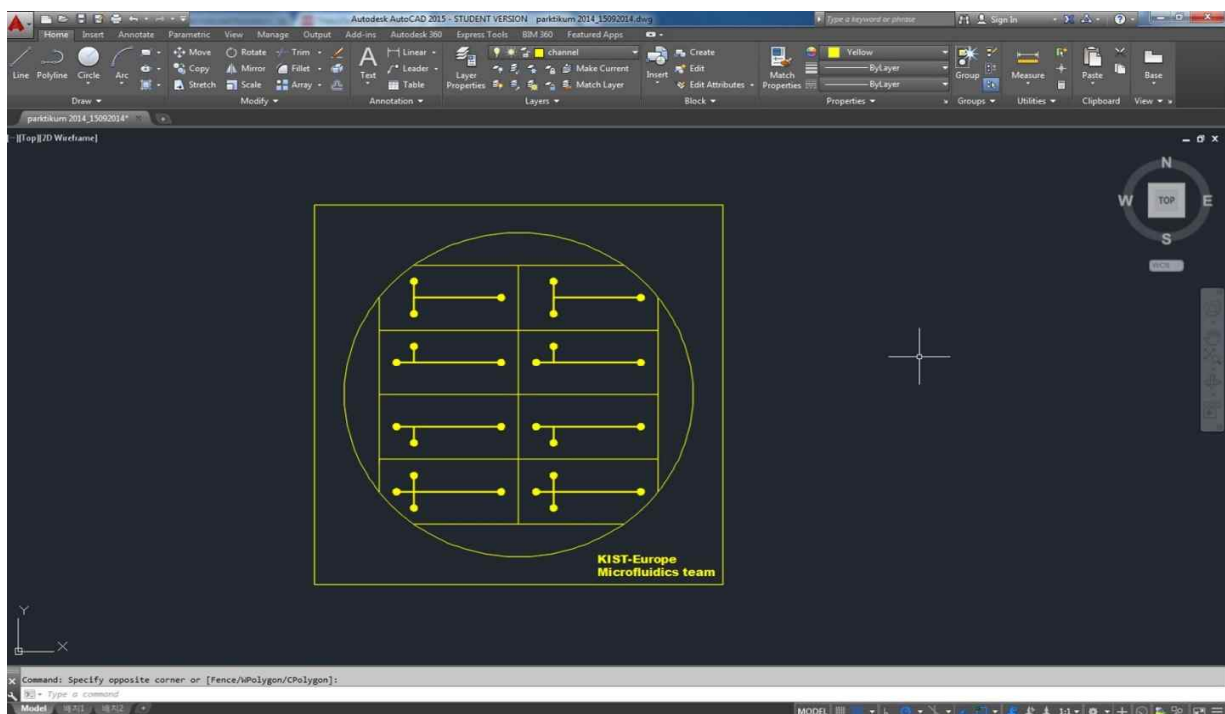
5.1 Chip fabrication and Sample injection methods for CE

5.1.1 Glass chip fabrication

As described in the previous chapter briefly about the construction of microfluidic system for on chip capillary electrophoresis. In order to fabricate the glass CE chip need a standard photolithography process. This process is consist with mainly two big part – patterning structure and etching process. Table 1 will be shown more detail parameters and processes for glass chip fabrication.

Design structure and glass wafer preparation

For the fabrication process of chip, first of all, design structure is needed. Normally, design chip layout can be done by some of professional drawing software such as AutoCAD or Cadence (Figure 4.1).



SPLIT-HUCE M1

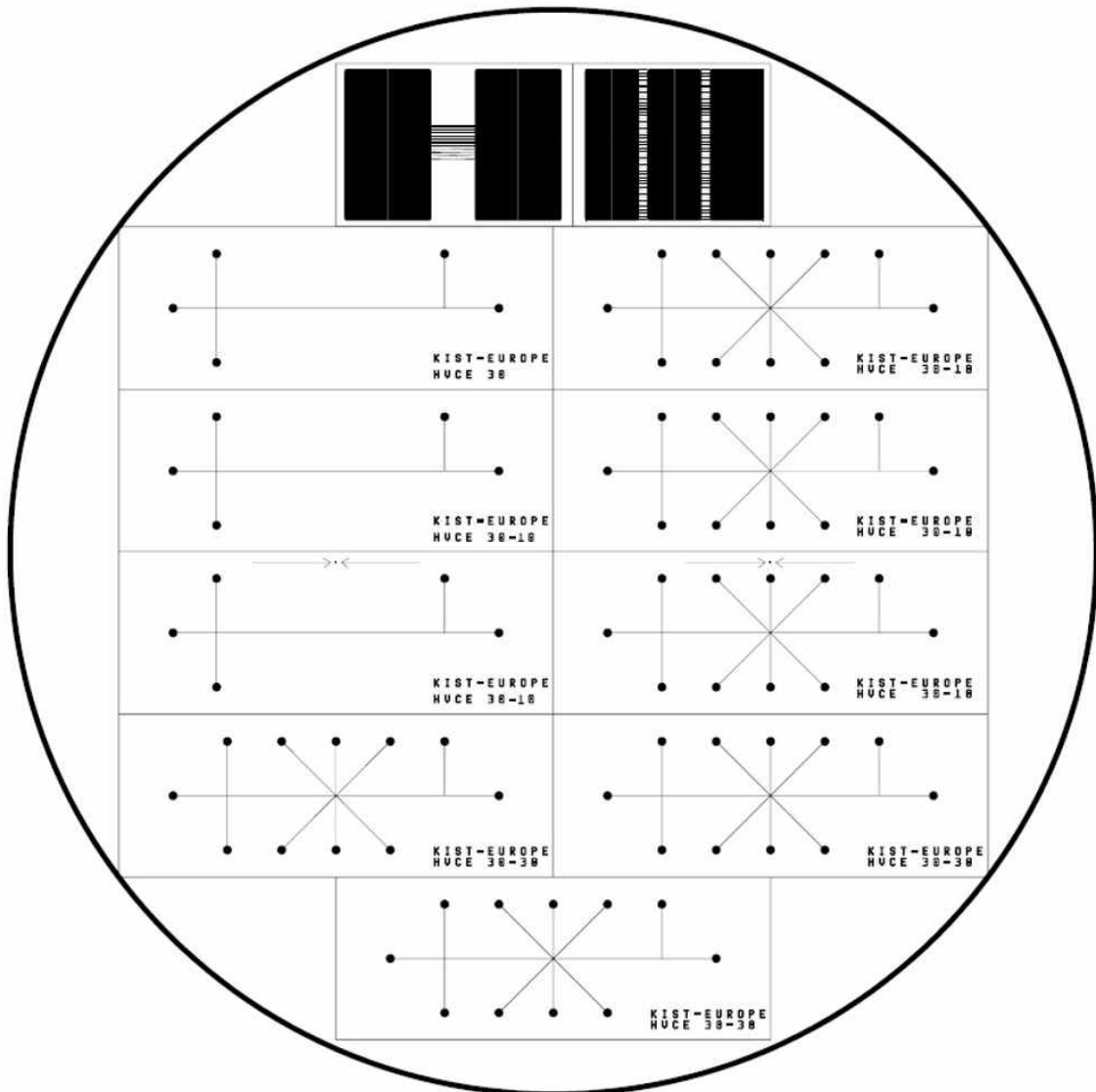


Figure 5.1. (Upper) Design the structure for glass chip fabrication process with AutoCAD software. (Bottom) control plot for 5inch Mask design.

After the design the structure, 5 inch size photo mask can be printed by professional mask printing company (in our case, we printed out our mask at “Rose Fotomasken GmbH, Germany). Depending on the size of structure, material of mask can be decided, for example, FCG (Film combine glass, normally $>10\mu\text{m}$ channel or line width), Cr mask (less than $5\mu\text{m}$ channel or line width). Once mask

is gotten, glass wafer needs to be prepared. In order to buy glass wafer, normally, special company for glass wafer was used for instance Plan optic GmbH Germany (for borosilicate 33 glass wafer). And then, for prevention of photoresist layer, masking layer needs to be sputtered onto the glass wafer. Generally, for the masking layer, Cr-Au is used which thickness is 200Å-1000Å (Figure 4.2).



Figure 5.2. Making layer deposition onto the glass wafer to prevent photoresist layer.

Patterning structure and etching metal layers

After finished the preparation of glass wafer, photoresist need to be spin coated. Depends on the size of the structure, the viscosity of photoresist needs to be decided. For example, AZ 1518 is a low viscosity photoresist which is suitable for thin channel or line width and AZ 4620 is higher viscosity photoresist than AZ1518 so, it is suitable for patterning thicker channel or line. For spin coating of photoresist needs to be followed standard protocol which is provided by the provider of photoresist (normally, 4000rpm for 30sec with 500rpm acceleration for 10~15sec.).



Figure 5.3. Spin coating photo resist onto the masking layer at 4000rpm for 30sec.

After spin coating of photoresist is done, glass wafer needs to be pre-baked on the hot plate at 95°C for 90sec. Then, the wafer with photoresist can be exposure by mask aligner. Usually, mask aligner has two different wavelength and power of UV light Ch1 (365nm, 18mW/cm²) and Ch2 (405nm, 30mW/cm²) so, before exposure UV light on the wafer, standard protocol for photoresist must be defined or checked. 5 inch mask (Cr or FCG photomask) is loaded and aligned, after that UV light is exposure by the following of standard protocol (Figure 4.4).

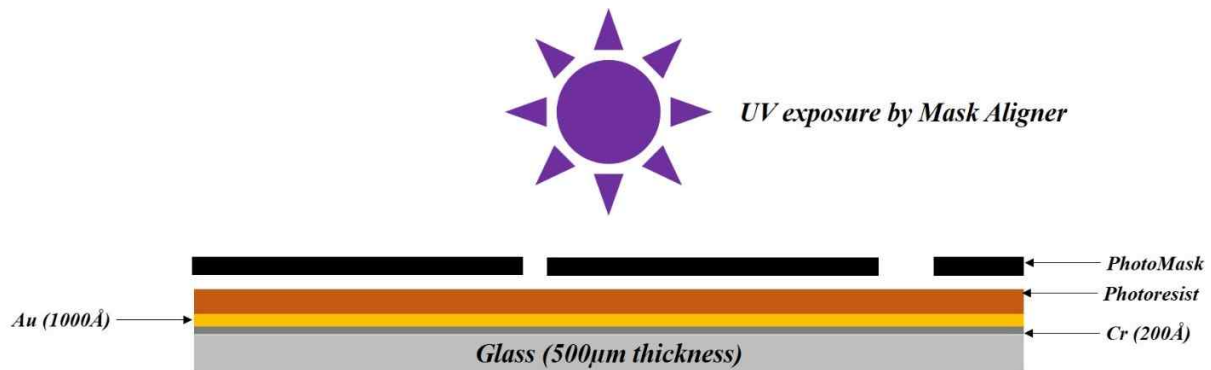


Figure 5.4. Glass wafer is exposure with UV light by Mask Aligner.

After the exposure, glass wafer have to be hard-baked (95°C for 2~3min.) before developing process. When the hard-baking process is finished, exposure wafer needs to be dip into developer solution (OPD4262) and the pattern onto the wafer is developed by the solution (Figure 4.5).

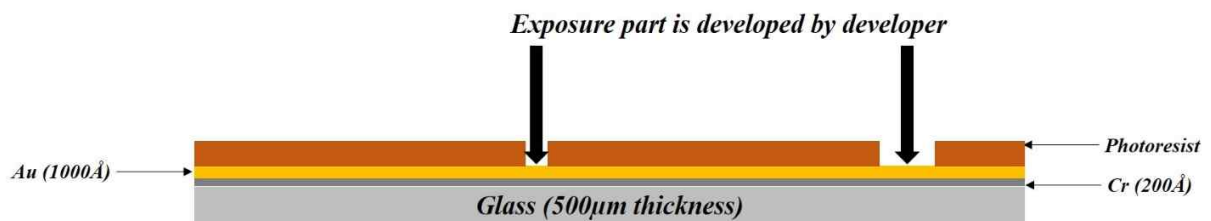


Figure 5.5. Exposure glass wafer is developed by developer

When the developing process is done, Cr-Au layer need to be etched by specific etchant. The composition of Au etchant is KI : I² : DI = 4g : 1g : 40ml. So, developed glass wafer need to be dip into gold etchant first and then gold layer needs to be etched until grey color of Cr layer visible. Then Cr layer can be etched by Cr etchant. The composition of Cr etchant is Ceric ammonium nitrate : Perchloric acid : DI = 10.9% : 4,25% : 84.85%. So, glass wafer need to be dip into the Cr etchant until the pattern can be seen transparent. After metal layers is etched properly, glass wafer is prepared completely to be etched for microfluidic channel. And then glass is etched by 25 % of fluoric acid (HF). Etching rate of 25% of HF is 1µm/min so, if the channel need to be 5µm depth then glass wafer need to be dip into the solution for 5 min (Figure 4.5). After done whole process for the etching, rest of photoresist can be removed by acetone and rest of Au-Cr layers can be removed by the etchants.

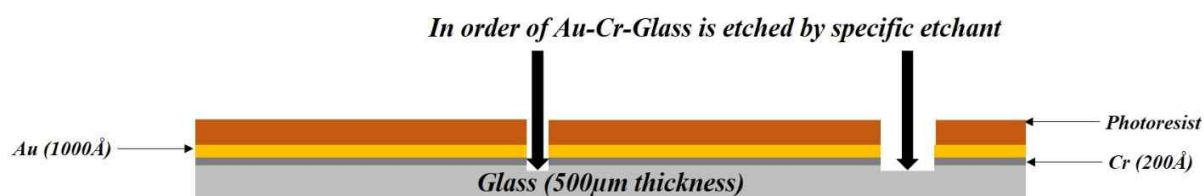


Figure 5.6. Metal layer etching and glass etching by specific etchant.

Powder blasting and glass bonding.

The most common method for making inlet and outlets is power blasting. For this process, another photomask need to be designed which is used only for the location of inlets and outlets on the structure. And, high viscosity photoresist should be spin coated and the in/outlets location need to be patterned by standard lithography process. Then, very fine powder is sprayed with very high pressure onto the patterned wafer and then in/outlet is made. Depends on the size of powder, the roughness can be decided between 0.8~2.5 μm. And then, upper glass substrate (powder blasted glass wafer) and bottom glass substrate (etched glass wafer) is bonded by thermal bonding process. After thermal bonding process, bonded glass wafer is ready to be diced by standard dicing protocol and diced (Chapter 6.1).

5.1.2. Sample injection method for CE

To get the high separation efficiency in CE, precise and optimal sample injection must be performed because of concerning total variance of band broadening which will be discussed in next chapter. Normally in CE, electro-kinetic sample injection method and hydrodynamic sample injection method is used. Both injection methods has fulfilled to inject precise sample amount into the capillary tube. However, depends on the application, injection methods needs to be decided after very careful consideration. Generally, hydrodynamic sample injection method is more precise and can inject optimal amount of sample into the capillary tube but, for viscous sample, hydrodynamic sample injection is cumbersome. So, electrokinetic sample injection methods is easier for higher viscosity of sample.

Electrokinetic sample injection method

Electrokinetic sample injection can be performed by electrokinetic force (Figure 4.5). So, injecting precise and optimal amount of sample, some of parameters need to be known such as,

electrophoretic mobility of sample, electroosmotic mobility, electric field strength, radius of capillary tube, concentration of sample and injection time. (Equation 5.1)

$$Q = (\mu_e + \mu_{eof}) * E\pi r^2 C t \quad (5.1)$$

Where, μ_e is electrophoretic mobility of sample, μ_{eof} is electroosmotic mobility, E is electric field strength, r is radius of capillary tube, C is concentration of sample and t is injection time. According to above equation, amount of injection sample into the capillary tube can be calculated and assumed.

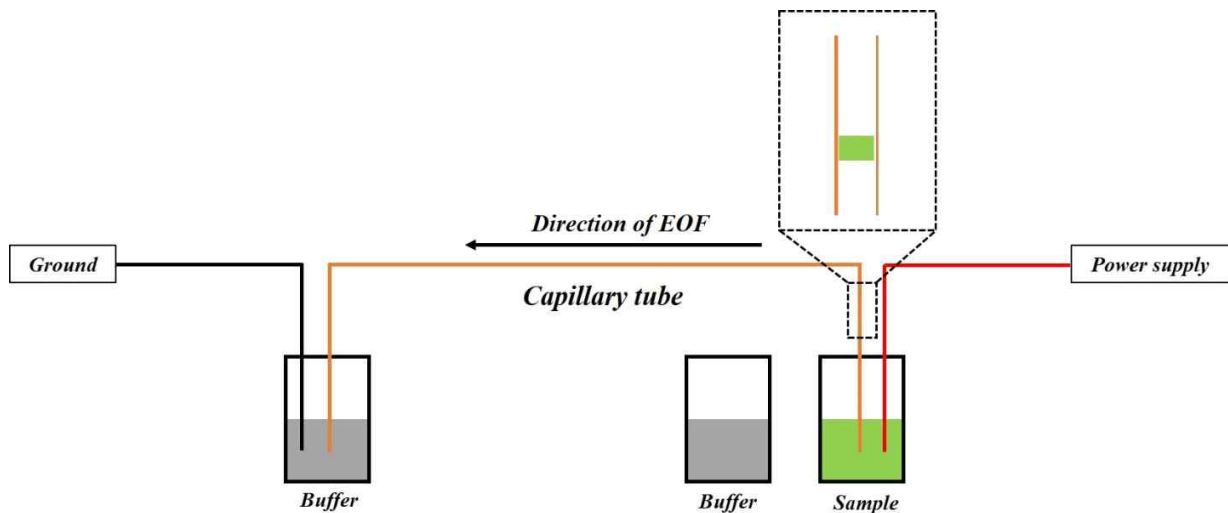


Figure 5.7. Schematic diagram of Electrokinetic injection method. Power supply connected into sample reservoir (red line) and ground electrode (black line) is connected into outlet side of buffer reservoir. Sample is injected by electrokinetic force by power supply (red dot rectangular box) which is occurred by the flow of EOF that is predominant inside of capillary tube.

Advantage of electrokinetic injection method is the same performance for any kinds of sample solution such as, high viscosity sample. Because, any sample can be moved by electroosmotic flow inside of capillary tube which is predominant flow. So, it is not the matter whether the sample has high viscosity or not. However, the different elevation between sample reservoir and buffer reservoir can make additional unexpected flow by difference of pressure which caused by height difference (capillary force). So, when the sample has low viscosity (like water), normally hydrodynamic sample injection method is more precise and less concerning for capillary force. Also, microfluidic chip electrokinetic sample injection method is frequently used because of its convenience to connect with conventional CE system, precise sample injection and easy to observe with microscope.

Hydrodynamic sample injection method

Hydrodynamic sample injection method is more precise and can inject more optimal amount of sample into capillary tube than electrokinetic sample injection method in specific sample condition (low viscosity of sample) and, this injection method doesn't need to concern about selective sample injection problem that can be happened by electrokinetic injection method because of different or opposite direction of mobility for sample electrolytes. Calculation of injection volume with hydrodynamic sample injection can be done by Poiseuille equation (Equation 5.2)

$$V = \frac{\Delta p d^4 \pi t}{128 \eta L} \quad (5.2)$$

Where, ΔP is pressure difference, d is the diameter of capillary tube, t is the injection time, η is the viscosity of sample and L is the total length of capillary tube. Usually, hydrodynamic injection system consists with high pressure pumps, injector, check valve and flow splitter (figure 5.6).

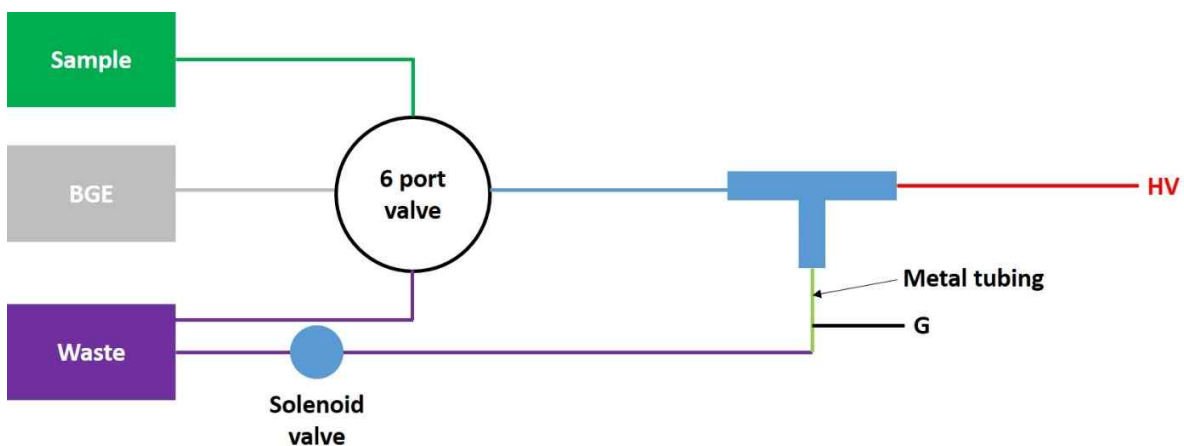
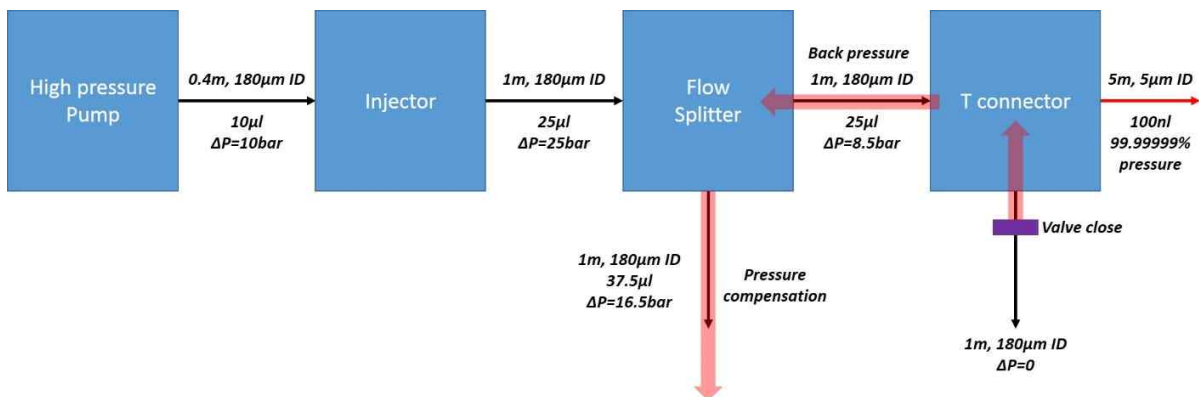


Figure 5.8. (Upper) Flow chart and flow calculation for hydrodynamic injection method. Hydrodynamic injection system consists with high pressure pump, injection, flow splitter and solenoid valve. (Bottom) Schematic diagram of hydrodynamic sample injection system.

5.1.3 On chip capillary electrophoresis

In this thesis, on chip electrophoresis is also considered. Because, miniaturization analytical method has lots of interest for many years. So, after development of microelectrical mechanical system (MEMS), capillary electrophoresis was also dramatically developed by combination with microfluidic system [1,2]. As known as, microfluidic chip electrophoresis has lots of advantages such, can be used for precise sample injection system, short separation channel, consume small amount of sample, easy to make hand held total analysis system and so on. The structure of the microfluidic chip for capillary electrophoresis is consisted with microfluidic channel systems which are connected with various features such as inlet and outlet reservoir that can be connected with electrode for applying voltage, separation chamber, mixing channel regions etc. The size of these microfluidic channel is typically in the range of a few micrometers. Also, normally microfluidic on chip capillary electrophoresis consumes sample from few picoliter to nanoliter for whole separation process. Therefore, on chip CE is one of the best separation method for some of applications such as proteomics or glycomics which need to be analyzed with tiny amount of sample [3-6].

Electrokinetic sample injection method

Sample injection method for on-chip CE need to be decided carefully depends on the application and sample. Normally, on-chip CE, electrokinetic sample injection method is used because of the convenience of experimental setup and easy to control the sample fluid. Hydrodynamic sample injection system for on-chip CE can make a precise sample injection but, this method needs an additional control system such as valve control system for sample flow channel and so on. Figure 1.12 shows brief introduction of electrokinetic sample injection method. Sample was injected and squeezed at the cross section area of CE chip by electrokinetic forces by applied voltage.

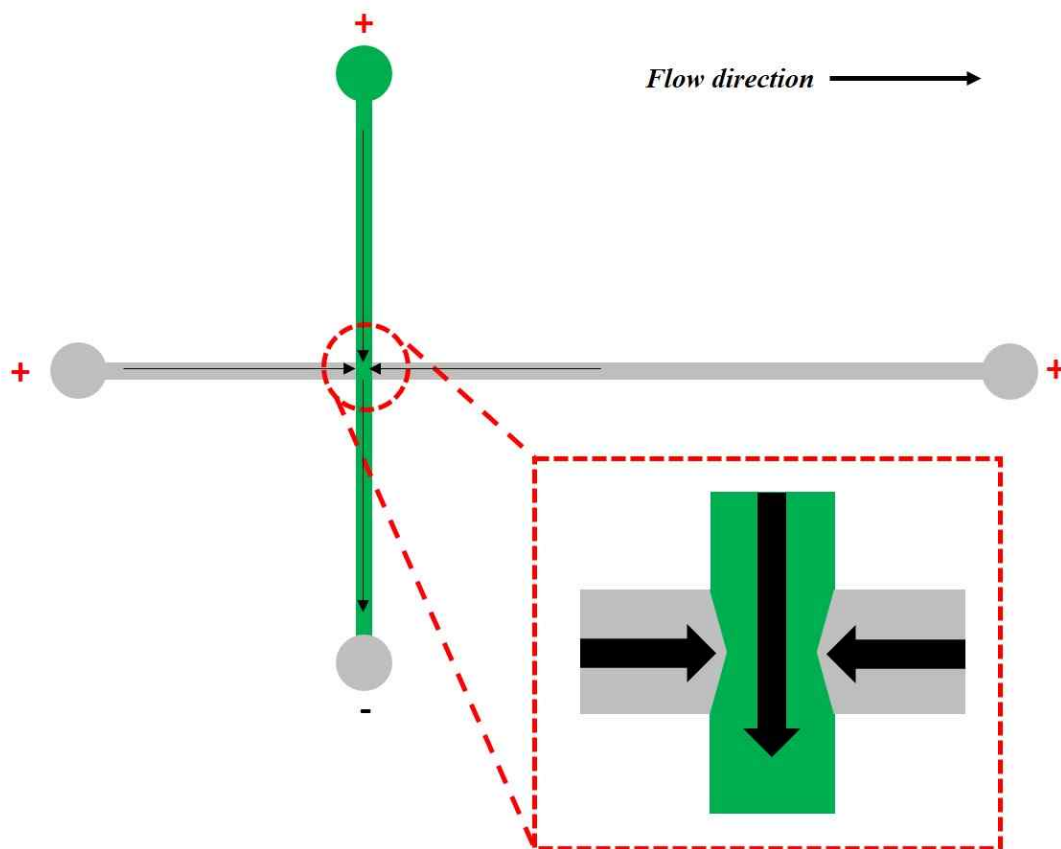
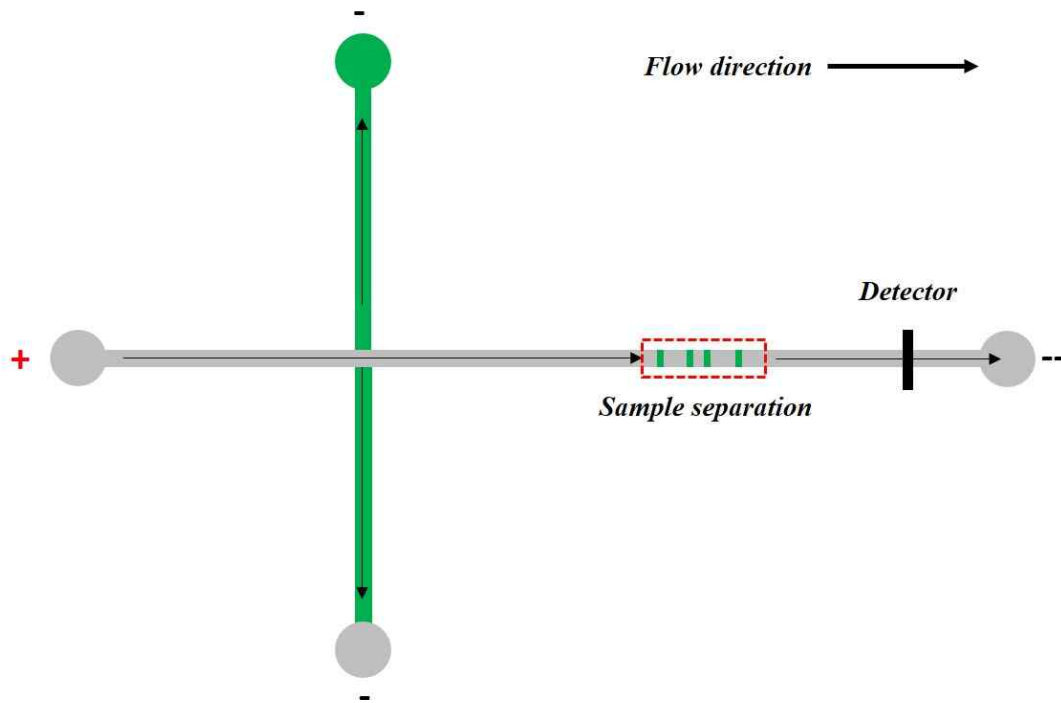


Figure 5.9. Electrokinetic sample injection method for on-chip CE (upper). Sample can be flow only upper to bottom and BGE can be flow to cross section area by electro kinetic force therefore, sample is squeezed (red dot box). Sample is separated by total electrical mobility (bottom). Total electrical mobility is determined the summation of electroosmitic flow and mobility of electrolyte.

Detection method for on-chip CE

Possibility of observation whole separation process through the microscope is the one of the best advantage for on-chip CE. Because of this advantage, fluorescence microscope is frequently used as a detection system for chip CE (Figure 1.13). In order to detect the signal from the separated sample, photomultiplier tube (PMT) is normally used because of its high sensitivity and fast response time. And, PMT signal is collected with the oscilloscope in real-time and then analyzed.

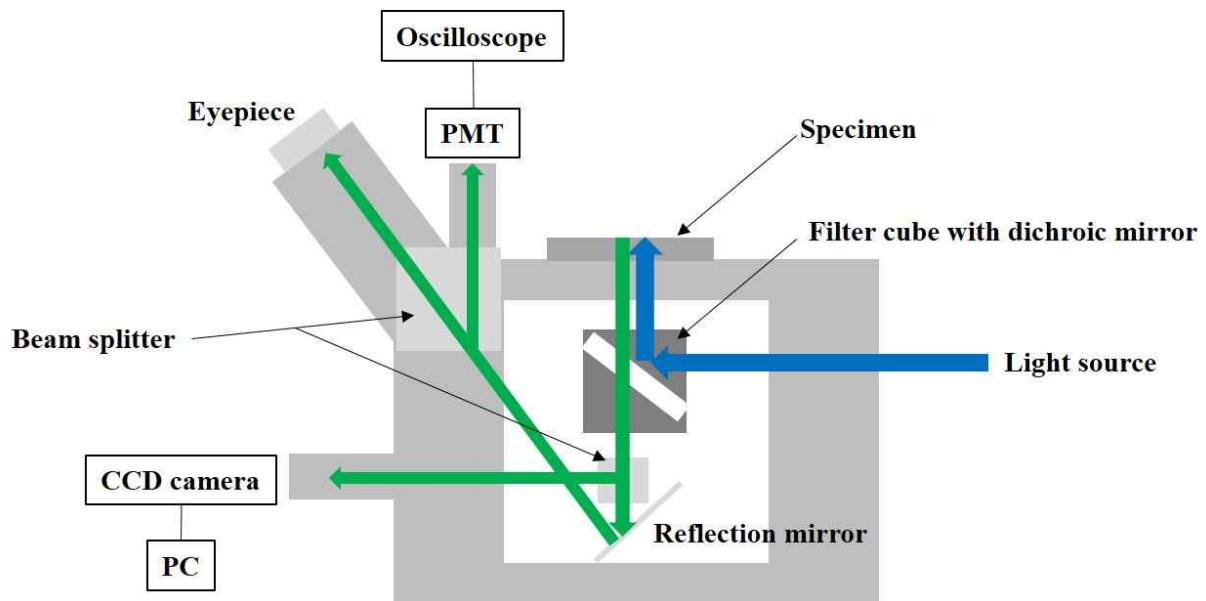


Figure 5.10. Microscopic detection system for on-chip CE. Emission light can be detected with photomultiplier tube (PMT) and oscilloscope is used for collecting signal from PMT.

5.1.4 References

1. Effenhauser, C.S., A. Manz, and H.M. Widmer, Glass chips for high-speed capillary electrophoresis separations with submicrometer plate heights. *Analytical Chemistry*, 1993. 65(19): p. 2637-2642.
2. Seiler, K., D.J. Harrison, and A. Manz, Planar glass chips for capillary electrophoresis: repetitive sample injection, quantitation, and separation efficiency. *Analytical Chemistry*, 1993. 65(10): p. 1481-1488.
3. Adam, T.W. and V.F. Hernan, Using Phase-Changing Sacrificial Materials to Fabricate Microdevices for Chemical Analysis, in *Handbook of Capillary and Microchip Electrophoresis and Associated Microtechniques*, Third Edition. 2007, CRC Press. p. 1419-1439.
4. Sanders, G.H.W. and A. Manz, Chip-based microsystems for genomic and proteomic analysis. *TrAC Trends in Analytical Chemistry*, 2000. 19(6): p. 364-378.
5. Callewaert, N., et al., Total serum protein N-glycome profiling on a capillary electrophoresis-microfluidics platform. *ELECTROPHORESIS*, 2004. 25(18-19): p. 3128-3131.
6. Vanderschaeghe, D., et al., High-Throughput Profiling of the Serum N-Glycome on Capillary Electrophoresis Microfluidics Systems: Toward Clinical Implementation of GlycoHepatoTest. *Analytical Chemistry*, 2010. 82(17): p. 7408-7415.

5.2 Split flow on-chip capillary electrophoresis (SCE)

5.2.1 Introduction

Capillary electrophoresis is one of well-known separation method since 1980s [1, 2]. Until now CE is widely used to separate biological substances and complex chemical compounds [3, 4]. Since middle of 1980s conventional CE based commercial instruments were developed [5, 6] and many researchers who is in the field of analytical chemistry and biology are frequently used the commercial instruments for sample separation method. But, the conventional CE system has some limitations, for example consume large amount of solutions, need long migration times, hard to control the size of sample plug and so on. In these reasons, from early 90s people have considered to use chip based CE system and tried to develop on-chip CE system [7-12]. Because microfluidic based CE chip can achieve many advantages such as lower sample consumption, faster separation time, easier to control sample plug and so on [13-15]. Thus, the on-chip CE technology is getting become promising method in the field of separation methods. However still on-chip CE has several limitations to increase efficiency and resolution. The separation efficiency in CE is very important factor to increase the chance of analysis. According to the equation for number of theoretical plate, the efficiency of CE is determined by applied voltage which means applying higher voltage for CE can achieve higher separation efficiency [16]. Also, achieving the higher resolution of CE people need good injector for sample injection otherwise, normally CE require longer separation channel [17]. But, both methods have a limitation to achieve high plate number in a short length of separation channel vs. high applied voltage and certain applied voltage vs. length of separation channel. For increasing separation efficiency, the application of high voltage is required. However, this is lead to occur joule heating phenomena which can make air bubble inside the capillary tube or channel [18, 19]. Moreover, using longer separation channel to increase resolution can be reason to increase the migration time and the problem of sample diffusion. So, the increase of both parameters is not easy to optimize.

In this chapter, I described “Split flow CE chip” which can easily increase the separation efficiency and resolution with geometrically modified split flow channel and also easy to connect with conventional CE system. With our novel chip, the injected sample plug can be divided proportionally during injection process and separation efficiency can be increased by assembling with conventional high voltage CE system.

5.2.2 Materials and Methods

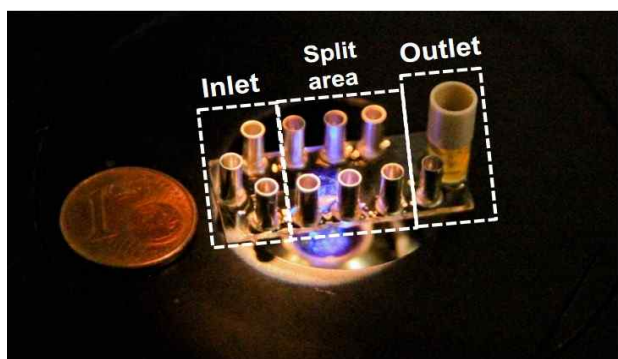
Reagents

Sodium phosphate, Fluorescein isothiocyanate (FITC), and, Amino acids (Glutamic acid, Glutamine, Arginine, Alanine and Lysine) was purchased from Sigma Aldrich (Germany). 99% Acetonitrile was purchased from VWR GmbH (Germany).

For the sample loading and injection, 50mM phosphate buffer was used as running buffer which has pH 9.38 and 0.2mM CTAB was added to the buffer for making reverse electroosmotic flow (EOF) also 15% volume ration of Acetonitrile was used for deproteinization inside of glass chip. 5 different kinds of amino acid were used as a target compound and the concentration of each amino acid was 10mM. For the fluorescence labelling of sample solution, each amino acids compounds was mixed to 5mL FITC which has 1mM and 5mM concentration and the mixture was stored in the dark condition for 12 hours.

Chip preparation

The microfluidic chip was designed using conventional layout editor. 4 inch pyrex glass wafer was used for upper and bottom substrate and general lithography process and glass etching process was used (see Table 5.1). The diameter of the channel was 30 μ m width, 5 μ m depth and the length of separation channel was 20 mm. For sample dividing during injection process, three split flow channels intersected the separation channel resulting in a star shaped geometry (Figure 5.11). And for the outlet, a bond port for 360 μ m OD capillary was connected to make easy for connecting normal capillary tube for further study. For comparison experiment, normal cross shape CE chip was also fabricated. Normal cross shape CE chip has same diameter and separation channel length as fabricated split flow CE chip.



- Width : 30 μ m
- Depth : 5 μ m
- Hole diameter : 800 μ m
- Separation channel: 15mm
- Material : Glass-Glass
- Manufactured in Twente university

Figure 5.11 Experimental picture for split flow CE chip which has 30 μm width and 5 μm depth. It was fabricated MESA⁺ at Twente University.

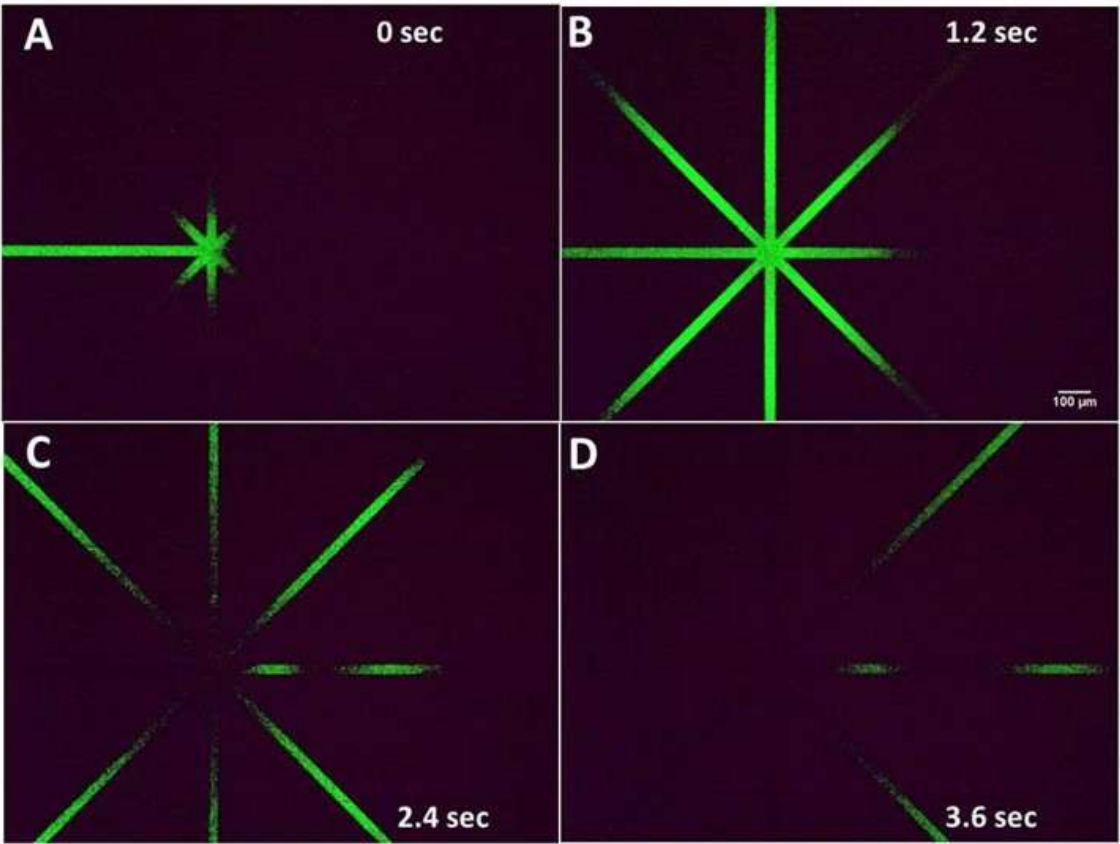
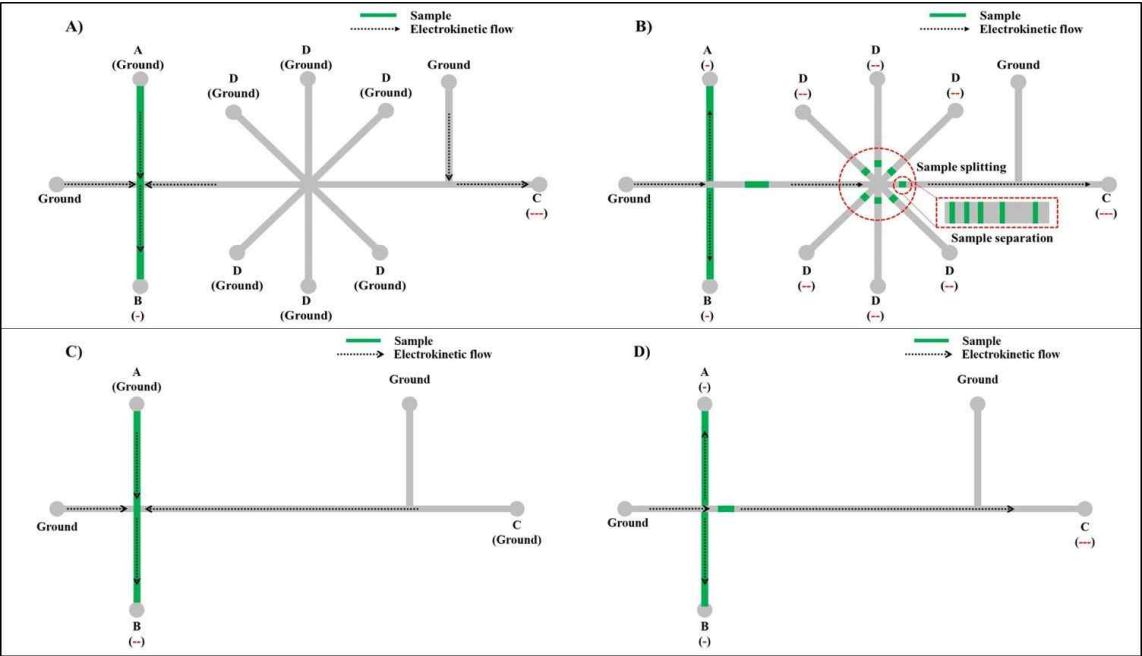


Figure 5.12 (Upper) Schematic diagram for sample loading process for SCE and normal CE chip, sample was squeezed in cross section by electro kinetic force (A) and sample injection process through SCE (B), sample was injected by electro kinetic force and the sample was divided at the split flow channel in the middle of separation channel. Each red dot circle and line indicate pictures from the experiment. Sample loading process for normal cross shape CE chip (C) and sample separation process in normal CE chip (D). (Bottom) Experimental picture for separation process at the split flow channel in the middle of SCE chip. Sample electrolytes are split at the star shape geometry.

Electrical equipment

Up to 3kV voltage potential was applied by programmable voltage sequencer (HVS448 3000D, LabSmith, USA). Each sample loading step and sample injection step was programmed by the software of sequencer. The sample separation was observed by fluorescence microscope (Axiovert 100, CarlZeiss GmbH, Germany) which was assembled with 470nm wavelength LED module (M470L3-C4, Thorlabs, USA) for sample excitation. And motorized stage was used to make sure the distance of the detection by photomultiplier tube (PMT). Experimental images were taken by monochromatic CCD camera (MFcool, Jenoptik GmbH, Germany). For the detection, Photomultiplier tube (PMT, H10722-01, Hamamatsu, Japan) was used to detect emitted light from separated sample band and, oscilloscope (DPO3014, Tektronix, Germany) collected amplified signal from the PMT. Data was processed by Origin software (Originlab, USA).

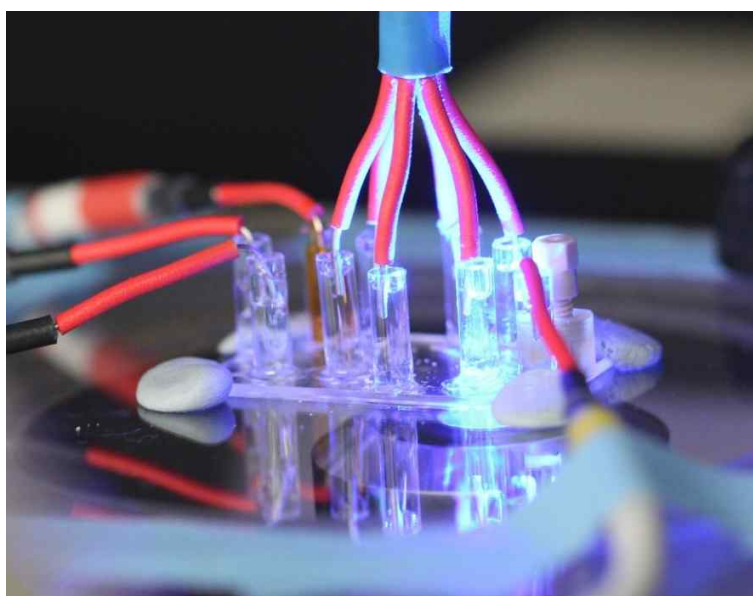


Figure 5.13 Experimental setup for split flow CE. 8 channel sequencer was used to apply voltage to each reservoirs and fluorescence microscope with PMT was used for detection. Data was collected with Oscilloscope.

Electric field simulation

Electric field through the separation channel was simulated for SCE and normal CE chip using LTspice IV (Linear technology, USA). Each channel was represented as a resistor which related with the length of channel and applied desired voltage potential through the separation channel.

On-chip CE experiment

Split flow intersected CE glass chip was used for sample loading and injection. CE chip is consisted of three part, inlet, split flow channel and outlet part. Electrode C (0kV) and D (1.5kV) were connected to sample inlet part for sample loading (Figure 5.11). For the sample injection, electrode was switched to A (0kV), B (3kV) and E (1kV) (Figure 3.1). Sample separation was detected in two locations; one is 8.5mm far from cross section (before split flow channel) and another one is 18.5mm far from the cross section which is placed after split flow channel. For the comparison experiment, normal cross shape CE chip was used (Figure 5.11).

5.2.3 Theoretical background

Equation for theoretical number of plate

In CE, the number of theoretical number of plate is determined by the applied voltage (V) (Equation 1.1). Usually to increase the separation efficiency of CE can be achieved by applying high voltage. However, generally applying high voltage to CE system can be occurred joule heating problem. And, accurate separation efficiency could be calculated with the consideration for total variance of band broadening. So, the number of theoretical plate for CE can be represented with the length of separation channel (L) and the total variance of band broadening (σ) value (Equation 5.2).

$$N = \frac{L^2}{\sigma^2} \quad (5.3)$$

According to equation 2, when the total variance of band broadening is decreased the number of theoretical plate can be increased. In term of the total variance of band broadening (σ) can be

consisted with the value for diffusion of analyte (σ_{diff}) and the length of injected sample plug (σ_{inj}) during the injection process (Equation 5.3).

$$\sigma_{total}^2 = \sigma_{diff}^2 + \sigma_{inj}^2 + \sigma_{joule\ heating}^2 + \dots \quad (5.4)$$

Each sigma value can be explained with the migration time (t_m), diffusion coefficient (D) and the length of injection plug (w) (Equation 5.4).

$$\sigma_{diff}^2 = 2Dt_m, \sigma_{inj}^2 = \frac{w^2}{12} \quad (5.5)$$

So, the number of theoretical plate could be calculated with the consideration for the total variance of band broadening (Equation 5.5)

$$N = \frac{L^2}{\sigma_{diff}^2 + \sigma_{inj}^2} = \frac{L^2}{2Dt_m + \frac{w^2}{12}} \quad (5.6)$$

According to the equation 5.5, separation efficiency for CE is increased by the decreasing the length of injected sample plug. Therefore, in this report we designed split flow channel intersected CE chip which could decreased the value for the total variance of band broadening by decreasing the length of injected sample plug during injection process.

Calculation for joule heating in CE chip

Increasing the separation efficiency for CE, applying high voltage is required. However, occasionally joule heating is occurred by current when the high voltage is applied for CE. In our case, we applied 3kV through the separation channel so, we needed to make sure our system is free from joule heating problem. For calculation of joule heating in glass chip, the heat release per unit volume in solution need to be calculated (Equation 5.6).

$$Q = E^2 \gamma \epsilon \quad (5.7)$$

So, the heat release per unit volume in solution (Q) is consist with electric field (E , V/m), molar conductivity of the solution (γ , $m^2/mol \cdot \Omega$), concentration of the solution (c , mol/m³) and the total porosity of the medium (ϵ) (Eqn. 6). In our case, molar conductivity of our buffer is 0.015 $m^2/mol \cdot \Omega$, porosity of the medium is 0.8 and the concentration of buffer is 50mM. Therefore, Q value in our case is 900W/m³. For the calculation of the temperature excess at the center of the microfluidic chip can be calculated with below equation (Equation 5.7).

$$\theta_{core} = \frac{Qd_c^2}{16k} \quad (5.8)$$

In equation 7, d_c and k represent diameter of core and thermal conductivity of solutions. According to the equation 6, we could substitute 900W/m^3 as a Q value, $5\mu\text{m}$ for diameter of the channel and $0.6\text{W/m}\cdot\text{K}$ for the thermal conductivity of buffer. So, the temperature excess in the core region of our glass chip is $2.3\text{E-}9$ kelvin. Therefore, joule heating problem is not occurred in our case. So, we could neglect the temperature effect for the total variance of band broadening.

5.2.4 Results and Discussions

Sample dividing in split flow channel

In order to the theoretical number of plate if the length of injected sample plug is divided, the separation efficiency of CE can be increased. Because, the number of theoretical plate is represented with the total variance of band broadening (σ), and the length of separation channel (L). The total variance of band broadening is the summation of the value for the diffusivity of sample and length of injected sample plug, joule heating, detection volume, and so on. But, in term of the sigma by diffusivity is the constant value of sample solution so it cannot be changed or modified. Therefore, decreasing the length of sample plug is one of method which can be considered to increase the separation efficiency in on-chip CE. So, in our case with the SCE during the injection process, 5amino acids sample mixture was divided by split flow channel. Each split flow channel divided sample plug evenly and the sigma (σ) value in total variance of band broadening (Eqn. 5.4) was decreased at the separation channel after split flow.

Simulation of electric field for normal CE chip and SCE

Electric field was simulated for normal CE chip and SCE with LTspice IV software (Figure 5.12).

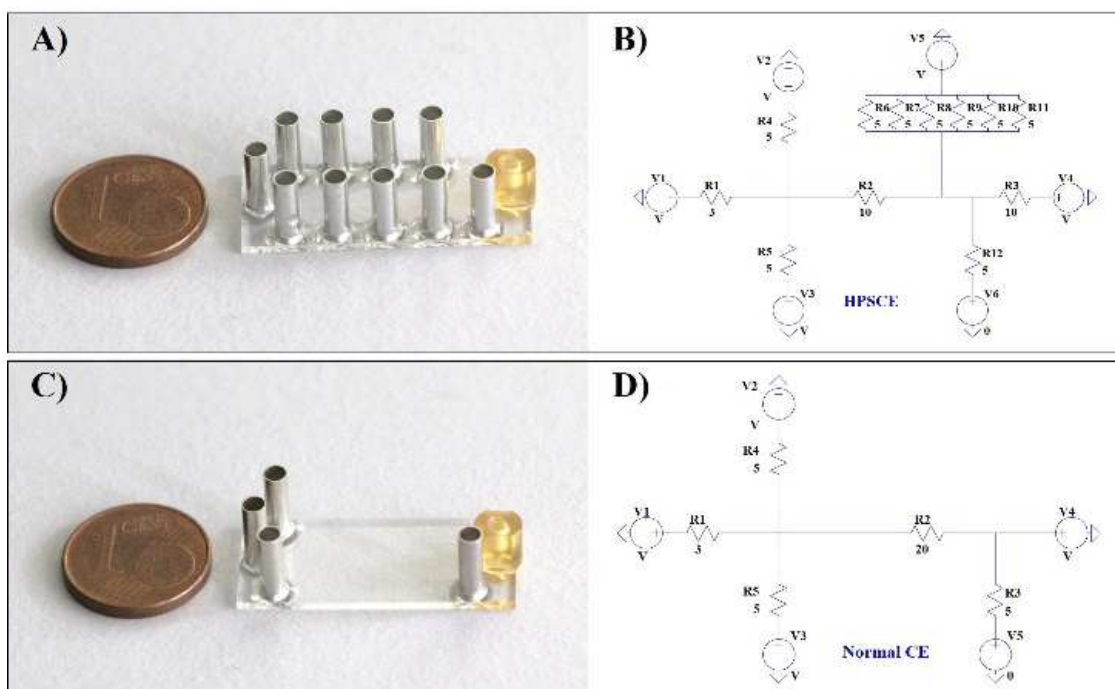


Figure 5.14. SCE (A) and circuit diagram for SCE (B) and Normal CE chip (C) and circuit diagram for normal CE chip (D)

Each microfluidic channel was represented as a resistor which related with the length of channel. According to the simulated result, 131V/mm potential was applied across to SCE and 134.5V/mm potential was applied to normal CE chip. So, the SCE has lower electric field at the separation channel than normal CE chip.

Comparison experiment of separation efficiency

5 amino acids sample mixture solution was loaded and separated by SCE (Figure 5.13 left) and normal cross shape CE (Figure 5.13right). Sample mixture were applied from reservoir A and the phosphate buffer was loaded to other reservoirs as running buffer for CE.

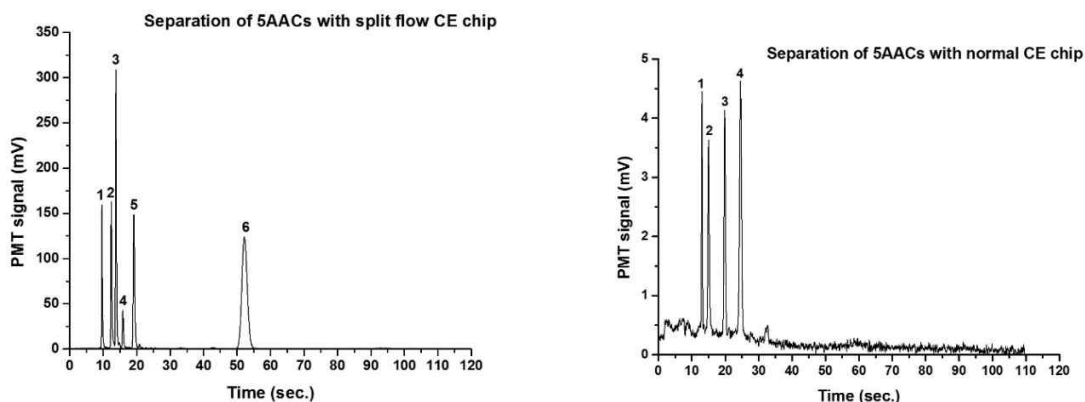


Figure 5.15. amino acids separation with SCE (Left) and normal cross shape CE chip (Right) at 18.5mm from the cross section. Each number represent 1: free FITC, 2: GLU, 3: GLN, 4: Ala, 5: Arg, 6: Lys

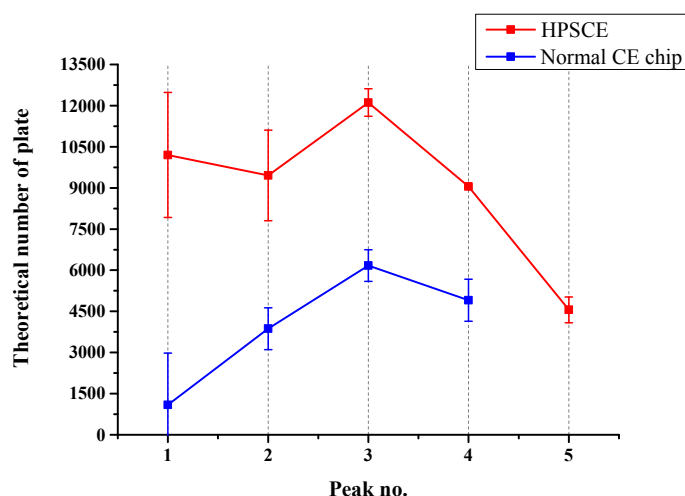


Figure 5.16. Comparison of theoretical number of plate for SCE and normal CE chip. SCE has approximately 300% better separation efficiency than normal CE chip.

Our split flow CE chip can separate 5 amino acids with higher separation efficiency than normal cross shape CE chip. The average of theoretical number of plate for split flow CE chip is 12000 which is approximately 300% higher than normal CE chip even the electric field was lower than normal one through the separation channel. Also, split flow CE chip could achieve high reproducibility and stable injection and separation (Table 3.1).

Unit: sec.

<i>Peak no.</i>	<i>First</i>	<i>Second</i>	<i>Third</i>	<i>Avg.</i>	<i>SD</i>
<i>1</i>	<i>9.26198</i>	<i>9.63267</i>	<i>9.83309</i>	<i>9.575913</i>	<i>± 0.289</i>
<i>2</i>	<i>11.88007</i>	<i>12.46391</i>	<i>12.80042</i>	<i>12.38147</i>	<i>± 0.465</i>
<i>3</i>	<i>13.08338</i>	<i>13.83407</i>	<i>14.27183</i>	<i>13.72976</i>	<i>± 0.601</i>
<i>4</i>	<i>15.00446</i>	<i>15.90529</i>	<i>16.44331</i>	<i>15.78435</i>	<i>± 0.727</i>
<i>5</i>	<i>17.99632</i>	<i>19.2073</i>	<i>19.97755</i>	<i>19.06039</i>	<i>± 0.998</i>
<i>6</i>	<i>52.32741</i>	<i>52.24366</i>	<i>51.81002</i>	<i>52.12703</i>	<i>± 0.277</i>

Table 5.2 Novel designed split flow CE chip could achieve high reproducibility for sample separation in CE.

5.2.5 Conclusion

In this chapter, novel shape split flow CE chip was described and explained. According to the result, SCE couldn't be achieved high separation efficiency but, could be shown star shape geometry can separate injected sample plug during separation process. For the further study, when experimental conditions (channel width, separation channel length etc.) will be optimized that high separation efficiency can be achieved. And also, the convenience for connecting with normal capillary tube by easy accessing bond port connector at the outlet, this chip can be easily assembled with our high voltage CE system which will be used for precise sample injection system.

5.2.6 Reference

1. Smith, R.D., C.J. Barinaga, and H.R. Udseth, Improved electrospray ionization interface for capillary zone electrophoresis-mass spectrometry. *Analytical Chemistry*, 1988. 60(18): p. 1948-1952.2.
2. Ewing, A.G., R.A. Wallingford, and T.M. Olefirowicz, CAPILLARY ELECTROPHORESIS. *Analytical Chemistry*, 1989. 61(4): p. 292A-303A.
3. Rizzi, A., Fundamental aspects of chiral separations by capillary electrophoresis. *ELECTROPHORESIS*, 2001. 22(15): p. 3079-3106.
4. Pedersen-Bjergaard, S. and K.E. Rasmussen, Liquid-Liquid-Liquid Microextraction for Sample Preparation of Biological Fluids Prior to Capillary Electrophoresis. *Analytical Chemistry*, 1999. 71(14): p. 2650-2656.
5. Zemann, A.J., et al., Contactless Conductivity Detection for Capillary Electrophoresis. *Analytical Chemistry*, 1998. 70(3): p. 563-567.
6. Lazaruk, K., et al., Genotyping of forensic short tandem repeat (STR) systems based on sizing precision in a capillary electrophoresis instrument. *ELECTROPHORESIS*, 1998. 19(1):p.86 -93.
7. Woolley, A.T., et al., Functional Integration of PCR Amplification and Capillary Electrophoresis in a Microfabricated DNA Analysis Device. *Analytical Chemistry*, 1996. 68(23): p. 4081-4086.
8. Poinot, V., et al., Recent advances in amino acid analysis by capillary electrophoresis. *ELECTROPHORESIS*, 2012. 33(1): p. 14-35.
9. Harrison, D.J., et al., Capillary electrophoresis and sample injection systems integrated on a planar glass chip. *Analytical Chemistry*, 1992. 64(17): p. 1926-1932.
10. Fritzsche, S., P. Hoffmann, and D. Belder, Chip electrophoresis with mass spectrometric detection in record speed. *Lab on a Chip*, 2010. 10(10): p. 1227-1230.

11. Effenhauser, C.S., et al., High-Speed Separation of Antisense Oligonucleotides on a Micromachined Capillary Electrophoresis Device. *Analytical Chemistry*, 1994. 66(18): p3. 2949-2953.
12. Woolley, A.T. and R.A. Mathies, Ultra-High-Speed DNA Sequencing Using Capillary Electrophoresis Chips. *Analytical Chemistry*, 1995. 67(20): p. 3676-3680.
13. Baldwin, R.P., et al., Fully Integrated On-Chip Electrochemical Detection for Capillary Electrophoresis in a Microfabricated Device. *Analytical Chemistry*, 2002. 74(15): p. 3690-3697.
14. Kenyon, S.M., M.M. Meighan, and M.A. Hayes, Recent developments in electrophoretic separations on microfluidic devices. *ELECTROPHORESIS*, 2011. 32(5): p. 482-493.
15. Fang, Q., G.-M. Xu, and Z.-L. Fang, A High-Throughput Continuous Sample Introduction Interface for Microfluidic Chip-based Capillary Electrophoresis Systems. *Analytical Chemistry*, 2002. 74(6): p. 1223-1231.
16. Jorgenson, J.W. and K.D. Lukacs, Zone electrophoresis in open tubular glass capillaries. *Analytical Chemistry*, 1981. 53(8): p.1298-1302.
17. Jacobson, S.C., et al., High-Speed Separations on a Microchip. *Analytical Chemistry*, 1994. 66(7): p. 1114-1118.
18. Grushka, E., R.M. McCormick, and J.J. Kirkland, Effect of temperature gradients on the efficiency of capillary zone electrophoresis separations. *Analytical Chemistry*, 1989. 61(3): p. 241-246.
19. Swinney, K. and D.J. Bornhop, Quantification and evaluation of Joule heating in on-chip capillary electrophoresis. *ELECTROPHORESIS*, 2002. 23(4): p. 613-620.

5.3 Supplement materials

5.3.1. Fabrication process for split flow CE glass chip.

Step	Process		Comment
1	Bottom wafer		
2	<p>Substrate Borofloat BF33- 500 μm (#subs114)</p>	<p>NL-CLR-Cupboard cleanroom Supplier: Schott Glas: www.schott.com/borofloat</p> <ul style="list-style-type: none"> • Type: Borofloat 33 • C.T.E.: $3.25 \times 10^{-6} \text{ K}^{-1}$ • T glass: 525°C • T anneal: 560°C • T softening: 820°C • Diameter: $100.0 \text{ mm} \pm 0.3 \text{ mm}$ • Thickness: $0.5 \text{ mm} \pm 0.025 \text{ mm}$ • Roughness: $< 1.0 \text{ nm}$ • TTV: $< 5 \mu\text{m}$ • Surface: DSP • Edge: C-edge • Flat: 32.5 mm (Semi) • Sec. Flat: 18 mm (acc to SEMI) • Price 40 euro • Etch rate HF 25%: $1 \mu\text{m}/\text{min}$ • Etch rate BHF (1:7): $20\text{-}25 \text{ nm}/\text{min}$ • Etch rate HF 1%: $8.6 \text{ nm}/\text{min}$ 	Number of wafers = 2
3	Clean HNO3 1&2 (#clean105)	<p>NL-CLR-WB16</p> <ul style="list-style-type: none"> • Beaker 1: HNO3 (99%) 5min • Beaker 2: HNO3 (99%) 5min 	
4	Quick Dump Rinse (QDR)	NL-CLR-Wet benches	

	(#clean119)	<p>Recipe 1 QDR: 2 cycles of steps 1 till 3,</p> <p>1- fill bath 5 sec</p> <p>2- spray dump 15 sec</p> <p>3- spray-fill 90 sec</p> <p>4- end fill 200 sec</p> <p>Recipe 2 cascade rinsing: continuous flow</p> <p>Rinse till the DI resistivity is > 10 ΩM</p>	
5	<p>Substrate rinsing/drying</p> <p>Semitool</p> <p>(#clean121)</p>	<p>NL-CLR-Wet Benches</p> <p>Semitool spin rinser dryer</p> <p>Apply always a single rinsing step (QDR)</p> <p>before using the Semitool</p> <p>Use dedicated wafer carrier of rinser dryer</p> <p>Parameters/step</p> <ul style="list-style-type: none"> • rinse in DI: 30 sec: 600 rpm • Qrinse in DI: 10.0 MΩ; 600 rpm • N2 purge: 10sec; 600 rpm • drying 1: 280 sec; 1600 rpm • drying 2: 0000 - 0000 <p>Unload wafer</p>	
6	<p>Sputtering of Cr</p> <p>(#film117)</p>	<p>NL-CLR-Sputterke Eq.Nr. 37</p> <p>Cr Target (gun #: see mis logbook)</p> <ul style="list-style-type: none"> • Use Ar flow to adjust process pressure. • Base pressure: < 1.0 e-6mbar • Sputter pressure: 6.6 e-3mbar • power: 200W 	10nm

		<ul style="list-style-type: none"> • Deposition rate = 15 nm/min 	
7	Sputtering of Au (#film136)	<p>NL-CLR-Eq.Nr. 37 / Sputter Au Target (gun #: see mis logbook)</p> <ul style="list-style-type: none"> • use Ar flow to adjust pressure • Base pressure: < 1.0 e-6mbar • Sputter pressure: 6.6 e-3mbar • power: 200W • Deposition rate = 45-50 nm/min. • MAX THICKNESS: 250 NM 	150nm
8	Dehydration bake (#lith102)	<p>NL-CLR-WB21/22</p> <p>dehydration bake at hotplate</p> <ul style="list-style-type: none"> • Temp. 120°C • time: 5min 	
9	Priming (liquid) (#lith101)	<p>NL-CLR-WB21/22</p> <p>Primer:HexaMethylDiSilazane (HMDS) use spin coater:</p> <ul style="list-style-type: none"> • program: 4000 (4000rpm, 30sec) 	
10	Coating Olin Oir 907-17 (#lith105)	<p>NL-CLR-WB21</p> <p>Coating: Primus spinner</p> <ul style="list-style-type: none"> • olin oir 907-17 • spin Program: 4000 (4000rpm, 30sec) <p>Prebake: hotplate</p> <ul style="list-style-type: none"> • time 90 sec • temp 95 °C 	1.7µm
11	Alignment & Exposure Olin OiR 907-17 (#lith121)	<p>NL-CLR- EV620</p> <p>Electronic Vision Group EV620 Mask Aligner</p> <ul style="list-style-type: none"> • Hg-lamp: 12 mW/cm² • Exposure Time: 4sec 	

12	Development Olin OiR resist (#lith111)	NL-CLR-WB21 After exposure Bake : hotplate • time 60sec • temp 120°C development: developer: OPD4262 • time: 30sec in beaker 1 • time: 15-30sec in beaker 2	
13	Quick Dump Rinse (QDR) (#clean119)	NL-CLR-Wet benches Recipe 1 QDR: 2 cycles of steps 1 till 3, 1- fill bath 5 sec 2- spray dump 15 sec 3- spray-fill 90 sec 4- end fill 200 sec Recipe 2 cascade rinsing: continuous flow Rinse till the DI resistivity is > 10 ΩM	
14	Substrate drying (#clean120)	NL-CLR-WB Single wafer dryer • speed: 2500 rpm, 60 sec with 30 sec N2 flow	
15	Post bake Olin OiR resist (#lith109)	NL-CLR-WB21 Post bake: Hotplate • temp 120°C • time 10min	
16	Inspection by optical microscope (#metro101)	NL-CLR- Nikon Microscope • Dedicated microscope for lithography inspection	
17	Cleaning by	NL-CLR-UV PRS 100 reactor	

	UV/Ozone (#clean109)	-To improve wetting for wet chemical etching of chromium and oxide layers coated with olin oir resist. -To remove resist residues Time: variable	
18	Etching of gold (#etch136)	NL-CLR-WB10 Use dedicated beaker with gold etch • recipe: KI:I2:DI = (4:1:40) • add 40g KI and 10g I2 to 400ml DI water • temp.: 20°C Etch rates = xx nm/min (check rate with dummy wafer!) Excessive under etching of Cr occurs because of a galvanic reaction with gold. To minimize this make sure you do not over etch the chromium.	
19	Quick Dump Rinse (QDR) (#clean119)	NL-CLR-Wet benches Recipe 1 QDR: 2 cycles of steps 1 till 3, 1- fill bath 5 sec 2- spray dump 15 sec 3- spray-fill 90 sec 4- end fill 200 sec Recipe 2 cascade rinsing: continuous flow Rinse till the DI resistivity is > 10 ΩM	
20	Etching of	NL-CLR-WB10	

	chromium (#etch134)	Use dedicated beaker with chromium etch (standard) <ul style="list-style-type: none"> • temp.:20°C Etch rates = 60nm/min, Check always the etch rate with dummy wafer!	
21	Quick Dump Rinse (QDR) (#clean119)	NL-CLR-Wet benches Recipe 1 QDR: 2 cycles of steps 1 till 3, 1- fill bath 5 sec 2- spray dump 15 sec 3- spray-fill 90 sec 4- end fill 200 sec Recipe 2 cascade rinsing: continuous flow Rinse till the DI resistivity is > 10 ΩM	
22	Etching of gold (#etch136)	NL-CLR-WB10 Use dedicated beaker with gold etch <ul style="list-style-type: none"> • recipe: KI:I2:DI = (4:1:40) • add 40g KI and 10g I2 to 400ml DI water • temp.: 20°C Etch rates = xx nm/min (check rate with dummy wafer!) Excessive under etching of Cr occurs because of a galvanic reaction with gold. To minimize this make sure you do not over etch the chromium.	
23	Quick Dump	NL-CLR-Wet benches	

	Rinse (QDR) (#clean119)	Recipe 1 QDR: 2 cycles of steps 1 till 3, 1- fill bath 5 sec 2- spray dump 15 sec 3- spray-fill 90 sec 4- end fill 200 sec Recipe 2 cascade rinsing: continuous flow Rinse till the DI resistivity is > 10 Ω M	
24	Etching of chromium (#etch134)	NL-CLR-WB10 Use dedicated beaker with chromium etch (standard) • temp.:20°C Etch rates = 60nm/min, Check always the etch rate with dummy wafer!	
25	Quick Dump Rinse (QDR) (#clean119)	NL-CLR-Wet benches Recipe 1 QDR: 2 cycles of steps 1 till 3, 1- fill bath 5 sec 2- spray dump 15 sec 3- spray-fill 90 sec 4- end fill 200 sec Recipe 2 cascade rinsing: continuous flow Rinse till the DI resistivity is > 10 Ω M	
26	Substrate rinsing/drying Semitool	NL-CLR-Wet Benches Semitool spin rinser dryer	

	(#clean121)	<p>Apply always a single rinsing step (QDR) before using the Semitool</p> <p>Use dedicated wafer carrier of rinser dryer</p> <p>Parameters/step</p> <ul style="list-style-type: none"> • rinse in DI: 30 sec: 600 rpm • Q rinse in DI: 10.0 MΩ; 600 rpm • N2 purge: 10sec; 600 rpm • drying 1: 280 sec; 1600 rpm • drying 2: 0000 - 0000 <p>Unload wafers</p>	
27	Surface profile measurement (#metro105)	NL-CLR-Veeco Dektak 8	Measure thickness stack, to allow measurement of channel depth afterward
28	Cleaning by UV/Ozone (#clean109)	<p>NL-CLR-UV PRS 100 reactor</p> <p>-To improve wetting for wet chemical etching of chromium and oxide layers coated with olin or resist.</p> <p>-To remove resist residues</p> <p>Time: variable</p>	
29	Etching in HF/HCl 25%/2.5% (#etch131UPDATE)	<p>NL-CLR-WB09 or 10</p> <p>Use private beaker for etching: HF (25%)</p> <p>Add one part HF (50%) to one part DI to dilute etch solution. Add one part HCl to 10 parts HF</p> <ul style="list-style-type: none"> • temp.: 20°C <p>Etch rates (function of load):</p> <ul style="list-style-type: none"> • borofloat BF33: 1 μm/min in 25% HF 	First etch step to about 4.8μm than slow etch toward 5.0μm using BHF

		BHF (1:7 dilution) for last step. Etch rate 23 nm/min.	
30	Quick Dump Rinse (QDR) (#clean119)	NL-CLR-Wet benches Recipe 1 QDR: 2 cycles of steps 1 till 3, 1- fill bath 5 sec 2- spray dump 15 sec 3- spray-fill 90 sec 4- end fill 200 sec Recipe 2 cascade rinsing: continuous flow Rinse till the DI resistivity is > 10 Ω M	
31	Substrate rinsing/drying Semitool (#clean121)	NL-CLR-Wet Benches Semitool spin rinser dryer Apply always a single rinsing step (QDR) before using the Semitool Use dedicated wafer carrier of rinser dryer Parameters/step • rinse in DI: 30 sec: 600 rpm • Q rinse in DI: 10.0 M Ω ; 600 rpm • N2 purge: 10sec; 600 rpm • drying 1: 280 sec; 1600 rpm • drying 2: 0000 - 0000 Unload wafers	
32	Surface profile measurement (#metro105)	NL-CLR-Veeco Dektak 8	
33	Repeat from 28, and continue etching untill depth=5um. Be aware subtract the PR/Cr/Au film from the		Precision required 5.0 \pm 0.2 μ m

	Profile meter data (PR thickness + 160 nm). Use BHF Er=23 nm/min for last etch steps to slow down.		
34	Quick Dump Rinse (QDR) (#clean119)	NL-CLR-Wet benches Recipe 1 QDR: 2 cycles of steps 1 till 3, 1- fill bath 5 sec 2- spray dump 15 sec 3- spray-fill 90 sec 4- end fill 200 sec Recipe 2 cascade rinsing: continuous flow Rinse till the DI resistivity is >10 ΩM	
35	Substrate rinsing/drying Semitool (#clean121)	NL-CLR-Wet Benches Semitool spin rinser dryer Apply always a single rinsing step (QDR) before using the Semitool Use dedicated wafer carrier of rinser dryer Parameters/step • rinse in DI: 30 sec: 600 rpm • Qrinse in DI: 10.0 MΩ; 600 rpm • N2 purge: 10sec; 600 rpm • drying 1: 280 sec; 1600 rpm • drying 2: 0000 – 0000 Unload wafers	
36	Clean HNO3 1&2 (#clean105)	NL-CLR-WB16 • Beaker 1: HNO3 (99%) 5min • Beaker 2: HNO3 (99%) 5min	Stripping resist
37	Lamination of BF 410 foil	NL-CLR-GBC 3500 PRO Laminator	

	(#lith145)	<p>Ordyl BF 410 dry resist foil</p> <p>Laminate BF 410 foil on one side</p> <ul style="list-style-type: none"> • Protect hotplate with Aluminum foil • Put wafer on hotplate, 100 °C, 180 sec • Remove thick PET layer from BF 410 foil • Apply BF 410 foil with roller • Protect carry-paper with plain A4 paper • Close carrier and laminate • Temp: 130 °C ('carry 'preset) • Speed: 2 ('carry 'preset) • Remove and cool down wafer • Cut the wafer out of foil 	
38	<p>Alignment and exposure BF410 (#lith135)</p>	<p>NL-CLR-EVG 20</p> <p>Electronic Vision Group 20 Mask Aligner</p> <ul style="list-style-type: none"> • Hg-lamp: 12 W.cm² • Exposure time: 20 sec (BF 410) <p>Remark: DSP alignment with foil on both sides</p> <ul style="list-style-type: none"> • Remove the foil with a "knife" to achieve a clear view of the aligning marks • After development protect the aligning mask with tape again! 	Using "hole" mask
39	<p>UV dicing foil (Adwill D-210) (#back104)</p>	<p>NI-CLR- Dicing foil</p> <p>Information:</p> <p>Thickness: 125um</p>	On other side as BF410

		<p>Material: 100um PET + 25um Acrylic (adhesive)</p> <p>Adhesion before UV: 2000 mN/25mm</p> <p>Adhesion after UV : 15 mN/25mm</p> <p>UV irradiation : Luminance > 120mW/cm²</p> <p>and Quality > 70mJ/cm² (wave length: 365nm)</p>	
40	<p>Development BF410 foil (#lith136)</p>	<p>Carre-TST-HCM Spray Developer</p> <p>Na₂CO₃: MERCK 1.06392.0500</p> <p>Na₂CO₃:H₂O = 15g : 7.5liters (+ 1 cup Antifoam)</p> <ul style="list-style-type: none"> • Temp: 32°C • Time: 3min • Rinsing • Spin drying <p>Due to non-uniform development turn sample by 180° after half the time (small features might need longer development time.)</p>	
41	<p>Powder blasting of glass (#etch120)</p>	<p>NL-Carre-BIOS Powder blaster</p> <p>For feature size >100µm</p> <ul style="list-style-type: none"> • Particles: 30µm Al₂O₃ • Pressure: 4.6bar • Mass flow: 3-12 g/min • Etch rate appr. 91µm per g/cm² 	

42	Removal of foil and particles after powder blasting (#clean139)	<p>Outside cleanroom - use own facility</p> <p>Start with removal of foil</p> <ul style="list-style-type: none"> • remove dicing foil manually • remove powder blast foil manually • rinse wafer with water (by spraying) to remove powder blast particles • strip foil in Na₂CO₃ solution, time >30 min • rinse wafer with water time > few minutes • ultrasonic cleaning in water, time >10 min • ultrasonic cleaning in fresh water, time >10 min • drying of substrate by spinning or N₂ gun <p>Note 1: For silicon substrates the stripping procedure in Na₂CO₃ solution is critical.</p> <p>The Na₂CO₃ solution may create a rough surface.</p> <p>#If wafer bonding is needed the silicon surface should be protected by an oxide film.</p>	
43	Removal of particles (#clean110)	<p>NL-CLR-Wet Bench11</p> <p>Removal of particles generated by powderblasting and /or metal lift-off.</p> <p>Use ultrasonic bath 1</p>	

		<p>Use dedicated metal beakers and carriers</p> <ul style="list-style-type: none"> • beaker 1: Aceton technical, > 10 min , ultrasonic • beaker 2: Isopropanol technical > 10min, ultrasonic • beaker 3: DI water > 10min, ultrasonic 	
44	<p>Quick Dump Rinse (QDR) (#clean119)</p>	<p>NL-CLR-Wet benches</p> <p>Recipe 1 QDR: 2 cycles of steps 1 till 3,</p> <p>1- fill bath 5 sec</p> <p>2- spray dump 15 sec</p> <p>3- spray-fill 90 sec</p> <p>4- end fill 200 sec</p> <p>Recipe 2 cascade rinsing: continuous flow</p> <p>Rinse till the DI resistivity is >10 ΩM</p>	
45	<p>Substrate drying (#clean120)</p>	<p>NL-CLR-WB</p> <p>Single wafer dryer</p> <ul style="list-style-type: none"> • speed: 2500 rpm, 60 sec with 30 sec N2 flow 	
46	<p>Surface profile measurement (#metro105)</p>	<p>NL-CLR-Veeco Dektak 8</p>	<p>In this step, exact channel depth is determined.</p>
47	<p>Etching gold layer (#etch136)</p>	<p>NL-CLR-WB10</p> <p>Use dedicated beaker with gold etch</p> <ul style="list-style-type: none"> • recipe: KI:I2:DI = (4:1:40) • add 40g KI and 10g I2 to 400ml DI water 	

		<ul style="list-style-type: none"> temp.: 20°C <p>Etch rates = xx nm/min (check rate with dummy wafer!)</p> <p>Excessive under etching of Cr occurs because of a galvanic reaction with gold.</p> <p>To minimize this make sure you do not over etch the chromium.</p>	
48	Etching of chromium (#etch134)	<p>NL-CLR-WB10</p> <p>Use dedicated beaker with chromium etch (standard)</p> <ul style="list-style-type: none"> temp.:20°C <p>Etch rates = 60nm/min,</p> <p>Check always the etch rate with dummy wafer!</p>	
49	Etching of gold (#etch136)	<p>NL-CLR-WB10</p> <p>Use dedicated beaker with gold etch</p> <ul style="list-style-type: none"> recipe: KI:I2:DI = (4:1:40) add 40g KI and 10g I2 to 400ml DI water temp.: 20°C <p>Etch rates = xx nm/min (check rate with dummy wafer!)</p> <p>Excessive under etching of Cr occurs because of a galvanic reaction with gold.</p> <p>To minimize this make sure you do not over etch the chromium.</p>	
50	Etching of chromium (#etch134)	<p>NL-CLR-WB10</p> <p>Use dedicated beaker with chromium etch (standard)</p>	

		<ul style="list-style-type: none"> • temp.:20°C <p>Etch rates = 60nm/min, Check always the etch rate with dummy wafer!</p>	
51	Clean HNO3 1&2 (#clean105)	<p>NL-CLR-WB16</p> <ul style="list-style-type: none"> • Beaker 1: HNO3 (99%) 5min • Beaker 2: HNO3 (99%) 5min 	Both new top wafer and bottom wafer
52	Clean Piranha		To obtain good pre-bond.
53	EV620 Aligning & Prebonding (#bond104)	<p>NL-CLR-EV620 mask aligner</p> <p>Program:</p> <ul style="list-style-type: none"> • SDB Direct Bond tool 4" • Bond chuck SDB • Substrate1 4" • Substrate2 4" • Separation 30 µm • No exposure • SDB Piston • Bond time 60 sec <p>Instructions:</p> <ul style="list-style-type: none"> • Align alignmarks of top wafer to crosshairs • Check prebonding by using IR-setup 	
54	<p>Position wafer stack in press</p> <ul style="list-style-type: none"> -Temp:650 °F - Apply force: 'Max.pressure Dorothee' *cleaning chuck with acetone *position of wafer : centre *turn on heating *Apply pressure T>550 °F *Max. pressure: if valve is closed tightly, max pressure 		

55	At Mic-Mec Lab. temp:600-650 °C, t=60min. Place stack on Si-wafer carrier		
56	Dicing of a Silicon wafer (#back101)	<p>NI-CLR- Disco DAD dicing saw</p> <p>Applications:</p> <p>Silicon wafers, bonded silicon-silicon wafers (max 1.1mm)</p> <p>See #back103 for laminate of Nitto STW T10 dicing foil (80 μm)</p> <p>See #back104 for laminate of UV dicing foil (250μm)</p> <p>Parameters dicing:</p> <p>Wafer work size: 110 mm for a standard 100mm silicon wafer</p> <p>Max. Feed speed: 10 mm/sec</p> <p>X, Y values: correspond respectively to Ch1 and Ch2 and those values are determined by mask layout</p> <p>Saw type NBC-Z 2050</p> <p>Select in blade menu: NBC-Z-2050</p> <p>Blade info:</p> <p>Exposure: 1.3 mm (maximum dicing depth for a new blade)</p> <p>Width: 50 um</p> <p>Spindle revolutions: 30. 000 rpm</p> <p>Depth settings:</p> <p>Maximum cut depth: 1.1 mm</p> <p>Foil thickness: See foil info</p> <p>Min. blade height: 50 μm</p>	For the dicing, bonded wafers need to be diced completely through the wafer.

5.3.2 Calculation for hydrodynamic sample injection system

As already mentioned at chapter 4, for precise sample injection into the capillary tube for CE, hydrodynamic sample injection system need to be considered. However, the difficulties of injection sample solution into very narrow capillary ID ($5\mu\text{m}$), “Flow splitter” should be placed and calculated for precise injection.

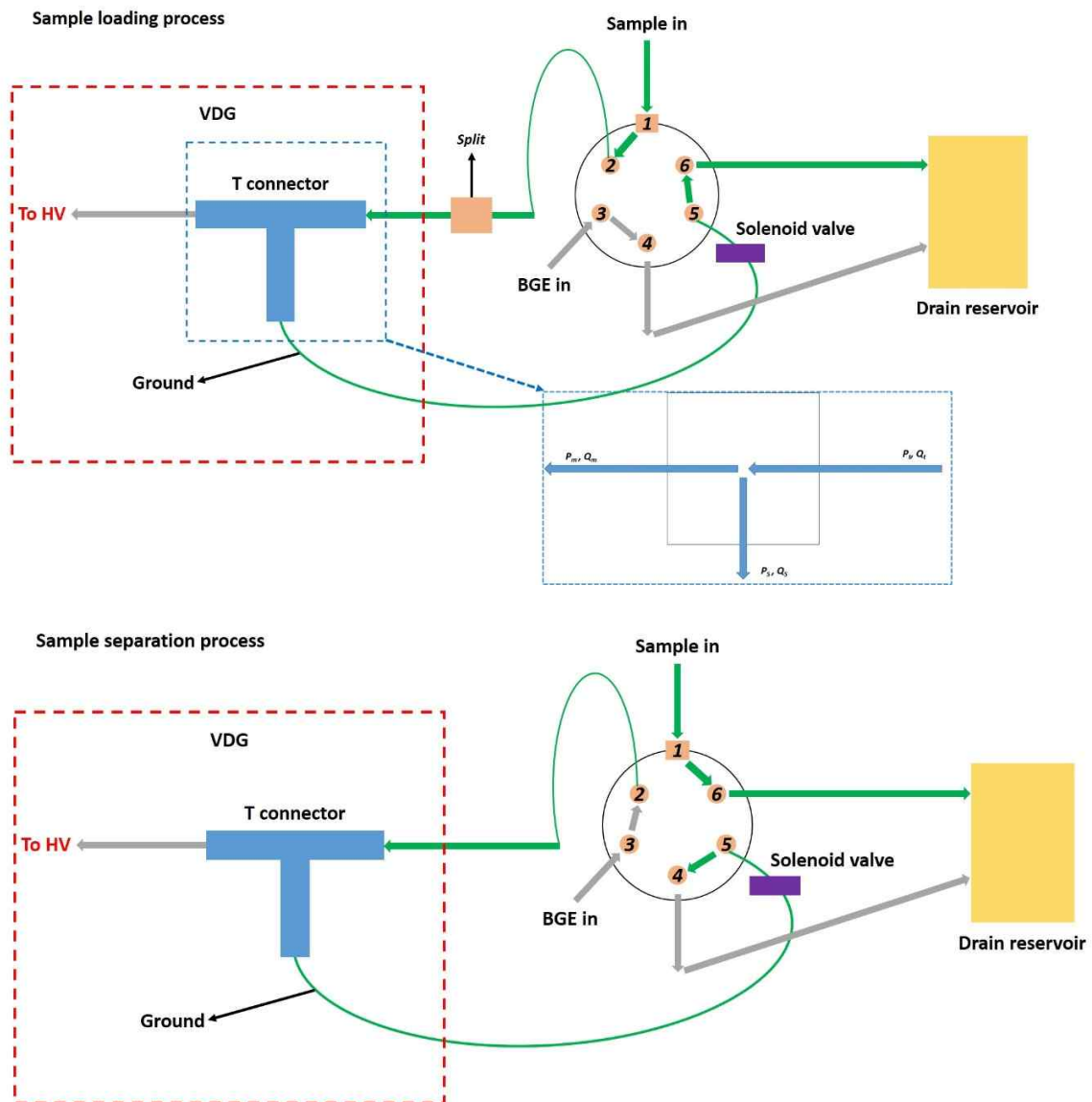


Figure 5.17 Schematic diagram of hydrodynamic sample injection system. (upper) Position of injector for sample loading process. (bottom) Position of injector for sample separation process.

For the calculation of exact injection volume, volume of tubing need to be determined.

Therefore, HPLC pump to injector port 3 (180 μ m ID PEEK tubing, 1m length) has 2.5nl, injector port 2 to “Flow splitter” inlet (180 μ m ID PEEK tubing, 1m length) has 2.5nl, “Flow splitter” outlet to T-connector (180 μ m ID PEEK tubing, 1.5m length) has 3.75nl. By the Hagen-Poiseuille equation, ΔP at the T-connector can be calculated to 211 bar when the flow rate from the HPLC is 7ml/min. (if, Solenoid valve is closed). According to those information, flow ratio between main channel (Q_m , 5 μ m ID and 6m length) and “Flow splitter” (Q_s , 100 μ m ID and 1m length) can be calculated by Eqn. 5.9

$$\frac{P_s}{P_m} = \frac{1.25 * 10^{-6} Q_s}{Q_m} \quad (5.9)$$

$Q_m=0.000125\%$ and $Q_s=99.99875\%$. So, if 7ml/min flow rate is used for the experiment, by the equation 5.10.

$$Q_t = Q_m + Q_s \quad (5.10)$$

$Q_m = 0.0725\text{nl/sec}$, $Q_s=57999.9275\text{nl/sec}$. Therefore, by the calculation of total volume for 5m and 5 μ mID capillary has 100nl. So, for the filling time for main capillary channel is 23min. and for the 1% sample volume injection for CE is 14sec. after close solenoid valve for pressure pulse injection.

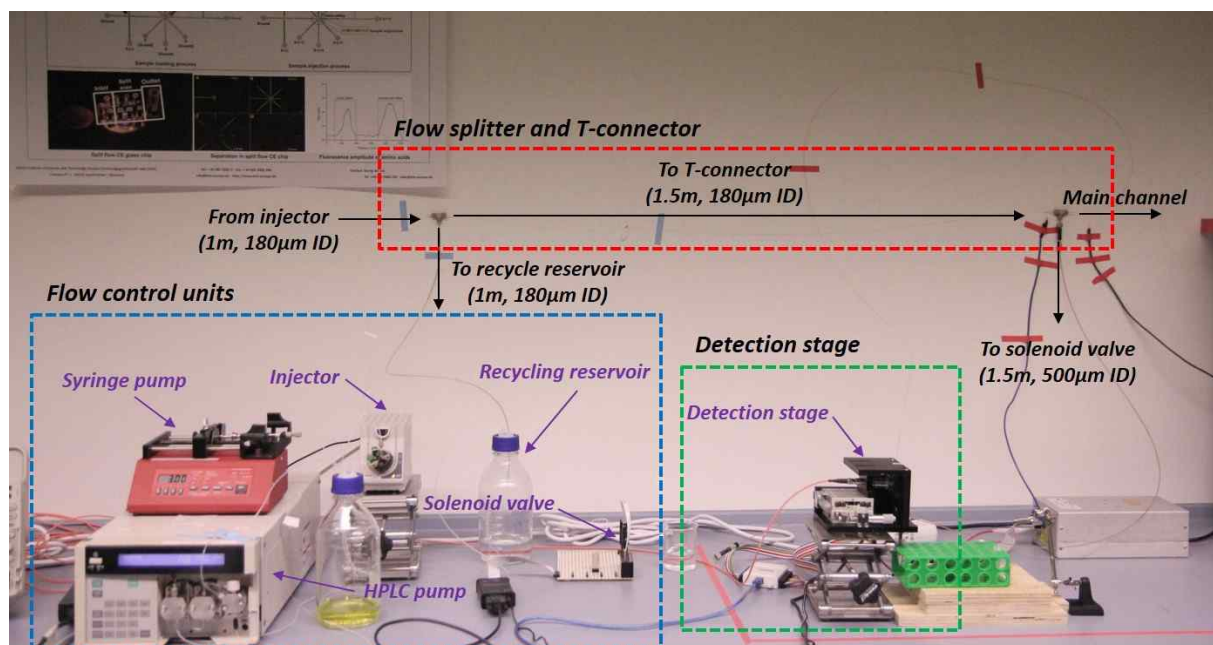


Figure 5.18 Hydrodynamic injection system with “Flow splitter” for pressure pulse injection.

Sample loading process

Sample injection process

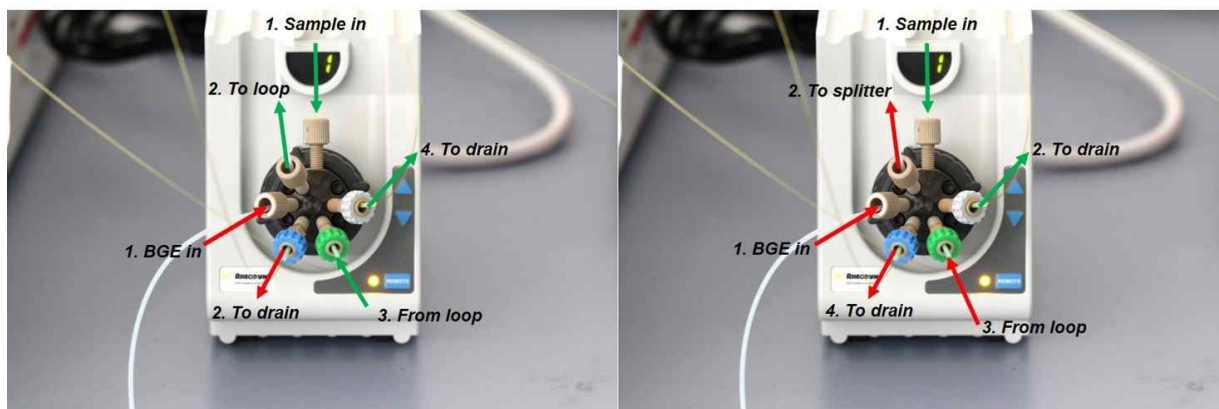


Figure 5.19 2-position flow injector for hydrodynamic sample injection system.

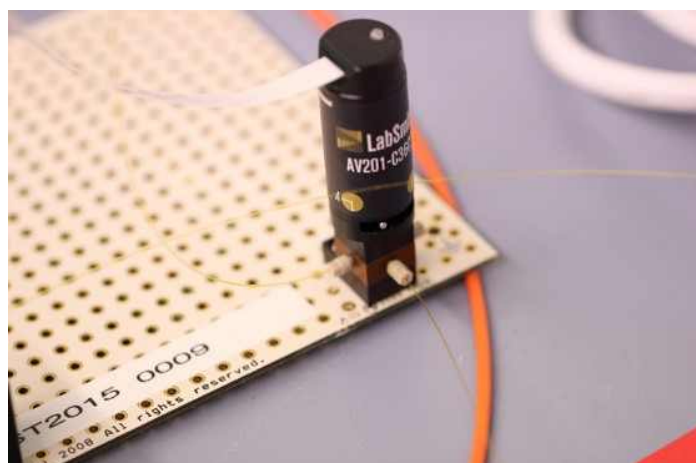


Figure 5.20 Solenoid valve for pressure pulse control

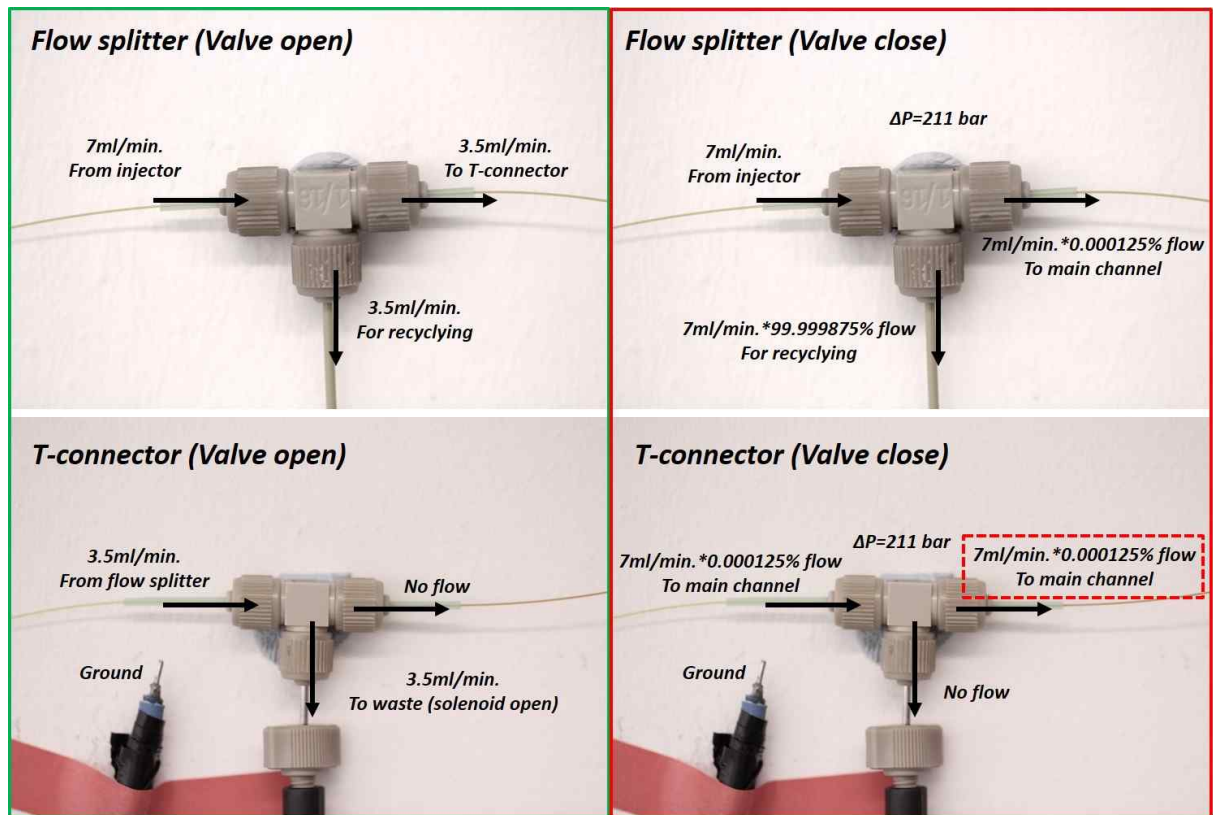


Figure 5.22 Flow splitter and T-connector for precise sample injection method into very narrow ID capillary tube ($5\mu\text{m}$)

5.3.3 High voltage measurement of VDG

VDG generates very high voltage with low current (350~900kV with 10~60 μ A) however, it can be used for CE, exact voltage measurement is needed. So, this chapter will describe about trial and error to measure direct high voltage from the VDG.

Theoretical understanding for voltage divide

Voltage divider can divide high (Alternating current or pulsating DC) voltage to low voltage by certain ratio of resistance. According to the simple circuit diagram. (figure 5.23)

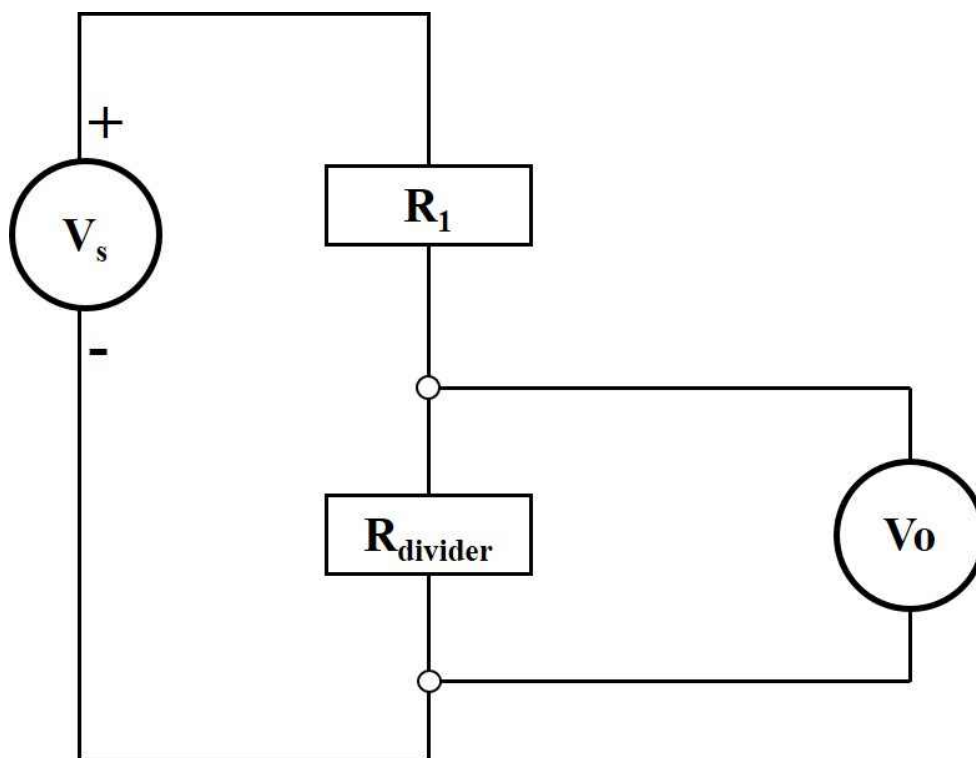


Figure 5.23 Schematic circuit diagram for resistive voltage divider.

The value of output voltage can be calculated with equation 5.11.

$$V_{out} = \frac{R_{\text{divider}}}{R_1 + R_{\text{divider}}} V_s \quad (5.11)$$

Where, V_{out} is output voltage, R_1 is the resistance of circuit, R_{divider} is the resistance for voltage dividing and V_s is output voltage from the instrument. For example, if the voltage source is 350kV, resistance of circuit is $35 \times 10^9 \Omega$, resistive voltage divider has $1 \text{M}\Omega$ then, the output voltage is 10V.

Using resistive capacitive voltage divider for VDG

According to the chapter 5.1.3, we bought the resistive capacitive voltage divider (CVD 600, HVP GmbH, Germany) and designed the measurement procedure for high voltage from VDG.

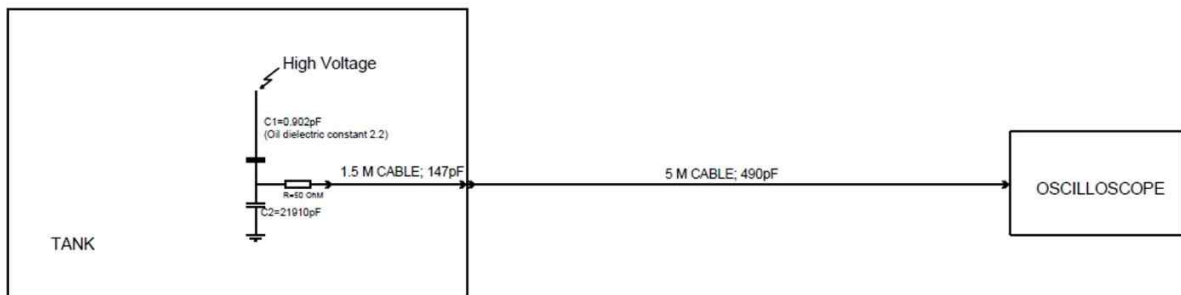


Figure 5.24 Resistive capacitive voltage divider for measurement of high voltage from VDG (upper), Measurement design with CVD 600 for high voltage measurement from VDG (Bottom).

However, high voltage measurement from the VDG was failed. Until the VDG was charged completely (less than 10 sec.), divided voltage was measured. But, the after certain period time (when the metal sphere was charged completely.). Hence, the measurement design needed to be reconsidered.

The definition of capacitor is an electrical component that stores electrical energy in the electric field. In this reason, capacitor can be used as a battery but, after some period the time the plates of the capacitor can be fully charged and there has no current flow anymore (figure 5.24). Therefore, the capacitor to DC current flow is at its maximum in the mega-ohms region and this is why capacitors block DC.

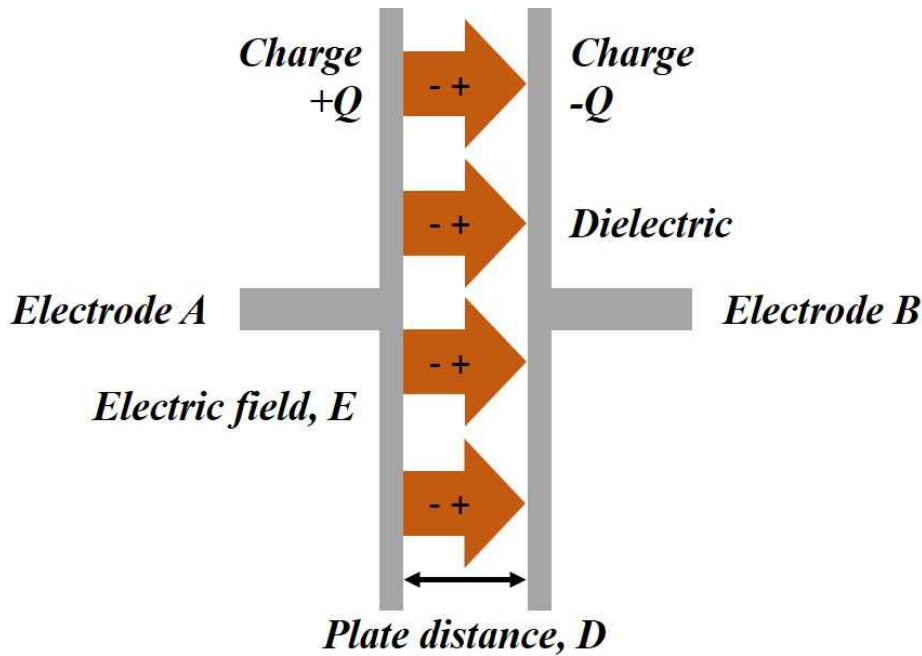


Figure 5.25 Schematic diagram of constant capacitor. Ideal capacitor consists with two plates which has certain distance in between. Charges inside of plates can make an internal electric field.

According to the capacitive reactance formula (Equation 5.4), if capacitive reactance is the function of the capacitance and the frequency of current.

$$X_c = \frac{1}{2\pi fC} \quad (5.12)$$

Where, X_c is the capacitive reactance in ohms, f is the frequency of current in hertz and C is the capacitance in farads. That is the reason (Equation 5.4), only alternating current (AC) or pulsating DC current can be used with resistive capacitive voltage divider (Figure 5.24 upper).

Electric field meter

Electric field meter is the instrument which can measure the strength of a static electric field. Especially, it is used to measure or predict the field strength in the atmosphere near thunderstorm clouds. Normally, electric field meter consists 2 pairs of electrode, shutter which connect with ground, AC amplifier and rotating motor for shutter (Figure 5.25). Electric field sensing electrode is exposed to the electric field and grounded by rotating shutter then, direct current from the high voltage source can become alternating current or pulsating DC after that, collected “high voltage potential” can be amplified by AC amplifier, finally, electric field strength can be measured.

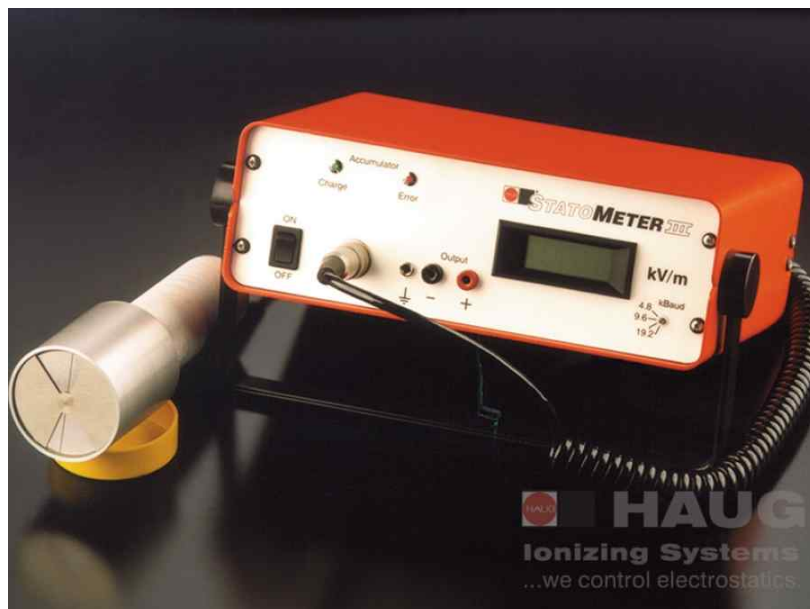
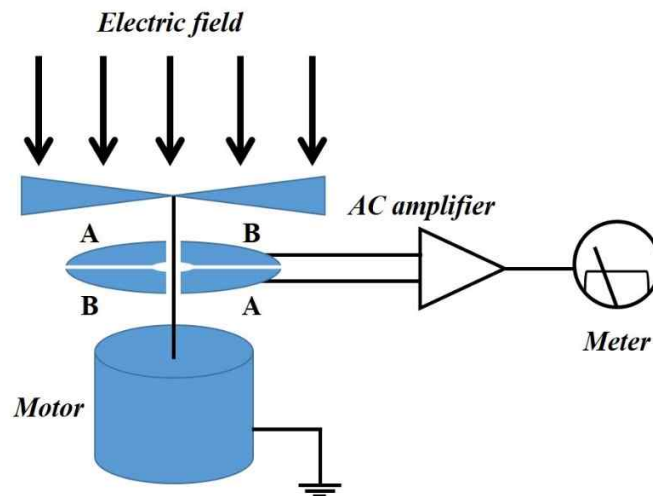


Figure 5.25 Schematic diagram of electric field meter. It consists with two pairs of measurement sensors, grounding shutter which connect with rotating motor and AC amplifier (upper). Commercialized electric field meter for measurement of high voltage from VDG (bottom).

In our case, VDG generate direct constant current therefore, the potential from the VDG need to be transformed to alternating or pulsating form artificially for measurement therefore, this type of electric field meter is the best solution to measure field strength directly from the VDG (Data was shown at chapter 2).

5.3.4 Electrical breakdown and heating problem from the AC motor of VDG

Electrical breakdown

Electrical breakdown can be occurred when the breakdown voltage is occurred by high electric field. According to the material, breakdown voltage can be differentiated. Normally, in the air, if the electric field is over 3MV/m, corona discharge can be observed (Figure 5.26). This means when we are doing the experiment with VDG, if you can see the corona discharge around the sphere of VDG that prove we are using high voltage.

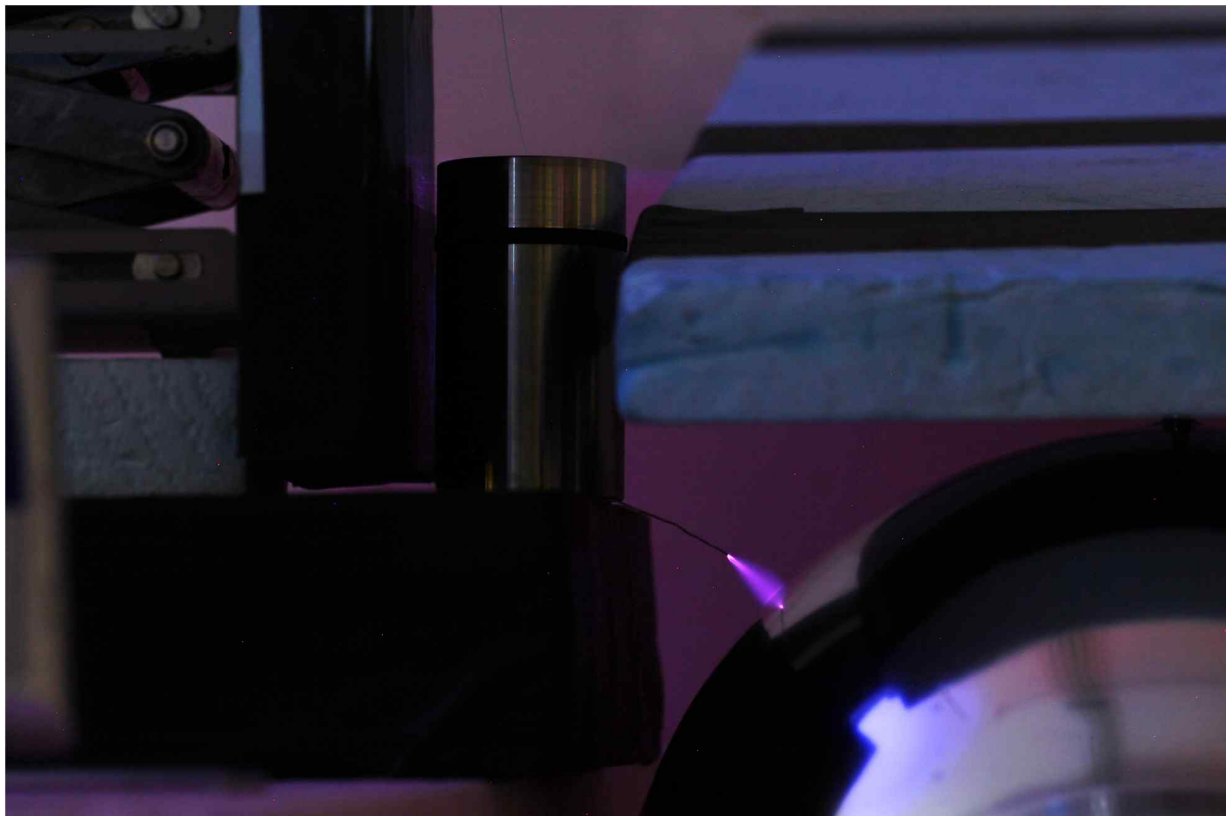


Figure 5.26 Corona discharge from VDG during separation experiment for CE.

But, the problem was when we were doing the separation experiment with 5 μ m and 1m length capillary, we could observe “capillary tube breaking” by high voltage from the VDG. Because, the dielectric strength of fused silica capillary is 4.2~7.5MV/m which is 4.5~7.2kV/180 μ m. So, if the field strength by the VDG is over 7.2kV/180 μ m, our capillary tube has high chance of break (Figure 5.27).

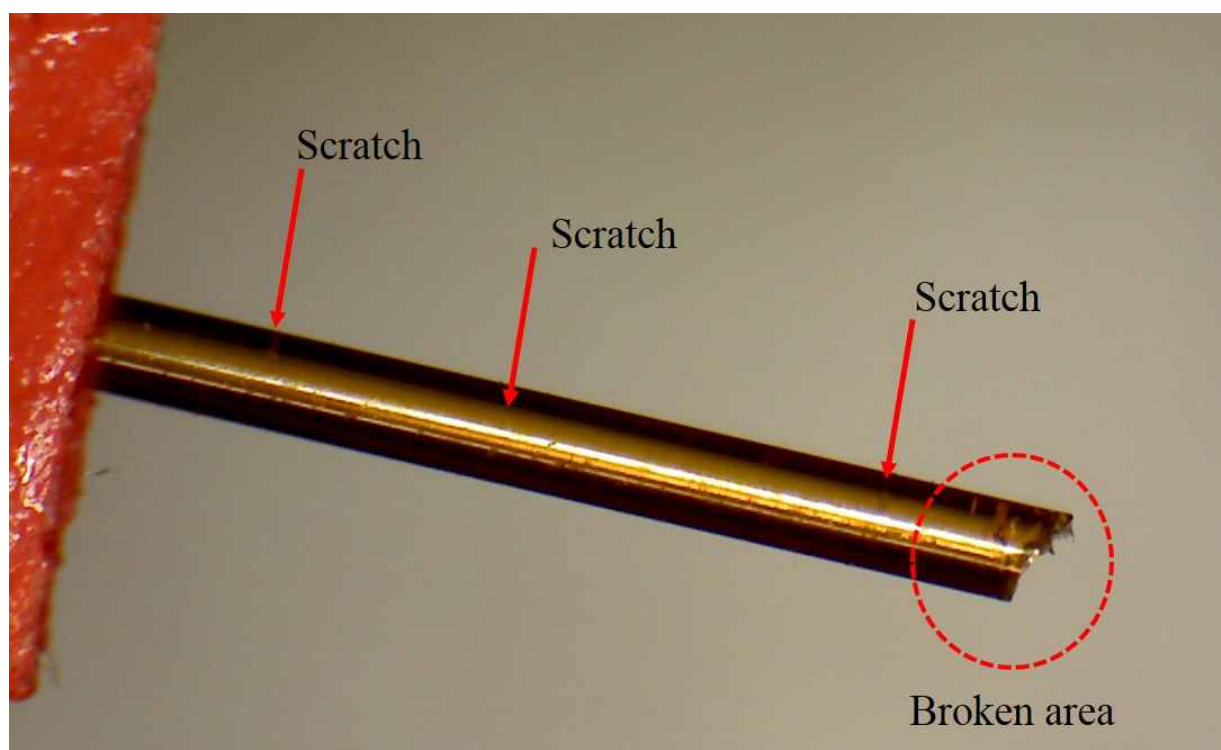


Figure 5.27 Brocken fused silica capillary by high electric field from VDG. When the electric field is too high, capillary is damaged (red arrow) and broken (red dot circle).

So, capillary tube needed to be shielded the material which has high dielectric strength. So, our capillary tube was covered with PEEK tubing (1mm wall thickness) which has 19kV/mm dielectric strength (Figure 5.28). Therefore, the total dielectric strength of fused silica capillary and PEEK shielding is 23.2~26.5kV/1180 μ m.

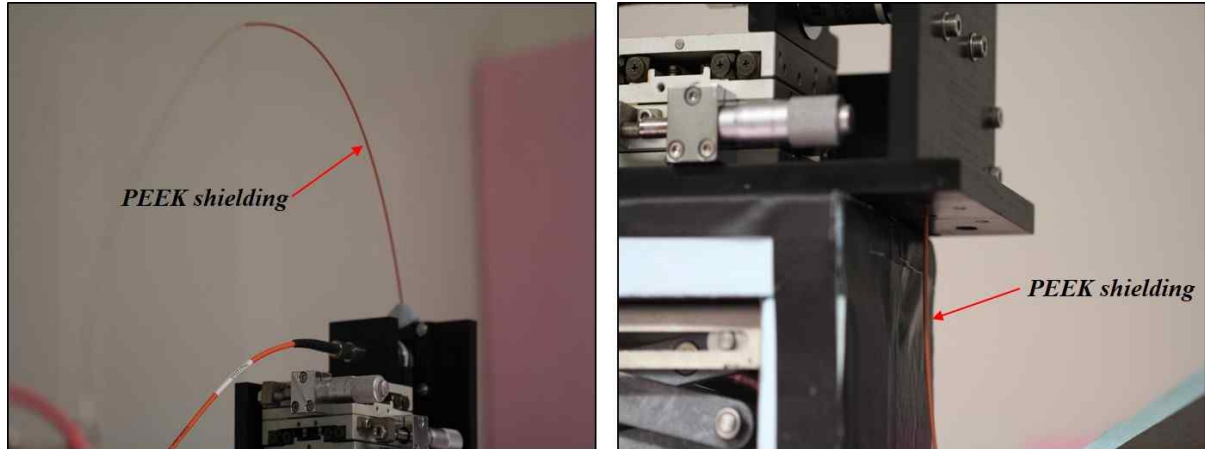


Figure 5.28 PEEK shielding to prevent breaking capillary tube by high voltage from VDG. By the shielding, total dielectric strength of capillary could be increased to 23.2~26.5kV/1180 μ m.

Heating problem from the AC motor of VDG

VDG is sensitive by the heat because of the rubber belt which carry the electron to the metal sphere. When the temperature around the rubber belt is increased, rubber belt can be expanded by the heat and can be loosen. Once the rubber belt is loosen it cannot be recover properly and it will carry less electrons or no electrons. Therefore, for the long-term running of VDG, heat dissipation need to be considered. In our case, when the VDG was run over 600 sec. the area of speed control knob and AC motor generated lots of heat (75~80°C) which was enough to make rubber belt loose. So, two Peltier elements that assembled with heating block and cooling fan were used for cooling element of those areas (Figure 6.13). The Peltier element can be cooled down to -20°C at 8.5A and it was controlled by DC power supply, by the cooling elements, the temperature of area for AC motor and speed control knob was decreased to 25°C~30°C which is much less surface temperature than without cooling elements. So, the life time of rubber belt for carrying electrons can be longer and stable for the long term experiment.

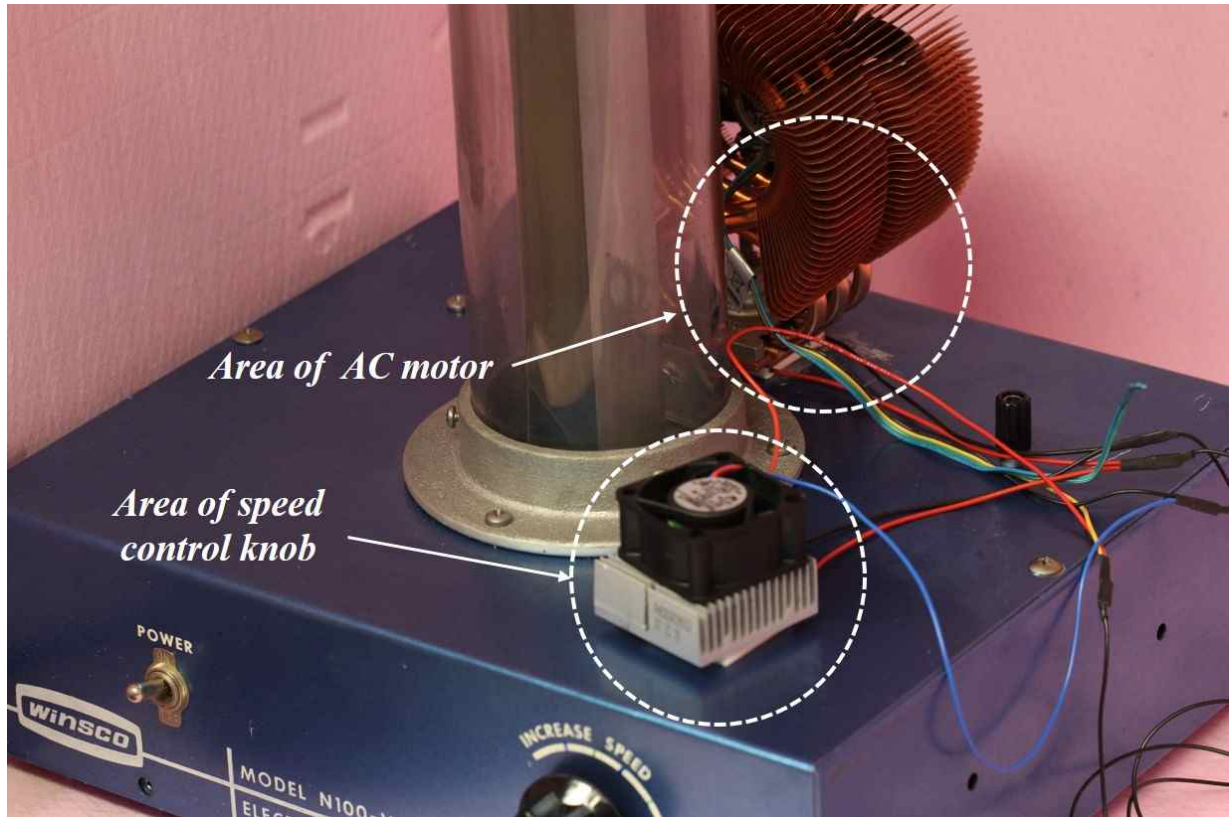


Figure 5.29 Heat control units from AC motor and speed control knob by Peltier elements.

5.3.5 Presentation materials for attended international conferences

MicroTAS 2014 (Poster presentation)

NOVEL SPLIT FLOW CHIP FOR CAPILLARY ELECTROPHORESIS

Seung Jae Lee, Eric Castro, Pavel Neuzil and Andreas Manz 

Introduction

- Capillary electrophoresis is a powerful electrical separation method.
- Its separation efficiency is determined by applied voltage.
- Applying higher voltages can generate heating which decrease separation performance.
- Decreasing the size of sample plug during the injection process, can increase separation efficiency.
- Our novel design split flow CE chip can decrease the size of sample plug during injection process.

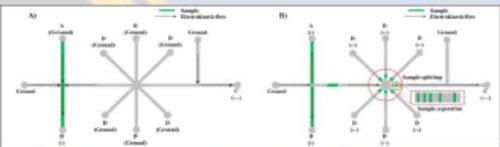
Theoretical number of plate (N)

$$N = \frac{L^2}{\sigma^2} = \frac{L^2}{\sigma_{diff}^2 + \sigma_{inj}^2} = \frac{L^2}{2Dt_m + \frac{w^2}{12}}$$

L: Length of separation channel
 σ : Total variance of band broadening
 σ_{diff}^2 : Variance due to diffusion
 σ_{inj}^2 : Variance due to sample plug
 $\sigma_{joule\ heating}^2$: Variance due to joule heating
 t_m : Migration time
w: Width of sample plug

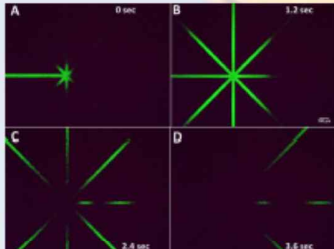
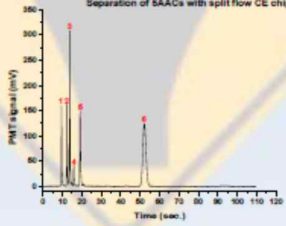
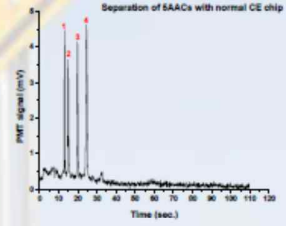
- Separation efficiency (N) is related to the total variance of band broadening.
- Decreasing the length of sample plug can be increased separation efficiency during injection process.

Working principle of split flow CE chip



- Applied voltage: 3kV for injection process
- Separation channel length: 23mm
- Running buffer: phosphate buffer
- Sample: Gln, Glu, Lys, Arg, Ala labelled with FITC
- Detection: laser induced fluorescence system
- Comparison with normal cross shape CE chip

Results and discussions

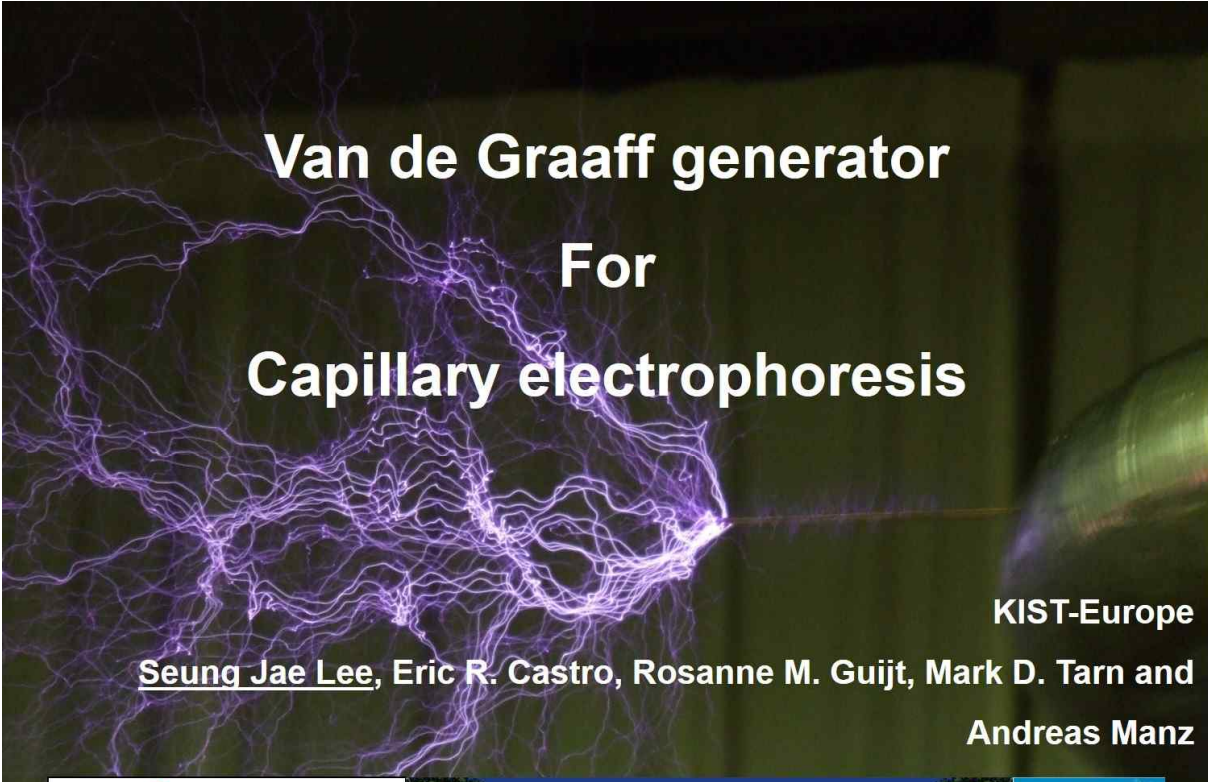
- Each peak represents 1: free FITC, 2: GLU, 3: GLN, 4: Ala, 5: Arg and 6: Lys
- Novel designed split flow CE chip can increase the separation efficiency compare with normal CE chip.
- The length of sample plug can be decreased during injection process.
- Split flow CE chip can be used to achieve high efficiency separation.
- Also, this high efficiency can be obtained using shorter separation channel length than conventional CE chips.

Korea Institute of Science and Technology Europe
Forschungsgesellschaft mbH (KIST)
Campus E7 1 - 66123 Saarbrücken - Germany

Tel: + 49 681 9382 0 · Fax: + 49 681 9382 240
info@kist-europe.de · <http://www.kist-europe.de>

Contact: Seung Jae Lee
Tel: +49 681 9382 230
E-mail: sjlee@kist-europe.de

40th ISCC Riva del Garda (Oral presentation)



Van de Graaff generator For Capillary electrophoresis

KIST-Europe
Seung Jae Lee, Eric R. Castro, Rosanne M. Guijt, Mark D. Tarn and
Andreas Manz

en:Z-pinches constrain the plasma filaments in an en:electrical discharge from a en:Tesla coil. Photo taken by Ian Tresman at the UK Teslathon in Derby, UK, on 27 May 2005.

Capillary electrophoresis to the extreme separation efficiency

- Applying 100kV to 150pL volume -

- *Separation efficiency is increased proportionally by applied voltage.*
- *Currently DC power supply has joule heating problem by high current.*
- *Van de graaff generator is constant current generator.*
- *Combination of VDG and high resistance of capillary can make extremely high separation efficiency.*

Seung Jae Lee, Rosanne M. Guijt and Andreas Manz

en:Z-pinches constrain the plasma filaments in an en:electrical discharge from a en:Tesla coil. Photo taken by Ian Tresman at the UK Teslathon in Derby, UK, on 27 May 2005.

Electrophoresis to the extreme

Seung Jae Lee¹, Rosanne M. Guijt² and Andreas Manz¹

¹Korea Institute of Science and Technology Europe, Campus E7 1 66123, Saarbruecken, Germany

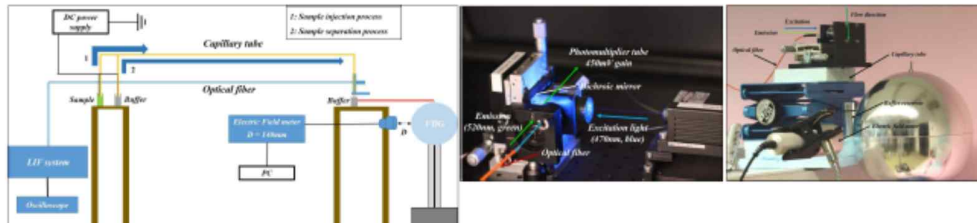
²School of Medicine and ACROSS, University of Tasmania, Private Bag26 Hobart TAS 7001, Australia

INTRODUCTION

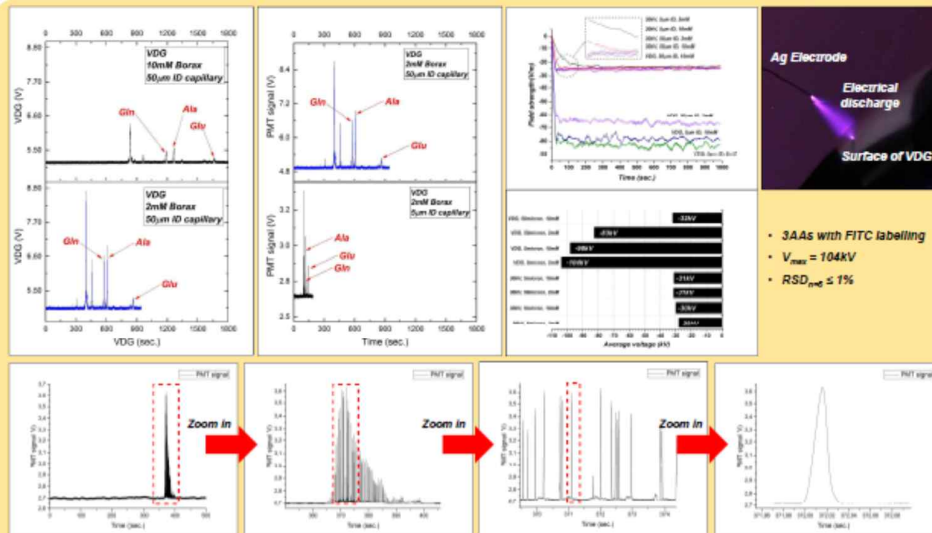
- Capillary electrophoresis (CE) is powerful separation method in analytical chemistry and biology.
- Higher voltage makes higher separation efficiency in CE
- Present CE method has a limitation of Joule heating.
- Low constant current (Van de Graaff generator (VDG)) can be a solution.
- VDG generate low current (10 μ A) and high voltage (360kV).
- By Ohm's law ($V=IR$), high resistance of capillary tube generate extremely high voltage with VDG.
- High resistance capillary smaller ID capillary, lower conc. BGE

Experimental setup

- Conventional CE setup and laser induced fluorescence (LIF) system was used.
- 6 μ m ID and 1m length fused silica capillary tube.
- Total volume of capillary tube is 16nL.
- Optimal sample injection volume is 150pL (1% of total volume).
- 2mM Sodium tetraborate buffer (pH 9.20) as BGE.
- Field strength was measured directly from VDG by electric field meter.
- For the comparison, 30kV DC power supply and 60 μ m ID capillary was used.
- Sample was injected by electrokinetic injection method.



Results



- Sigma (σ) of peak is 0.0072 sec. (7.2msec.) and the length of analyte zone is 15 μ m.
- Separation efficiency is $2.7 \cdot 10^9$ which is 1000 times higher than commercial CE instrument.

Contact information : Prof. Dr. Andreas Manz (E-mail: manz@kist-europe.de, Tel: +49 681 9382 210)

Seung Jae, Lee (E-mail: sjlee@kist-europe.de, ricky0730@gmail.com, Tel: +49 681 9382 371)